nature aging

Article

https://doi.org/10.1038/s43587-024-00594-3

Restoration of neuronal progenitors by partial reprogramming in the aged neurogenic niche

Received: 1 March 2023

Accepted: 13 February 2024

Published online: 29 March 2024

Check for updates

Lucy Xu[1,2], Julliana Ramirez-Matias[1], Max Hauptschein[1], Eric D. Sun[1,3], Judith C. Lunger[1], Matthew T. Buckley[1] & Anne Brunet[1,4,5]

Partial reprogramming (pulsed expression of reprogramming transcription factors) improves the function of several tissues in old mice. However, it remains largely unknown how partial reprogramming impacts the old brain. Here we use single-cell transcriptomics to systematically examine how partial reprogramming influences the subventricular zone neurogenic niche in aged mouse brains. Whole-body partial reprogramming mainly improves neuroblasts (cells committed to give rise to new neurons) in the old neurogenic niche, restoring neuroblast proportion to more youthful levels. Interestingly, targeting partial reprogramming specifically to the neurogenic niche also boosts the proportion of neuroblasts and their precursors (neural stem cells) in old mice and improves several molecular signatures of aging, suggesting that the beneficial effects of reprogramming are niche intrinsic. In old neural stem cell cultures, partial reprogramming cell autonomously restores the proportion of neuroblasts during differentiation and blunts some age-related transcriptomic changes. Importantly, partial reprogramming improves the production of new neurons in vitro and in old brains. Our work suggests that partial reprogramming could be used to rejuvenate the neurogenic niche and counter brain decline in old individuals.

Long thought to be irreversible, aging is in fact a malleable process. Several interventions can slow or even reverse aspects of aging[1–8]. Among these, partial reprogramming has emerged as a potentially powerful way to restore function in old tissues[9,10]. Expression of reprogramming transcription factors (OCT4 (POU5F1 or OCT3/4), SOX2, KLF4, c-MYC or 'OSKM'), which converts somatic cells into embryonic-like stem cells, erases many hallmarks of aging in vitro[11–15]. This is likely because reprogramming mimics aspects of the resetting process between generations that naturally occurs during gametogenesis and fertilization. However, for in vivo applications, full reprogramming to embryonic-like stem cells would be detrimental because of loss of cell identity and increased tumorigenic potential[16–18]. Interestingly, the 'rejuvenating' effects of reprogramming can be uncoupled from loss of cell identity by controlling expression of reprogramming factors through pulsed or cell type-targeted expression ('partial reprogramming')[19–31]. Partial reprogramming improves function in a variety of tissues in mice[20,29–34], including pancreas and muscle, to different extents depending on the cell type[22,27,28]. In the central nervous system, partial reprogramming has shown promising effects in the spinal cord of old mice[20] and in the optic nerve, hippocampus and striatum of young to middle-aged mice[26,30,33,34]. However, the impact of partial reprogramming on the brains of older mice remains largely uncharacterized. The brain has a remarkably

[1]Department of Genetics, Stanford University, Stanford, CA, USA. [2]Department of Biology, Stanford University, Stanford, CA, USA. [3]Department of Biomedical Data Science, Stanford University, Stanford, CA, USA. [4]Wu Tsai Neurosciences Institute, Stanford University, Stanford, CA, USA. [5]Glenn Center for the Biology of Aging, Stanford University, Stanford, CA, USA. e-mail: abrunet1@stanford.edu

large number of different cell types, and unbiased characterization at single-cell resolution is critical to understand how different cells are impacted by in vivo partial reprogramming.

The adult brain contains neurogenic niches in the hippocampus and the subventricular zone (SVZ) that are unique regions to examine the effects of brain aging and rejuvenation[35–40]. In particular, the SVZ neurogenic niche encompasses many cell types (neural stem cells (NSCs), neuroblasts, microglia, endothelial cells, etc.) and has regenerative potential, as NSCs from this niche can give rise to newborn neurons (neurogenesis) and glia throughout adulthood in mammals[41–46]. Normally quiescent, NSCs can also activate and proliferate and commit to neuronal precursors (neuroblasts)[41,42,47]. In mice, SVZ neuroblasts migrate a long distance to the olfactory bulb and differentiate into newborn neurons, which are important for olfactory discrimination and learning[48–51]. NSCs from the SVZ are also critical for repair after brain injury or stroke[52–54]. However, the process of SVZ neurogenesis declines strikingly with age[55–60]. Rejuvenation strategies such as parabiosis (the sharing of blood between young and old mice), exercise and rapamycin have been shown to improve old neurogenic niches with various degrees of efficacy[61–67], suggesting that aspects of these age-related changes are malleable.

Here, we show that partial reprogramming in old mice, either in the whole body or targeted to the SVZ niche itself, restores the neuroblast proportion to a younger level and reverses several molecular signatures associated with aging. Partial reprogramming also improves the proportion of neuroblasts during differentiation in old primary NSCs, suggesting a cell-autonomous effect. Finally, partial reprogramming improves the production of new neurons both in vitro and in old brains, a characteristic of youthfulness. Our work raises the possibility that partial reprogramming in already old individuals could rejuvenate the neurogenic niche and counter brain decline with aging or neurodegeneration.

Results

Partial reprogramming boosts neuroblast proportion in old mice

We leveraged single-cell transcriptomics to unbiasedly examine how partial reprogramming affects the SVZ neurogenic niche in old mice. To this end, we generated aging cohorts of a genetically engineered mouse line[68] that allows doxycycline-inducible expression of the four reprogramming factors OCT4, SOX2, KLF4 and c-MYC in the whole body (Fig. 1a) (hereafter iOSKM mice). In these iOSKM mice, a reverse tetracycline transactivator (rtTA) is constitutively and ubiquitously expressed (from the *ROSA26* locus), and doxycycline treatment induces expression of OCT4, SOX2, KLF4 and c-MYC (from the *Col1a1* locus)[68]. We first verified induction of the reprogramming factors both in vivo and in culture. Treatment of iOSKM mice with doxycycline for 2 d led to increased expression of OCT4 in the whole SVZ niche and the olfactory bulb by western blot analysis (Fig. 1b) as well as in more than ten other tissues at varying levels (Extended Data Fig. 1a). We also confirmed SOX2 expression by western blot (Extended Data Fig. 1b). To assess OSKM expression in SVZ NSCs in these iOSKM mice (and not solely in blood cells present in the tissue, for example), we isolated NSCs from the brain and added doxycycline to these primary NSC cultures. Western blot analysis showed that rtTA was constitutively expressed in NSCs from iOSKM mice and that OCT4 was induced by doxycycline in a dose- and time-dependent manner (Extended Data Fig. 1c,d). Reverse transcription followed by quantitative PCR (RT–qPCR) confirmed expression of *Oct4* (*Pou5f1*) and the polycistronic OSKM messenger RNA (mRNA) (primers specific for *Oct4-P2A*, *Sox2-T2A* and *E2A-c-Myc*) upon doxycycline treatment in iOSKM NSCs (Fig. 1c). Expression of the reprogramming factors declined following doxycycline withdrawal (Extended Data Fig. 1e). Thus, the iOSKM mouse model allows pulsed expression of reprogramming factors in culture and in vivo in multiple tissues, including the SVZ neurogenic niche.

To unbiasedly examine how partial reprogramming affects the SVZ neurogenic niches of old mice in vivo, we aged cohorts of iOSKM mice for ~2 years and performed single-cell transcriptomics upon pulsed induction of the reprogramming factors. Old iOSKM mice (two independent cohorts, 18–20 months for cohort 1 and 24–26 months for cohort 2) were treated with a partial reprogramming regimen of 2 d of doxycycline in drinking water, followed by 5 d of withdrawal, repeated three times (Fig. 1d and Extended Data Fig. 2a,b). A pulsed doxycycline regimen was chosen because it was shown to improve pancreas repair in middle-aged mice and lifespan in an accelerated aging disease model[19]. We verified that this regimen did not negatively impact weight or survival of old iOSKM mice during treatment (Extended Data Fig. 1f,g). We collected SVZ neurogenic niches from partially reprogrammed old mice immediately after the last 2-d pulse of doxycycline ('old + OSKM') and from untreated old mice as well as from untreated young mice for cohort 2 and then performed single-cell RNA sequencing (RNA-seq) (Fig. 1d and Extended Data Fig. 2b). Dimensionality reduction and clustering (uniform manifold approximation and projection (UMAP) and Louvain clustering) based on the transcriptomes of single cells identified the major cell types previously observed[54,69–73], including the NSC lineage (astrocytes and quiescent NSCs (qNSCs), activated NSCs and neural progenitor cells (aNSCs–NPCs) and neuroblasts) and other cell types (for example, microglia, oligodendrocytes, endothelial cells) (Fig. 1e and Extended Data Fig. 2j, cohort 2; Extended Data Fig. 2d, cohort 1).

We examined how partial reprogramming affects cell composition in old SVZ neurogenic niches (Fig. 1f,h). As previously reported[69,73–76], old age led to a decline in neuroblasts and their precursors: aNSCs–NPCs (Fig. 1g and Extended Data Fig. 2h). This age-dependent decline was also observed, especially for neuroblasts, when calculated as a proportion of cells recovered from the NSC lineage (astrocytes–qNSCs, aNSCs–NPCs and neuroblasts), which is less sensitive to variation in microdissection of the SVZ (Fig. 1h). Interestingly, partial reprogramming in old mice ('old + OSKM') led to an increase in the proportion of neuroblasts that was consistent across both aging cohorts, either when calculated as a fraction of the entire niche ($P = 0.11$; Fig. 1g and Extended Data Fig. 2h) or of the NSC lineage (Fig. 1h). We also validated these cell type proportion changes using immunostaining approaches (Fig. 3 and Extended Data Fig. 4). By contrast, reprogramming did not strongly affect the proportion of neuroblast precursors (aNSCs–NPCs) in old mice (Fig. 1g,h and Extended Data Fig. 2h). Partial reprogramming also led to an increase in the proportion of mural cells and a drop in the fraction of oligodendrocyte precursor cells (OPCs) in the neurogenic niche of old mice, although the total number of these cells captured was very low (Extended Data Fig. 2h,i). Importantly, partial reprogramming did not result in the production of new cell types (for example, 'undifferentiated') (Fig. 1e,f and Extended Data Fig. 2d–g). Thus, partial reprogramming mainly affects neuroblasts in the old SVZ neurogenic niche, increasing their proportion within the NSC lineage to more youthful levels.

To quantify the impact of partial reprogramming on all cell type proportions in the old niche, we trained a machine learning model to predict chronological age by linear regression using as features the proportions of ten annotated cell types from single-cell RNA-seq data (astrocytes–qNSCs, aNSCs–NPCs, neuroblasts, oligodendrocytes, microglia, etc.) (Methods). For the training data, we leveraged an independent dataset of single-cell RNA-seq from the SVZ neurogenic niches of 28 mice spanning an age of 3–29 months[77]. This cell proportion linear regression model had good accuracy in predicting the chronological age of the mice ($R = 0.63$, $P = 0.00035$; Extended Data Fig. 2k). Applying this cell proportion model to our single-cell RNA-seq dataset revealed that partial reprogramming in old mice decreased median predicted age ('rejuvenation') by 2.7 months (Fig. 1i), although this change was not significant at the mouse level (Fig. 1i and Extended Data Fig. 2l).

https://doi.org/10.1038/s43587-024-00594-3

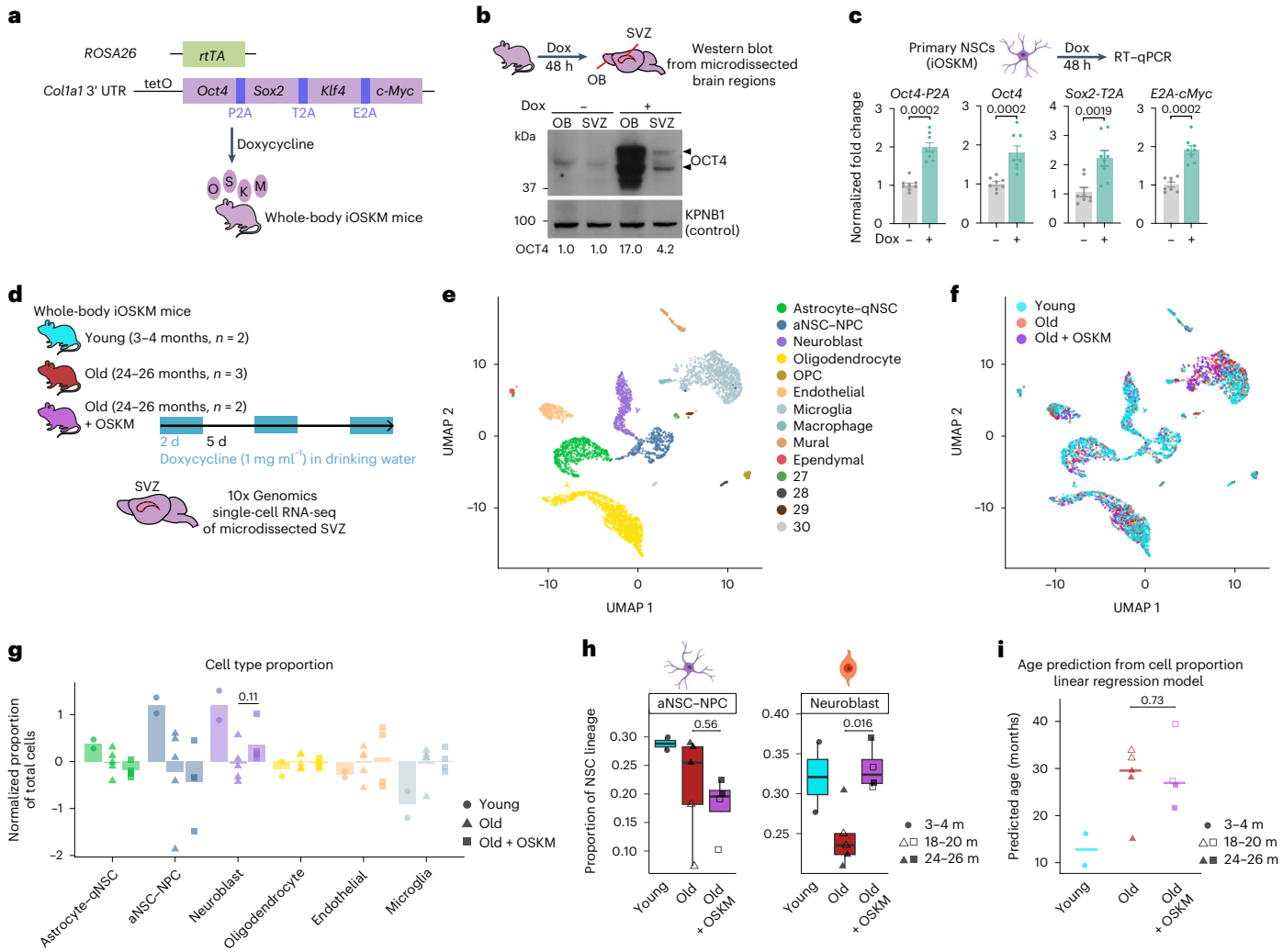

Fig. 1 | Effect of whole-body in vivo partial reprogramming on the old SVZ neurogenic niche by single-cell transcriptomics. a, Transgenic whole-body 'iOSKM' mouse for doxycycline-inducible expression of OSKM reprogramming factors. P2A, T2A, E2A, self-cleaving peptides; tetO, tetracycline-responsive operator; UTR, untranslated region. **b**, Western blot from microdissected brain regions after in vivo doxycycline (Dox) treatment. OB, olfactory bulb; arrowheads, OCT4 bands; KPNB1, karyopherin subunit beta 1 (loading control). Normalized densitometry quantification of OCT4 is indicated below each lane. **c**, RT–qPCR on primary NSC cultures treated with doxycycline. $n = 4$ young (3 months, two males and two females) and $n = 4$ old (24–26 months, two males and two females) cultures, each from one mouse. *Oct4-P2A*, *Sox2-T2A*, *E2A-c-Myc*, primers specific to the polycistronic OSKM mRNA. Each dot represents one culture. Mean ± s.e.m.; *P* values, two-sided Wilcoxon rank-sum test. **d**–**f**, Single-cell RNA-seq. $n = 2$ young (3–4 months, two males), $n = 3$ old (24–26 months, two males and one female) and $n = 2$ old + OSKM (24–26 months, one male and one female) samples. See Extended Data Fig. 2b–f for another cohort. **d**, Experimental design for single-cell RNA-seq of the SVZ after whole-body partial reprogramming using iOSKM mice. **e**,**f**, UMAP on single-cell transcriptomes of 3,857 high-quality cells. Each dot represents one cell. Colors indicate cell type (**e**) or condition (**f**). **g**–**i**, Combined results from two independent experiments (Supplementary Table 1 and Source data). $n = 2$ young (3–4 months, two males), $n = 5$ old (18–20 months or 24–26 months, four males and one female), 4 old + OSKM (18–20 months or 24–26 months, three males and one female) samples. **g**, Proportion of each cell type from single-cell RNA-seq of the SVZ as a fraction of total cells recovered per mouse, normalized as $\log_2$ (fold change) over the mean of old control mice per experiment. Each dot, triangle or square represents one mouse. Bar, mean; *P* values, two-sided Wilcoxon rank-sum test. **h**, Proportion of aNSCs–NPCs and neuroblasts from single-cell RNA-seq, as a fraction of total cells within the NSC lineage per mouse. Each dot, triangle or square represents one mouse. Median (center line), upper and lower quartiles (box limits) and 1.5× interquartile range (whiskers); shape, experimental cohort; *P* values, two-sided Wilcoxon rank-sum test. m, months. **i**, Predicted age per mouse from a linear regression model of cell type proportions in the SVZ neurogenic niche, trained on 28 mice at 3–29 months. Each dot, triangle or square represents one mouse. Line, median; shape, experimental cohort; *P* values, two-sided Wilcoxon rank-sum test.

Thus, whole-body partial reprogramming in vivo can boost neuroblast proportion in old mice, countering one aspect of age-associated cell proportion changes in the SVZ neurogenic niche.

Partial reprogramming improves some signatures of aging

We examined transcriptomic changes for each cell type in the SVZ after whole-body partial reprogramming. Differential gene expression analysis revealed significant gene expression changes during aging (old versus young) and in response to reprogramming (old + OSKM versus old) across cell types (Fig. 2a,b and Extended Data Fig. 3a). To examine molecular signatures affected by age and reprogramming, we performed gene set enrichment analysis (GSEA) and compared the direction of changes with age and reprogramming in each cell type using a scatterplot (Fig. 2c and Extended Data Fig. 3b). Several signatures were increased with age and changed in the opposing direction with reprogramming (Fig. 2c). As previously reported[69,74,75,78], inflammation and adhesion signatures were upregulated in most cell types in old individuals (although inflammation was downregulated in neuroblasts

and adhesion signatures were downregulated in astrocytes–qNSCs with aging) (Fig. 2e,f and Extended Data Fig. 3d,e). RNA processing signatures were also mostly upregulated with age (Fig. 2c and Supplementary Tables 3 and 4), similar to previous reports[73]. Interestingly, reprogramming 'reversed' some of these age-dependent signatures (Fig. 2c). For example, RNA processing and cell adhesion signatures were reversed by partial reprogramming in aNSCs–NPCs and oligodendrocytes (Fig. 2d,e and Extended Data Fig. 3e). Generally, aNSCs–NPCs, neuroblasts, endothelial cells and mural cells had a high fraction of pathways that trended in opposing directions with aging and after partial reprogramming (Fig. 2c and Extended Data Fig. 3d–g). By contrast, partial reprogramming exacerbated many age-related signatures in some cell types (microglia, astrocytes–qNSCs) (Fig. 2c). Inflammation was further increased by reprogramming in many cell types including microglia (Fig. 2f,k). This is consistent with the observation that cell-specific aging clocks built to predict age from single-cell transcriptomes[77] did not detect strong 'rejuvenation' by partial reprogramming (Extended Data Fig. 3c), as these clocks include many inflammation genes[77]. Differences between cell types could reflect differing levels of and responses to reprogramming factor expression. Thus, reprogramming has both positive and negative transcriptomic effects, with some cells (for example, aNSCs–NPCs) exhibiting more of the positive effects.

We next specifically examined transcriptomic changes in neuroblasts, the main cell type for which the proportion increased upon partial reprogramming (Fig. 1g), and their immediate precursors, aNSCs–NPCs. Surprisingly, there were very few significant pathway changes in neuroblasts with partial reprogramming (Fig. 2h and Extended Data Fig. 3b). By contrast, aNSCs–NPCs exhibit reversal in several signatures, including RNA processing and cell adhesion (Fig. 2d,e,g,i,j), which could contribute to the observed boost in neuroblast proportion.

Neuroblast proportion increases in situ after partial reprogramming

While single-cell RNA-seq is a powerful tool to capture different cell types, it requires cell dissociation. As an orthogonal validation approach, we used immunostaining of the intact SVZ niche. We collected brain sections containing the SVZ niche from young (3–4 months) and old (20–26 months) iOSKM mice, with or without whole-body in vivo partial reprogramming (old + OSKM) (Fig. 3a–c and Extended Data Fig. 4a). Immunostaining with antibodies against DCX, a neuroblast marker in the SVZ niche, confirmed that old SVZ niches exhibit a strong decrease in the proportion of neuroblasts compared to young counterparts (Fig. 3d), as shown previously[56,58]. Importantly, partial reprogramming in old mice boosted the proportion of DCX$^+$ neuroblasts in the SVZ niche (Fig. 3d). This increase was also observed when we measured DCX$^+$ cell density (Fig. 3e and Extended Data Fig. 4b) or DCX intensity (Extended Data Fig. 4c). Additionally, the results were similar using PSA-NCAM, another marker of neuroblasts (Fig. 3f–i and Extended Data Fig. 4f–i). These findings provide orthogonal validation of the neuroblast proportion increase observed in our single-cell RNA-seq data.

By contrast, partial reprogramming did not affect the proportion (and density) of proliferating cells (Ki-67$^+$, which includes aNSCs and NPCs; Fig. 3b,c and Extended Data Fig. 4d,e) or the proportion (and density) of epidermal growth factor (EGF) receptor (EGFR)$^+$ cells (aNSCs and NPCs) in the old SVZ (Fig. 3f,g and Extended Data Fig. 4j,k). This observation is consistent with our single-cell RNA-seq data, which did not show an increased proportion of aNSCs–NPCs. Hence, the increase in neuroblasts upon reprogramming may be due to increased neuroblast differentiation (and possibly neuroblast survival) rather than enhanced proliferation.

Thus, partial reprogramming of the whole body restores in part the proportion of neuroblasts in the SVZ of old mice, which could improve neurogenesis.

A mouse model for partial reprogramming targeted to the SVZ

In the iOSKM mouse model, reprogramming factors are expressed not only in the SVZ neurogenic niche but also in other brain regions and organs, which could thereby influence neuroblast production indirectly. To test the direct effect of partial reprogramming in the SVZ niche itself, we established a mouse line to control OSKM expression in both a spatial and temporal manner. This mouse line has a *lox*-STOP-*lox* cassette before the sequences encoding rtTA (to allow Cre-dependent cell- and/or tissue-specific expression) and OSKM under the control of the tetracycline response element (to control timing of expression with doxycycline) (Fig. 4a). In these mice, expression of Cre recombinase (which can be spatially restricted) is required to trigger excision of the *lox*-STOP-*lox* cassette and subsequent expression of rtTA and an enhanced green fluorescent protein (EGFP) reporter (Fig. 4a). Doxycycline treatment then induces expression of the OSKM reprogramming factors. Thus, this mouse line, when coupled with Cre, allows for inducible expression of OSKM in specific tissues (hereafter Cre-dependent and inducible OSKM or c+iOSKM).

To target the SVZ neurogenic niche, we delivered Cre by stereotaxic viral injection into the lateral ventricle in close proximity to the SVZ of c+iOSKM mice. We used an adeno-associated virus (AAV) variant (SCH9) that is capable of infecting adult SVZ NSCs (and can also infect other cells)[79] to deliver Cre and an mCherry reporter (AAV-SCH9 *Ef1a-mCherry*-IRES-*Cre* or 'AAV-mCherry-Cre') (Fig. 4b). Using immunostaining on brain sections, we verified that stereotaxic AAV injection delivered Cre and mCherry to the neurogenic niche and that there was a good overlap between Cre and mCherry (Fig. 4b,c). Co-staining with cell type markers showed that AAV infection (assessed by mCherry) occurred in NSCs (GFAP$^+$ (also expressed in astrocytes) or SOX2$^+$) and also other cell types (for example, SOX2$^-$ cells and a small number of DCX$^+$ neuroblasts) in the neurogenic niche (Fig. 4d and Extended

Fig. 2 | Transcriptomic pathway changes in the old neurogenic niche after whole-body in vivo partial reprogramming. a, Differential gene expression by MAST for each cell type from single-cell RNA-seq, comparing old versus young untreated iOSKM mice. Each dot is the *Z* score for one gene. Positive *Z* score indicates upregulation with age. Color indicates false discovery rate (FDR) < 0.2. **b**, As in **a**, but comparing old + OSKM versus old samples. Each dot is the *Z* score for one gene. Positive *Z* score, upregulation with whole-body reprogramming; color, FDR < 0.2. **c**, Scatterplots showing normalized enrichment scores from GSEA with reprogramming (old + OSKM versus old) versus age (old versus young) for each cell type. The gene list from MAST was ranked by *Z* score, and enrichment analysis was performed with Gene Ontology (GO) pathways using fgsea (Methods). Each point is the normalized enrichment score for one pathway. For **c**–**h**, adjusted *P* values (P_{adj}) are Benjamini–Hochberg (BH)-adjusted two-sided fgsea *P* values. Pathways where $P_{adj} < 0.05$ for at least one comparison are shown. Filled circles, significant enrichment ($P_{adj} < 0.05$) after reprogramming. Pathways in the top left quadrant and bottom right quadrant change in opposing directions with aging and after reprogramming. **d**–**f**, Dot plots of GSEA comparing the effects of aging and reprogramming on expression of selected pathways related to RNA processing (**d**), cell adhesion (**e**) and inflammation (**f**) across cell types. Names of GO pathways are listed on the left. Size of dot reflects P_{adj} values. Color, normalized enrichment score (NES), where positive values (red) indicate increase with age ('aging') or increase with reprogramming ('OSKM'). **g**,**h**, Dot plot showing normalized enrichment score from GSEA in aNSCs–NPCs (**g**) or neuroblasts (**h**) after reprogramming (old + OSKM versus old). GO pathway names are listed on the left. Significantly enriched pathways ($P_{adj} < 0.05$) are shown. Color, P_{adj}. Size of dot reflects the number of genes in the set. **i**–**k**, Violin plots of gene expression in aNSCs–NPCs and neuroblasts from single-cell RNA-seq. Each dot is the summed expression of genes within the RNA processing (**i**), cell adhesion molecule binding (**j**) or inflammatory response (**k**) GO pathway for a single cell. Line, median; *P* values, two-sided Wilcoxon rank-sum test.

https://doi.org/10.1038/s43587-024-00594-3

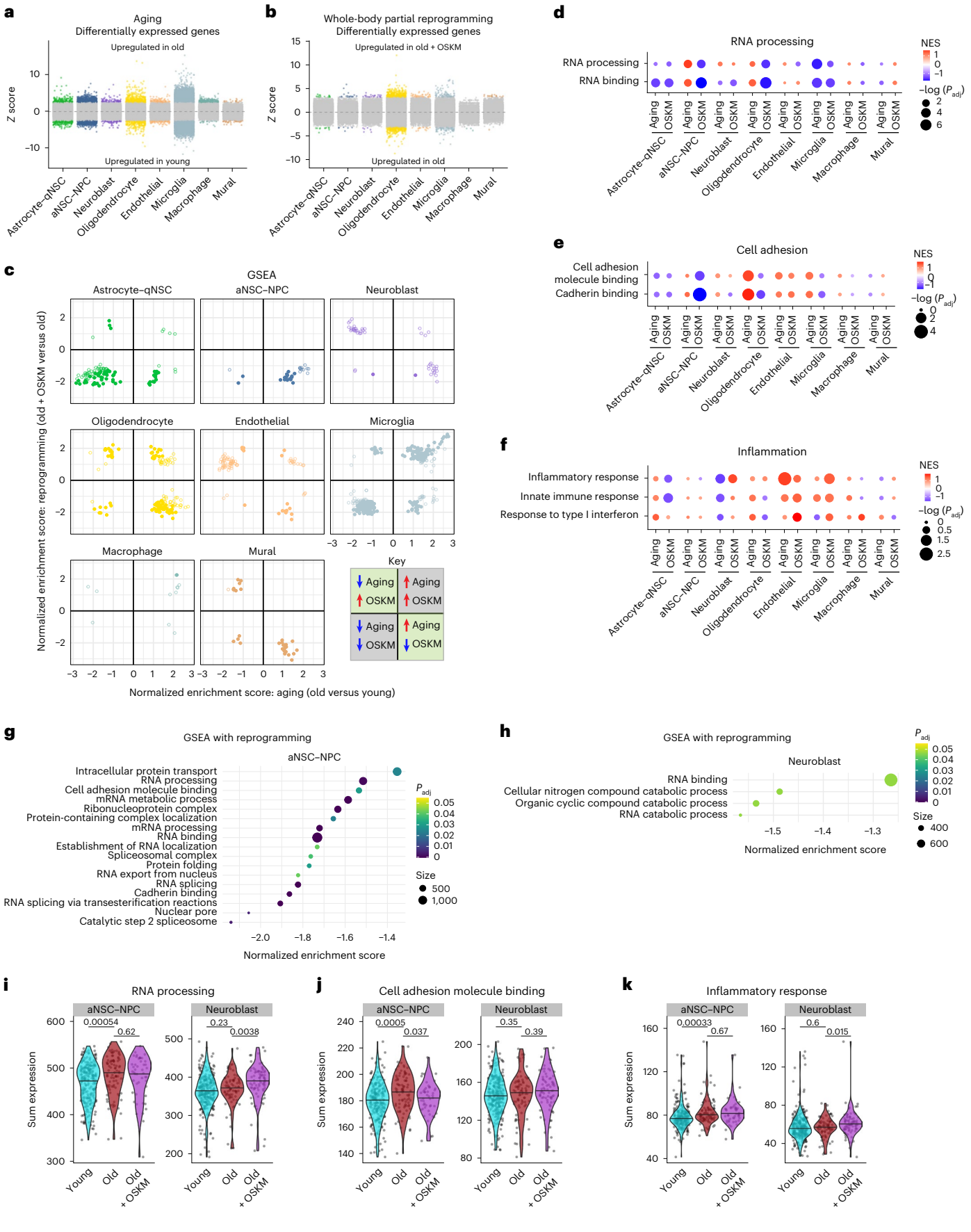

https://doi.org/10.1038/s43587-024-00594-3

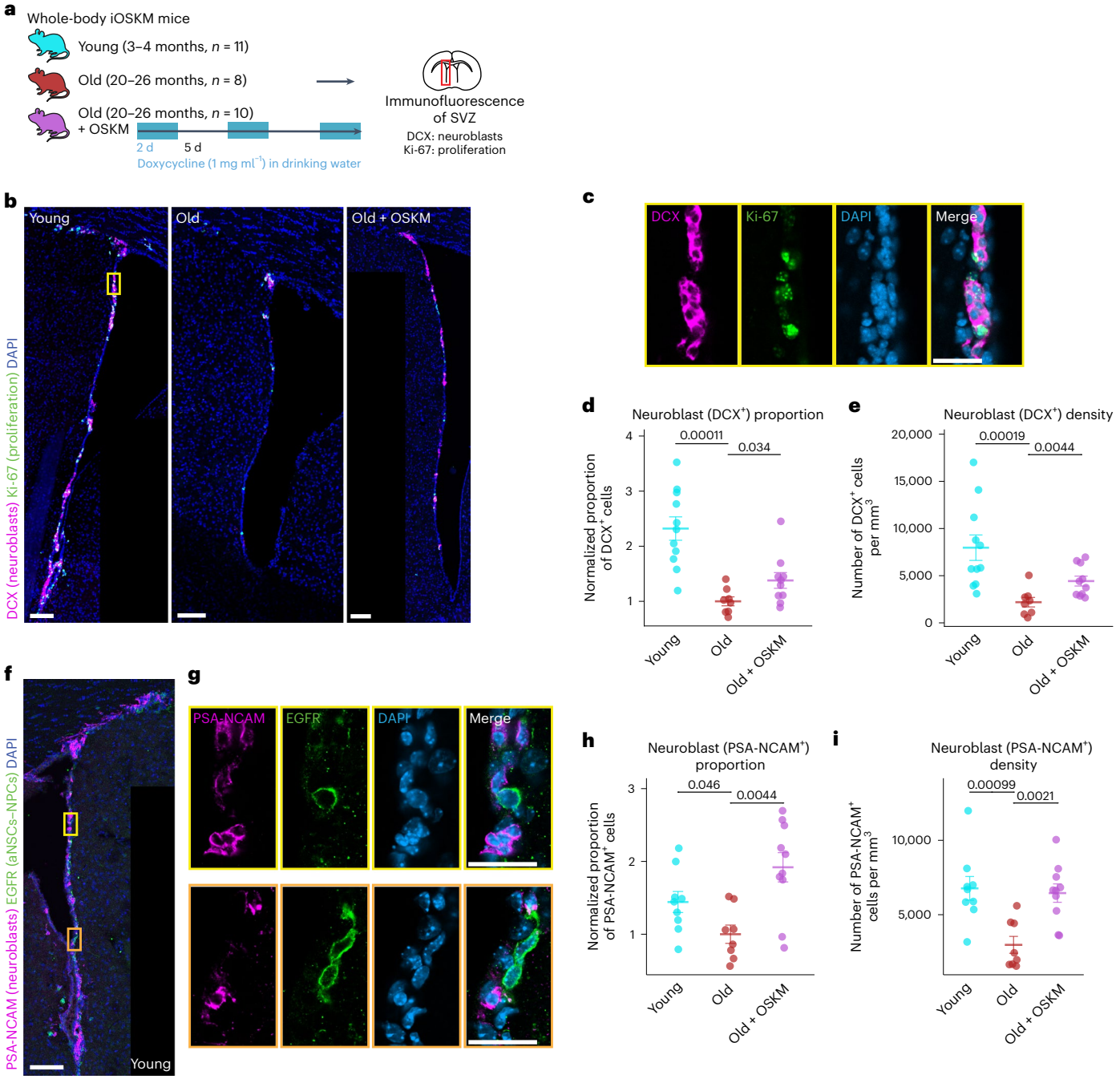

Fig. 3 | Validation of neuroblast proportion changes after whole-body partial reprogramming. a, Experimental design to assess SVZ neuroblast proportion in situ after whole-body partial reprogramming. The red rectangle shows the region in **b**. **b**, Representative images for immunofluorescence staining of the SVZ in coronal brain sections after in vivo partial reprogramming. Dorsal, up; lateral, left. Magenta, DCX (neuroblasts); green, Ki-67 (proliferative cells); blue, 4′,6-diamidino-2-phenylindole (DAPI) (nuclei). The yellow rectangle is the region shown in the insets in **c**. Scale bars, 100 µm. Note that only tiles containing the SVZ were imaged; black boxes are areas where no imaging data were acquired (Methods). **c**, Inset region from **b**. One optical section of a confocal image acquired using a ×20 objective. Scale bar, 25 µm. **d**,**e**, Quantification of immunofluorescence. Multiple optical sections a total of 8 µm thick were acquired for each SVZ, and both hemispheres in five coronal sections at 120-µm intervals were quantified per mouse (Methods). $n = 11$ young (3–4 months, five males and six females), $n = 8$ old (20–26 months, three males and five females) and $n = 10$ old + OSKM (20–26 months, four males and six females) mice over three independent experiments (for individual experiments, see Source data). Each dot represents one mouse. Mean ± s.e.m.; *P* values, two-sided Wilcoxon rank-sum test. **d**, Neuroblast proportion (DCX^+ over $DAPI^+$) in the SVZ per mouse, normalized to the mean of old control mice. **e**, Neuroblast density (number of DCX^+ cells per mm^3) in the SVZ per mouse. **f**, Representative immunofluorescence images. Dorsal, up; lateral, right. Magenta, PSA-NCAM (neuroblasts); green, EGFR (aNSCs–NPCs); blue, DAPI (nuclei). Yellow and orange rectangles are the regions shown in the insets in **g**. Scale bar, 100 µm. **g**, High magnification of inset regions from **f**. One optical section of a confocal image acquired using a ×63 objective. Scale bars, 25 µm. **h**,**i**, Quantification of immunofluorescence, as above. $n = 9$ young (3–4 months, four males and five females), $n = 8$ old (20–26 months, three males and five females) and $n = 10$ old + OSKM (20–26 months, four males and six females) mice over three independent experiments (Source data). Each dot represents one mouse. Mean ± s.e.m.; *P* values, two-sided Wilcoxon rank-sum test. **h**, Neuroblast proportion ($PSA\text{-}NCAM^+$ over $DAPI^+$) in the SVZ per mouse, normalized to the mean of old control mice. **i**, Neuroblast density (number of $PSA\text{-}NCAM^+$ cells per mm^3) in the SVZ per mouse.

https://doi.org/10.1038/s43587-024-00594-3

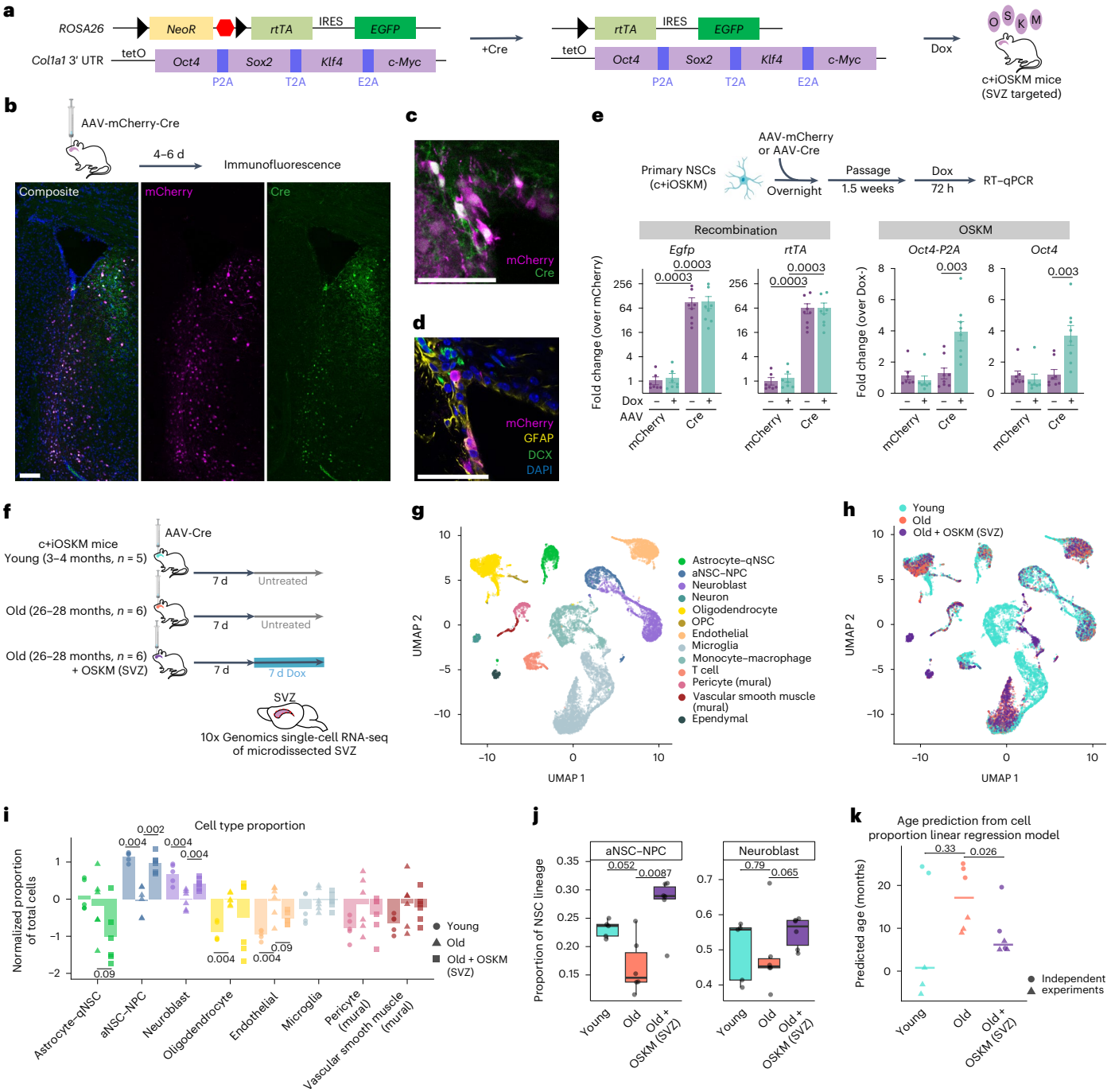

Fig. 4 | Effect of partial reprogramming targeted to the SVZ neurogenic niche by single-cell transcriptomics. a, Mouse model for conditional and inducible expression of OSKM (c+iOSKM). Stereotaxic injection of Cre targets expression of the reprogramming factors to the SVZ. **b**–**d**, Immunofluorescence of coronal sections after stereotaxic viral injection (AAV-mCherry-Cre, AAV serotype SCH9 carrying *Ef1a-mCherry*-IRES-*Cre*) into the lateral ventricle. **b**, Markers of viral infection (magenta, mCherry; green, Cre); blue, DAPI. Scale bar, 100 µm. **c**, Magenta, mCherry; green, Cre. Scale bar, 50 µm. **d**, Magenta, mCherry; yellow, GFAP (NSCs/astrocytes); green, DCX (neuroblasts); blue, DAPI. Scale bar, 50 µm. **e**, RT–qPCR in NSCs isolated from c+iOSKM mice and infected with AAV-mCherry (AAV-SCH9 *Ef1a-mCherry*) or AAV-Cre (AAV-SCH9 *Ef1a-Cre*) in culture. $n = 4$ young (3–4 months, three males and one female) and $n = 4$ old (20–23 months, three males and one female) cultures for AAV-Cre, $n = 3$ young (3–4 months, two males and one female) and $n = 4$ old (20–23 months, three males and one female) cultures for AAV-mCherry, over one independent experiment. Each dot represents one culture isolated from one mouse. Mean ± s.e.m.; *P* values, two-sided Wilcoxon rank-sum test. **f**, Experimental design for single-cell RNA-seq after SVZ-targeted reprogramming. Stereotaxic injection of AAV-Cre (AAV-SCH9 *Ef1a-Cre*) was performed in c+iOSKM mice. $n = 5$ young (two males and three females), $n = 6$ old (four males and two females) and $n = 6$ old + OSKM (SVZ) (three males and three females) samples over two independent experiments. **g**,**h**, Dimensionality reduction (UMAP) on single-cell transcriptomes of 16,291 high-quality cells, colored by cell type (**g**) or condition (**h**). Each dot represents one cell. **i**, Proportion of each cell type from single-cell RNA-seq as a fraction of total cells recovered per mouse, normalized as $\log_2$ (fold change) over the mean of old control mice. Each dot, triangle or square represents one mouse. Bar, mean; *P* values, two-sided Wilcoxon rank-sum test. **j**, Proportion of aNSCs–NPCs and neuroblasts from single-cell RNA-seq, as a fraction of total cells recovered from the NSC lineage. Each dot represents one mouse. Median (center line), upper and lower quartiles (box limits) and 1.5× interquartile range (whiskers); *P* values, two-sided Wilcoxon rank-sum test. **k**, Predicted age per mouse after SVZ-targeted reprogramming from a linear regression model of cell type proportions in the SVZ neurogenic niche. Each dot or triangle represents one mouse; shape denotes experiment. Line, median; *P* values, two-sided Wilcoxon rank-sum test.

Data Fig. 5a–c). There was no AAV infection (assessed by mCherry) detected in other areas of the brain, including the olfactory bulb and the cerebellum (Extended Data Fig. 5d). In NSCs isolated from c+iOSKM mice, we confirmed proper excision of the *lox*-STOP-*lox* cassette after in vitro infection with AAV expressing Cre ('AAV-Cre') (Extended Data Fig. 5e,f). Flow cytometry and immunofluorescence staining showed that both AAV infection and Cre recombination in NSCs were efficient and dose dependent and that AAV-Cre-infected NSCs expressed EGFP, indicative of Cre recombination at this locus (Extended Data Fig. 5g–k). Importantly, doxycycline treatment of cultured NSCs isolated from c+iOSKM mice after Cre recombination triggered *Oct4* expression from the inducible OSKM transgene as detected by RT–qPCR (Fig. 4e and Extended Data Fig. 5l,m) and western blotting (Extended Data Fig. 5n). Thus, this c+iOSKM mouse system combined with stereotaxic delivery of Cre allows for targeted reprogramming of cells, including NSCs, within the SVZ niche.

SVZ-targeted partial reprogramming boosts neuroblast proportion

To systematically probe the impact of reprogramming targeted to the SVZ niche, we aged cohorts of c+iOSKM mice for over 2 years and performed single-cell transcriptomics. We stereotaxically injected AAV-Cre into two independent cohorts of young (3–4 months) and old (26–28 months) c+iOSKM mice and then 7 d later treated them with doxycycline for another 7 d for targeted expression of OSKM in the SVZ (+OSKM (SVZ)) (Fig. 4f). Targeted OSKM expression allows for longer continuous doxycycline treatment (7 d compared to 2 d) without the mortality previously observed for long-term whole-body expression[17,19,28,30,80]. After this SVZ-targeted partial reprogramming, we performed single-cell RNA-seq of the SVZ niche (Fig. 4f). UMAP and Louvain clustering analysis indicated that all major cell types were recovered (Fig. 4g,h). We verified that AAV infection and Cre-mediated recombination indeed led to expression of *rtTA*-IRES-*EGFP*, which was detected mostly in the aNSC–NPC cluster but also in other cell types (Extended Data Fig. 6c).

We performed cell proportion analysis of single-cell RNA-seq data, comparing aging and reprogramming. There was a strong age-dependent decline in the proportion of aNSCs–NPCs and neuroblasts in c+iOSKM mice (Fig. 4i and Extended Data Fig. 6a), consistent with results from other mouse lines[69,73–76]. The proportions of other cell types in the niche were either not affected by age (astrocytes–qNSCs) or increased with age (oligodendrocytes, endothelial cells). Interestingly, SVZ-targeted partial reprogramming led to an increase in the proportion of both aNSCs–NPCs and neuroblasts in old mice, when normalized either by total cells (Fig. 4i) or by cells from the NSC lineage (Fig. 4j; $P = 0.065$ for neuroblasts). SVZ-targeted partial reprogramming also led to a trending ($P = 0.093$) decrease in the proportion of astrocytes–qNSCs and endothelial cells (Fig. 4i and Extended Data Fig. 6a). There was variability between mice in the proportions of mural cells and oligodendrocytes (Fig. 4i and Extended Data Fig. 6a). Finally, we noted a high prevalence of immune cells such as T cells in young mice in this model, perhaps due to an immune response to surgery and/or viral infection in young mice, which makes interpretation of changes by reprogramming in immune cells difficult (Fig. 4g,h and Extended Data Fig. 6a,b). Thus, SVZ-targeted partial reprogramming increases the proportion of neuroblasts (albeit less than whole-body partial reprogramming) and their precursors (aNSCs–NPCs) and may also impact other cells in the niche.

To quantify the impact of SVZ-targeted partial reprogramming on all cell type proportions in the old niche, we used our cell type proportion linear regression model for predicting age (Extended Data Fig. 2k). This cell proportion model indicated that SVZ-targeted partial reprogramming decreased median predicted age ('rejuvenation') by 10.9 months (Fig. 4k and Extended Data Fig. 6d). The rejuvenating effect of SVZ-targeted reprogramming was larger than that of the whole-body reprogramming and could be due to the more pronounced effect on multiple cell types (including aNSC–NPC and astrocyte–qNSC proportions) in the niche.

Thus, SVZ-targeted partial reprogramming in the neurogenic niche itself in old mice leads to an increased proportion of neuroblasts and their precursors, aNSCs–NPCs. This suggests that partial reprogramming targeted to the SVZ has a direct and intrinsic effect in this niche.

Signatures affected by SVZ-targeted partial reprogramming

We asked which molecular signatures are impacted upon in vivo partial reprogramming targeted to the SVZ. Analysis of differential gene expression in our single-cell RNA-seq dataset revealed significant transcriptomic changes across cell types with aging and after SVZ-targeted partial reprogramming (Fig. 5a,b). We compared the direction of molecular signature changes with age and reprogramming across cell types using scatterplots to identify pathways most 'rejuvenated' by this intervention (Fig. 5c and Extended Data Fig. 6c). These pathways include chromatin and transcription factors in neuroblasts, oligodendrocytes, endothelial cells and microglia (Fig. 5d,i, Extended Data Fig. 6g and Supplementary Tables 5 and 6), and pathways related to RNA processing and ribosomes in aNSCs–NPCs and endothelial cells (Fig. 5e, Extended Data Fig. 6f and Supplementary Tables 5 and 6). Changes in cell adhesion pathway expression with age were also reversed by reprogramming in aNSCs–NPCs and oligodendrocytes (Fig. 5f,j). Immune and inflammation pathways increased in many cell types upon SVZ-targeted partial reprogramming, although they appeared to decrease with age, probably related to immune cell infiltration in young mice (Extended Data Fig. 6b,d and Supplementary Tables 5 and 6). As with whole-body reprogramming, cell-specific transcriptomic aging clocks did not show strong improvements in predicted age across cell types (Extended Data Fig. 6g), potentially due to these opposing effects on inflammation.

Fig. 5 | Transcriptomic pathway changes after partial reprogramming targeted to the SVZ. a,**b**, Differential gene expression by MAST for each cell type, comparing old versus young (**a**) or old + OSKM (SVZ) versus old (**b**). Each dot represents the *Z* score for one gene. Color, FDR < 0.2. **c**, Scatterplots showing normalized enrichment scores from GSEA with SVZ-targeted reprogramming (old + OSKM (SVZ) versus old) versus age (old versus young) for each cell type. The gene list from MAST was ranked by *Z* score, and enrichment analysis was performed with GO pathways using fgsea (Methods). Each point is the normalized enrichment score for one pathway. For **c**–**h**, P_{adj}, BH-adjusted two-sided fgsea *P* value. Pathways where $P_{adj} < 0.05$ for at least one comparison are shown. Filled circles indicate $P_{adj} < 0.05$ after reprogramming. Pathways in the top left and bottom right quadrants change in opposing directions with aging and SVZ-targeted reprogramming. **d**–**f**, Dot plots of GSEA comparing the effects of aging and SVZ-targeted reprogramming on expression of pathways related to chromatin and/or transcription (**d**), RNA processing (**e**) or cell adhesion (**f**) across cell types. Names of GO pathways are listed on the left. Size of dot reflects P_{adj} values. Color indicates NES, where positive values (red) indicate increase with age ('aging') or increase with SVZ-targeted reprogramming ('OSKM'). **g**,**h**, Dot plot showing NES from GSEA in aNSCs–NPCs (**g**) or neuroblasts (**h**) after SVZ-targeted reprogramming (old + OSKM (SVZ) versus old control). GO pathway names are listed on the left. Color reflects P_{adj} values. Size of dot reflects the number of genes in the set. Pathways are filtered by $P_{adj} < 0.03$ for **g** and $P_{adj} < 0.01$ for **h**, and the top and bottom pathways ranked by NES are shown. cGMP, cyclic GMP; ncRNA, noncoding RNA; rRNA, ribosomal RNA. **i**–**k**, Violin plots of gene expression from single-cell RNA-seq. Each dot is the summed expression of genes within the chromatin binding (**i**), cell-cell adhesion (**j**) or neuron migration (**k**) GO pathway for a single cell. The line represents median. *P* values, two-sided Wilcoxon rank-sum test. **l**,**m**, Heatmaps showing NES from GSEA in aNSCs–NPCs (**l**) and neuroblasts (**m**), comparing whole-body (old + OSKM versus old) and SVZ-targeted (old + OSKM (SVZ) versus old) in vivo partial reprogramming. GO pathway names are listed on the right. Color reflects NES. Selected pathways are shown.

https://doi.org/10.1038/s43587-024-00594-3

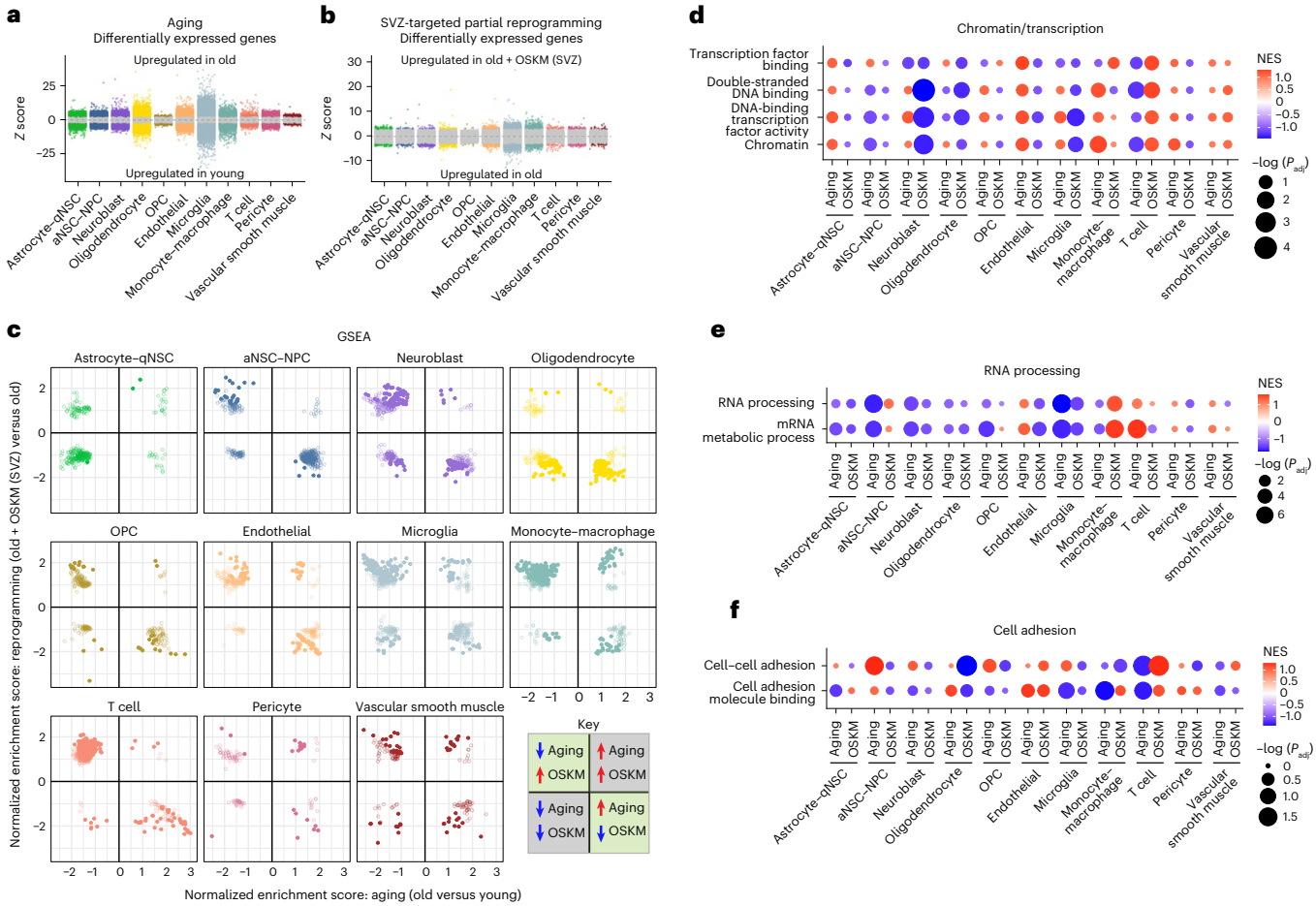

https://doi.org/10.1038/s43587-024-00594-3

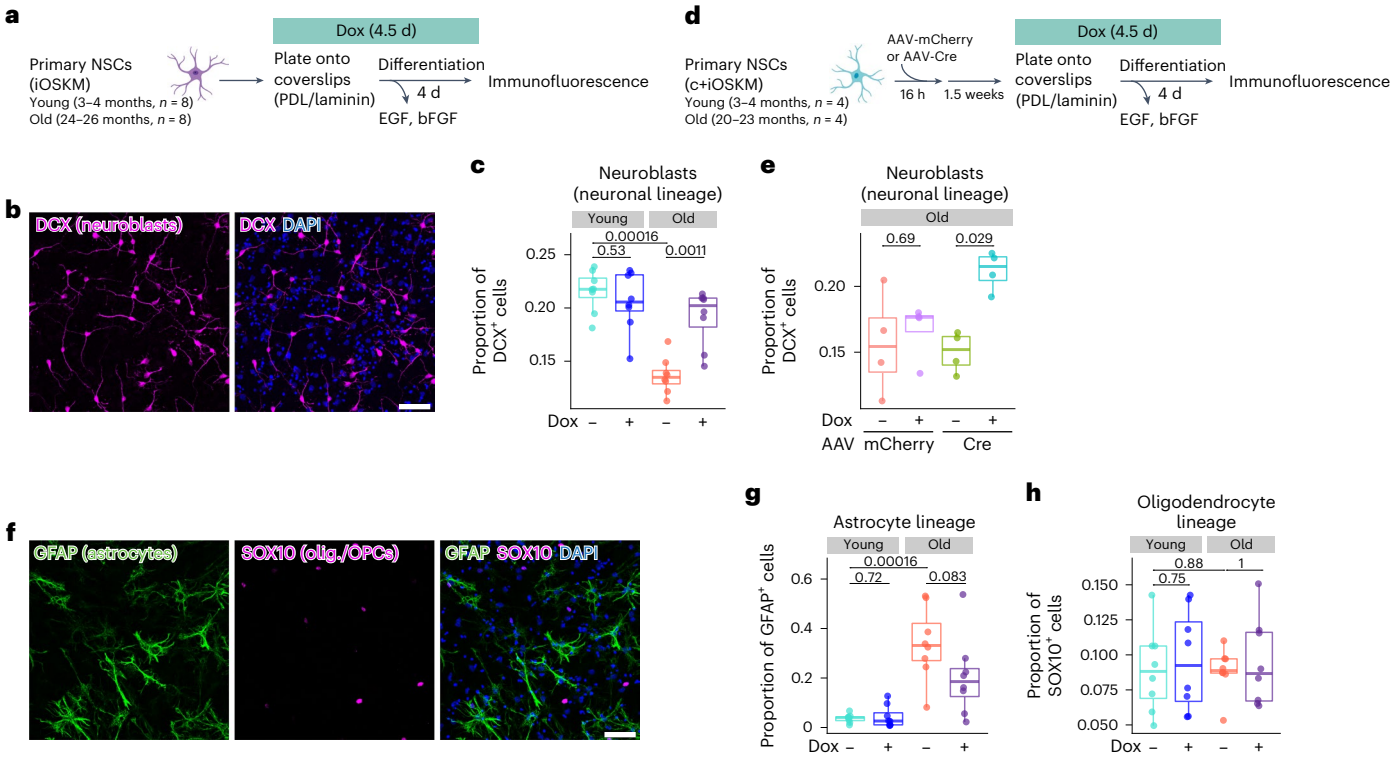

Fig. 6 | Impact of aging and reprogramming on primary NSC differentiation. **a**, Experimental schematic for differentiation of primary NSC cultures from iOSKM mice with partial reprogramming (**c**,**g**,**h**). PDL, poly-D-lysine. $n = 8$ young (3–4 months, four males and four females) and $n = 8$ old (24–26 months, four males and four females) samples over two independent experiments. Each culture was isolated from one mouse. **b**, Representative image of immunofluorescence staining for neuroblasts (DCX, magenta) after in vitro differentiation for 4 d. Scale bar, 50 µm. **c**, Quantification of immunofluorescence staining for neuroblasts (DCX^+ over $DAPI^+$). Each dot represents the neuroblast proportion for one culture isolated from one iOSKM mouse. Median (center line), upper and lower quartiles (box limits) and 1.5× interquartile range (whiskers); *P* values, two-sided Wilcoxon rank-sum test. **d**, Experimental schematic for differentiation of primary NSC cultures from c+iOSKM mice for 4 d with partial reprogramming. Primary NSCs were infected with AAV carrying genes for mCherry (control) or Cre and then passaged to allow for recovery before in vitro differentiation with or without reprogramming. $n = 4$ young (3–4 months, three males and one female) and $n = 4$ old (20–23 months, three males and one female) samples over one independent experiment. Each culture was isolated from one mouse. **e**, Quantification of immunofluorescence staining for neuroblasts (DCX^+ over $DAPI^+$). Each dot represents the neuroblast proportion for one culture; each culture was isolated from one c+iOSKM mouse. Median (center line), upper and lower quartiles (box limits) and 1.5× interquartile range (whiskers); *P* values, two-sided Wilcoxon rank-sum test. **f**, Representative images of immunofluorescence staining for astrocytes (GFAP, green) and oligodendrocytes (olig.) and OPCs (transcription factor SOX10, magenta) after in vitro differentiation for 4 d. Scale bar, 50 µm. **g**,**h**, Quantification of immunofluorescence staining for astrocytes ($GFAP^+$ over $DAPI^+$) (**g**) and oligodendrocytes and OPCs ($SOX10^+$ over $DAPI^+$) (**h**). Each dot represents the astrocyte proportion for one culture, and each culture was isolated from one iOSKM mouse. Median (center line), upper and lower quartiles (box limits) and 1.5× interquartile range (whiskers); *P* values, two-sided Wilcoxon rank-sum test.

We next focused on aNSCs–NPCs and neuroblasts (Fig. 5g,h and Extended Data Fig. 6f,g). SVZ-targeted partial reprogramming reversed the age-associated increase in single-cell expression of cell adhesion-related gene signatures in these cells (Fig. 5j) (similar to whole-body reprogramming for aNSCs–NPCs). In this case, neuroblasts also showed 'rejuvenation' changes in many molecular signatures upon partial SVZ-targeted reprogramming, including pathways related to neuron development and morphology, cell migration and projections (Fig. 5h,k, Extended Data Fig. 6g and Supplementary Tables 5 and 6).

Finally, we compared the molecular signatures regulated by whole-body and SVZ-targeted partial reprogramming. We examined pathways with enrichment scores that were either positive or negative in both paradigms (Extended Data Fig. 7a,b). Immune response and immune signaling pathways in neuroblasts and endothelial cells were upregulated by both whole-body and SVZ-targeted reprogramming strategies (Fig. 5m and Extended Data Fig. 7c,e). Cell morphogenesis, adhesion and migration pathways in aNSCs–NPCs and neuroblasts were downregulated by both reprogramming strategies (Fig. 5l,m and Extended Data Fig. 7d,e). Interestingly, chromatin-related pathways in neuroblasts were downregulated only in SVZ-targeted reprogramming (Fig. 5m and Extended Data Fig. 7e). Differences between whole-body and SVZ-targeted partial reprogramming paradigms could reflect the influence of cell non-autonomous and systemic factors or differences in the protocols (for example, length of doxycycline induction, use of viruses).

Thus, SVZ-targeted partial reprogramming reverses some aspects of age-dependent changes within the niche, including cell type proportion changes and transcriptional signatures in the NSC lineage, indicating that the effects of reprogramming are at least in part intrinsic to the neurogenic niche.

Partial reprogramming in old NSCs improves neuronal lineage differentiation

While stereotaxic injection in c+iOSKM mice allows spatial restriction of reprogramming to the SVZ niche, a key question remains: whether targeting a single cell type in the NSC lineage could recapitulate the effects of partial reprogramming. Cell type-specific in vivo reprogramming is limited by the tools needed to target only one cell state within the NSC lineage. We thus leveraged a primary NSC culture system[63,81] to assess how cell-autonomous reprogramming affects NSCs' ability to differentiate into neuroblasts, given the increase in neuroblast proportion uncovered by single-cell RNA-seq.

https://doi.org/10.1038/s43587-024-00594-3

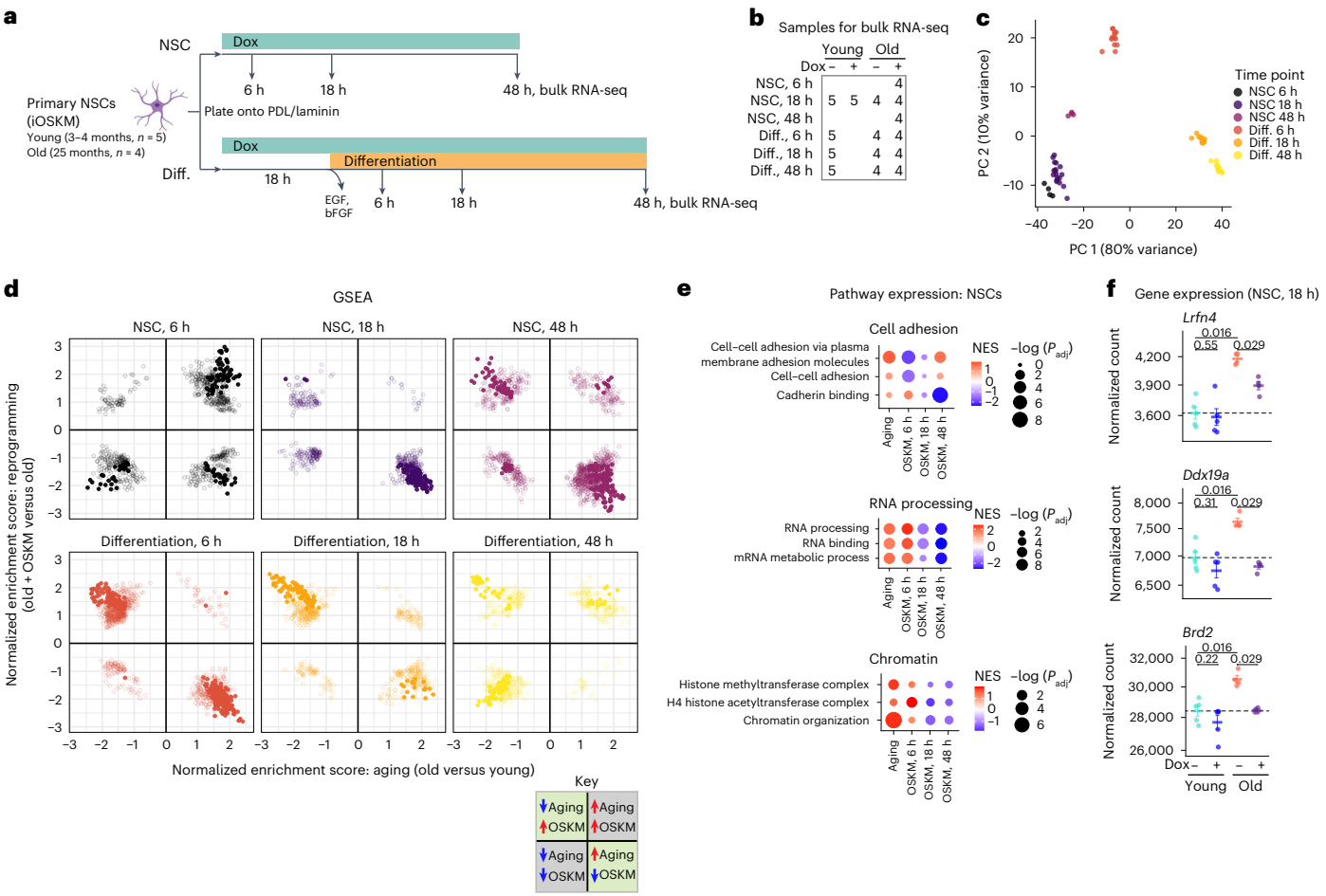

Fig. 7 | Gene expression in primary NSCs with aging, reprogramming and differentiation. a, Experimental schematic for bulk RNA-seq time course of partial reprogramming and differentiation in primary NSC cultures from iOSKM mice. $n = 5$ young (3–4 months, two males and three females) and $n = 4$ old (25 months, two males and two females) samples. Each culture was isolated from one mouse. In the top row ('NSC'), primary NSCs are treated with doxycycline for 6 h, 18 h or 48 h. In the bottom row ('Diff.', differentiation), primary NSCs are treated with doxycycline for 18 h before inducing differentiation and doxycycline treatment is continued for an additional 6 h, 18 h or 48 h. **b**, Table of the number of biological replicates collected for each condition at each time point for bulk RNA-seq. Each culture was isolated from one mouse. **c**, Dimensionality reduction (PCA) on all samples from bulk RNA-seq. Each dot represents one sample. PC, principal component. **d**, Scatterplots showing normalized enrichment scores from GSEA with partial reprogramming (old + OSKM versus old) versus aging (old versus young) for each time point. Each point represents the normalized enrichment score for one GO pathway. For **d**,**e**, P_{adj}, BH-adjusted two-sided fgsea P value. Pathways where $P_{adj} < 0.05$ for at least one comparison are shown. Filled circles indicate $P_{adj} < 0.05$ in both comparisons. Pathways in the top left quadrant and the bottom right quadrant change in opposing directions with aging and after reprogramming. **e**, Dot plots of GSEA comparing the effects of aging and 6 h, 18 h and 48 h of partial reprogramming in primary NSCs on expression of pathways related to cell adhesion, RNA processing and chromatin and histone marks. Names of GO pathways are listed on the left. Size of dot reflects P_{adj} values. Color, NES. **f**, Expression of selected genes in primary NSCs at the 18-h time point. Each dot represents the normalized count for one culture. Dashed line, mean expression level in young control samples; mean ± s.e.m.; P values, two-sided Wilcoxon rank-sum test.

Proliferative NSCs in primary cultures can be induced to differentiate into a mixed population of both neuronal and glial cells by withdrawal of EGF and basic fibroblast growth factor (bFGF) from the cell culture medium[81]. Using immunofluorescence staining, we first verified that this NSC differentiation protocol led to the appearance of neuroblasts (DCX$^+$), astrocytes (GFAP$^+$) and oligodendrocytes and OPCs (SOX10$^+$) after 4 d (Fig. 6a,b,f and Extended Data Fig. 8a) and neurons (TUJ1$^+$(TUBB3), NeuN$^+$), astrocytes (GFAP$^+$) and oligodendrocytes (O4$^+$) after 8 d (Extended Data Fig. 8b).

We then analyzed how age and reprogramming influenced primary NSC differentiation. We isolated primary NSCs from young (3–4 months) and old (24–26 months) iOSKM mice and verified that doxycycline also induced OSKM expression in these cells (Fig. 1c and Extended Data Fig. 1b–d). To induce reprogramming and differentiation of NSCs, we treated NSC primary cultures with doxycycline overnight before inducing differentiation and throughout the 4-d differentiation protocol (Fig. 6a). As expected, old NSC cultures produced fewer neuroblasts than their young counterparts after 4 d of differentiation (Fig. 6b,c and Extended Data Fig. 8k,l). In line with our in vivo data, partial reprogramming of old NSCs restored this age-associated deficit in neuroblast formation (Fig. 6c and Extended Data Fig. 8l). Partial reprogramming of young NSCs did not boost the neuroblast proportion (Fig. 6c and Extended Data Fig. 8l). Importantly, before differentiation, reprogramming in old NSCs did not impact cell type marker expression (nestin, EGFR) or proliferation status (Ki-67, 5-ethynyl-2′-deoxyuridine (EdU)) and did not induce a spurious increase in neuroblast differentiation (DCX) (Extended Data Fig. 8c–j). Partial reprogramming did not increase the proportion of proliferative cells (Ki-67$^+$) after differentiation (Extended Data Fig. 8m), suggesting that this intervention ameliorates differentiation (or neuroblast survival) rather than promoting NSC expansion in differentiation conditions. Partial reprogramming also increased the neuroblast proportion in NSC cultures from old c+iOSKM mice infected with Cre virus and treated with doxycycline throughout differentiation (Fig. 6d,e and Extended Data Fig. 8o,p).

https://doi.org/10.1038/s43587-024-00594-3

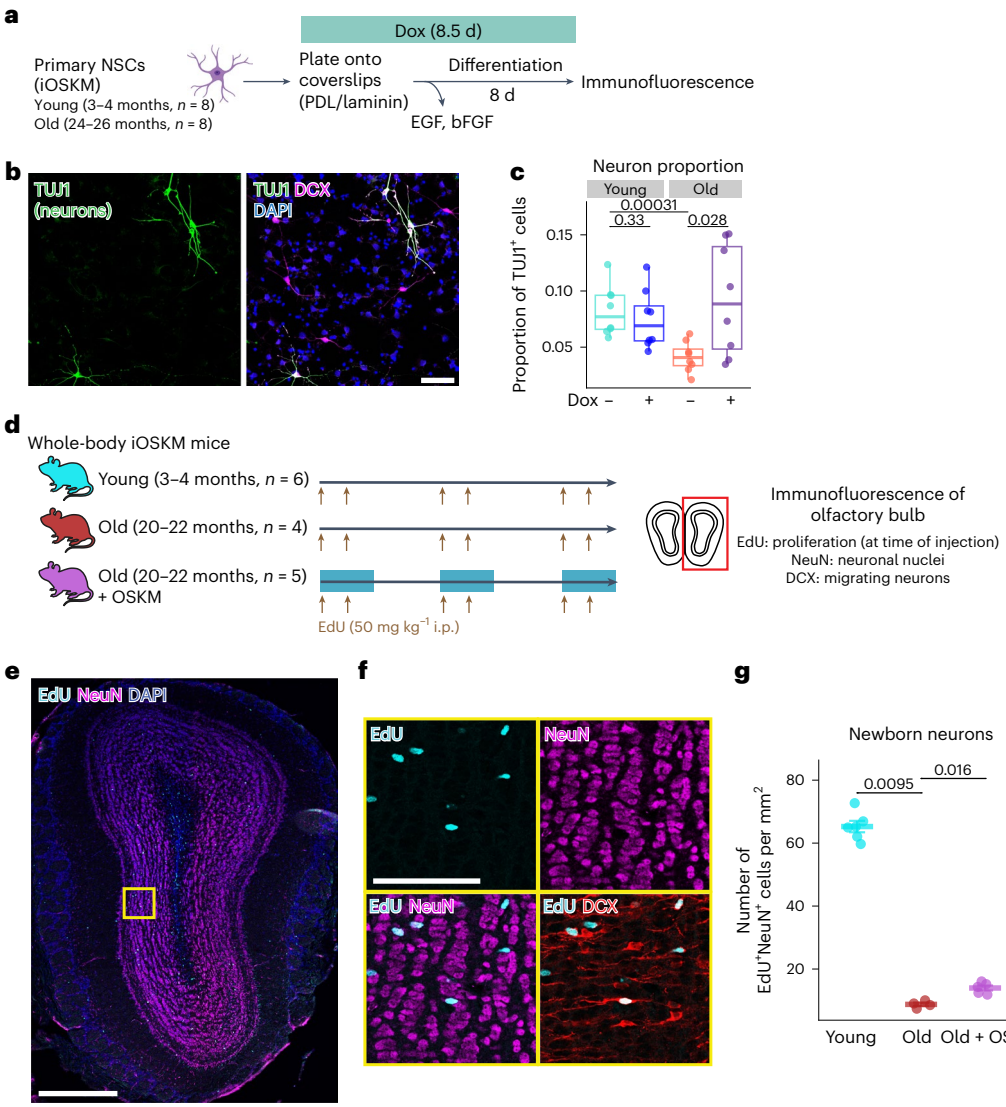

Fig. 8 | Newborn neuron production with partial reprogramming. **a**, Experimental schematic for differentiation of primary NSC cultures for 8 d with partial reprogramming. $n = 8$ young (3–4 months, four males and four females) and $n = 8$ old (24–26 months, four males and four females) samples over two independent experiments. Each culture was isolated from one mouse. **b**, Representative image of immunofluorescence staining for immature neurons after in vitro differentiation for 8 d. Green, TUJ1 (neurons); magenta, DCX (neuroblasts and immature neurons); DAPI (nuclei). Scale bar, 50 µm. **c**, Quantification of immunofluorescence staining for neurons (TUJ1$^+$ over DAPI$^+$). Each dot represents the neuron proportion for one culture, and each culture was isolated from one mouse. Box plot indicates median (center line), upper and lower quartiles (box limits) and 1.5× interquartile range (whiskers). *P* values, two-sided Wilcoxon rank-sum test. **d**, Experimental design to assess the number of newborn neurons in the olfactory bulb after in vivo whole-body partial reprogramming. Blue bars represent doxycycline treatment (2 d on, 5 d off). EdU was administered once daily as indicated with brown arrows. i.p., intraperitoneal. **e**, Representative image for immunofluorescence staining of the olfactory bulb. Dorsal is up. Cyan, EdU; magenta, NeuN (neuronal nuclei); blue, DAPI (nuclei). The yellow square is the region shown in insets in **f**. Scale bar, 500 µm. **f**, Higher-magnification images of the olfactory bulb. Cyan, EdU; magenta, NeuN (neuronal nuclei); red, DCX (migrating neurons). Scale bar, 100 µm. **g**, Number of newborn neurons (EdU$^+$NeuN$^+$ cells per mm^2) in the olfactory bulb per mouse. Both hemispheres in five coronal sections at 120-µm intervals were quantified per mouse (Methods). $n = 6$ young (3–4 months, three males and three females), $n = 4$ old (20–22 months, two males and two females) and $n = 5$ old + OSKM (20–22 months, three males and two females) samples. Each dot represents one mouse. Data are mean ± s.e.m.; *P* values, two-sided Wilcoxon rank-sum test.

Thus, partial reprogramming in culture boosts the ability of old NSCs to generate neuroblasts, suggesting a direct, cell-autonomous effect of reprogramming on old NSCs.

Aging is also accompanied by a 'glial skew' of NSCs during differentiation, with a decrease in the proportion of new neurons and an increase in the proportion of glial cells (mostly astrocytes)[82]. Indeed, after 4 d of differentiation, cultures differentiated from old NSCs exhibited a large increase in the proportion of astrocytes (GFAP$^+$) compared to young counterparts (Fig. 6f,g and Extended Data Fig. 8n). Partial reprogramming blunted this age-dependent increase in astrocytes (Fig. 6g) (and did not affect oligodendrocytes, Fig. 6h). Hence, partial reprogramming reverses the glial skew of old NSCs, favoring the production of neuroblasts, a feature of youthful NSCs.

To identify transcriptional changes that could mediate the effects of reprogramming on old NSCs and their differentiation, we performed bulk RNA-seq on primary NSCs throughout a time course of differentiation and partial reprogramming (Fig. 7a,b and Extended Data Fig. 9c). As expected, principal-component analysis (PCA) separated samples by differentiation time points (Fig. 7c), with a decline in cell cycle genes (for example, *Pclaf*, *Mki67*) and increases in neuronal (for example, *Slc1a1*, *Draxin*) and glial (for example, *Gfap*, *Mbp*) genes across differentiation (Extended Data Fig. 9a,b). Global GSEA in NSCs

revealed a host of changes with age, some of which were reversed by reprogramming (Fig. 7d and Extended Data Fig. 9d,f). Similar to in vivo findings, primary NSCs exhibited increased expression of cell adhesion, RNA processing and chromatin-related gene pathways with age, and partial reprogramming in old NSCs reversed expression of these signatures (Fig. 7e and Extended Data Fig. 9d,j). Interestingly, we identified a cluster of genes for which expression increased with age and that were restored to a youthful expression level by partial reprogramming (Fig. 7f and Extended Data Fig. 9i). These include *Lrfn4*, involved in neurite outgrowth and cell motility, *Ddx19a*, encoding a putative RNA helicase and the transcriptional regulator encoded by *Brd2*. Such genes and pathways may represent interesting candidates that mediate the age-specific effect of partial reprogramming on old NSC function.

Thus, partial reprogramming of NSCs during differentiation in culture is sufficient to boost the resulting proportion of neuroblasts, indicating a direct effect of partial reprogramming on old NSCs. While in vitro assays cannot fully recapitulate in vivo conditions, these results also suggest that the boost in neuroblast proportion after in vivo partial reprogramming may be due at least in part to improved differentiation of NSCs.

Newborn neuron production improves with partial reprogramming

Can partial reprogramming boost not only the production of neuroblasts but also the generation of differentiated neurons? We first tested the impact of partial reprogramming in NSCs on mature neuron formation in culture. Using the in vitro differentiation protocol for 8 d (Fig. 8a,b), we found that old primary NSCs led to fewer neurons ($TUJ1^+$) than young primary NSCs (Fig. 8c). Partial reprogramming in old NSCs, starting before and continuing through differentiation, increased the production of more mature neurons (Fig. 8c and Extended Data Fig. 8q).

In vivo, neuroblasts from the SVZ migrate to the olfactory bulb where they terminally differentiate into neurons[42,83]. To test the effect of partial reprogramming on the formation of newborn neurons in the olfactory bulb in vivo, we injected old mice with EdU to label all proliferating cells (including aNSCs–NPCs and proliferating neuroblasts) during each cycle of doxycycline treatment (Fig. 8d–f). As neurons are postmitotic, EdU-positive neurons (labeled by the neuronal nuclear marker NeuN) are newly born from these labeled aNSCs and neuroblasts. Immunostaining showed that the number of newborn neurons (EdU^+NeuN^+) in the olfactory bulb declines dramatically with age, as has been previously observed (Fig. 8g). Interestingly, partial reprogramming in old mice increased the number of newborn neurons in the olfactory bulb (neurogenesis) (Fig. 8g).

Thus, partial reprogramming in old NSCs and old mice increases the number of newborn neurons, an important aspect of youthfulness.

Discussion

Using single-cell transcriptomics and immunostaining validation, we find that whole-body partial reprogramming in old mice partly reverses the age-associated defect in neuroblast proportion in the SVZ neurogenic niche. This 'rejuvenation' effect can be recapitulated by targeting the SVZ itself for partial reprogramming, indicating a niche-intrinsic phenomenon. Furthermore, partial reprogramming in old NSCs in culture cell autonomously improves their differentiation into neuronal precursors. Our study uncovers the impact of partial reprogramming in old brains by systematically probing its effect on multiple different cell types. Previous studies in the nervous system had found rejuvenation of visual acuity and bulk DNA methylation and transcriptome upon OSK expression in the optic nerve of 11–12-month-old mice[30], improvement in remyelination after injury with c-MYC (M) expression in oligodendrocyte progenitor cells of 18-month-old mice[20], improvement in epigenetic marks and memory in the hippocampus of 6–10-month-old mice upon OSKM expression[26], improved neurodegeneration phenotypes in an Alzheimer's mouse model with OSKM expression in neurons[33] and improved recovery after ischemic injury in 2–4-month-old mice with OSKM expression[34]. Our study uses older animals (18–28 months old) and a combination of systematic single-cell RNA-seq analysis and immunocytochemistry validation, which reveal that NSCs and neuroblasts are key cell types influenced by partial reprogramming in a neurogenic niche of old brains.

We find that partial reprogramming of the SVZ itself in vivo recapitulates some of the effects of whole-body partial reprogramming, suggesting that at least some of the beneficial effects are intrinsic to the SVZ niche. In muscle stem cells (satellite cells), the intrinsic effects of partial reprogramming have been assessed with various results[19,22,28,29]: a genetic strategy to target reprogramming to the muscle stem cells in vivo does not seem to improve their function (in young mice)[28], while ex vivo reprogramming in old muscle stem cells and reimplantation in old muscles does seem sufficient to improve repair after injury[29]. The levels of reprogramming factor expression[22], the exact combination of factors used, the age of onset and duration of treatment could all be important factors to explain differences.

We do not observe any appearance of a 'new' cell type (for example, embryonic-like stem cell) by single-cell RNA-seq after in vivo partial reprogramming. However, the possibility that transdifferentiation of another cell type might contribute to the increase in neuroblast proportion cannot be excluded in vivo. Using a culture system, we find that partial reprogramming of NSCs is sufficient to rescue the age-associated decline in neuroblast proportion, suggesting that at least some effects of in vivo partial reprogramming are due to improvement of NSCs. An alternative possibility could be that partial reprogramming factors directly promote neuronal differentiation[84] independent of a 'rejuvenation' effect. Our observation that the effect of partial reprogramming is specific to old NSCs in vitro suggests that this is unlikely. Nevertheless, it will be important to distinguish the impact of partial reprogramming on rejuvenation versus cell fate.

Interestingly, reprogramming factors, which normally induce stemness, promote more fate-committed progenitor cells and boost the production of new neurons in the context of old mice. This is consistent with the idea that reprogramming factors could rescue aspects of age-associated defects in the neural lineage, thereby increasing neurogenesis. Partial reprogramming in 6–10-month-old mice did not show increased neurogenesis in the hippocampus[26], perhaps because mice were too young. However, the authors observed increased neuroblast and neuron migration[26], reminiscent of the changes in cell adhesion signatures we observe here, and this could be a possible step in the neurogenesis process affected by reprogramming. Partial reprogramming could thus improve aging hallmarks in old NSCs, favoring their commitment and differentiation toward the neuronal lineage.

Many avenues for future study remain. It remains unknown how long the effects of reprogramming last and whether pulses of expression are more beneficial than continuous expression. It would be interesting to examine how long transcriptomic changes persist following doxycycline withdrawal, in addition to determining whether cell type proportion changes are stable or dependent on recent OSKM expression. The long-term effect on survival and the impact of seemingly negative effects like increased inflammation will be key to determine. Importantly, the c+iOSKM mouse, combined with strains allowing cell type-specific expression of Cre, could enable cell type-specific partial reprogramming in vivo as well as genetic lineage tracing, which should help elucidate cell-intrinsic effects, cell fate and population heterogeneity. Finally, it will be important to test whether partial reprogramming in the old SVZ leads to beneficial effects on behavior and whether pathways affected by reprogramming could be directly targeted to improve neurogenesis.

Systemic rejuvenation interventions (exercise, young blood, dietary restriction) have different effects on cell proportions within the SVZ neurogenic niche. Exercise also boosts neuroblast proportion in the aged SVZ, whereas heterochronic parabiosis does not[77,85].

There might be some overlapping mechanisms between reprogramming and exercise, and each intervention could improve specific aspects of aging (for example, neuroblast formation) while also having detrimental or orthogonal effects on the aging process (for example, inflammation). Comparing the effect of interventions on different cell types could help elucidate common or synergistic mechanisms to counter aging.

Methods

Animal housing and protocols

All animal procedures were performed according to protocols approved by the IACUC and AAPLAC of Stanford University (protocol 8661). Mice were housed with 12-h light–dark cycles, ad libitum access to food and water in the cage, a temperature of ~21 °C and ~50% humidity. Mice were maintained under the care of the Stanford Veterinary Service Center and housed at the Stanford Comparative Medicine vivarium and the ChEM-H/Neuro vivarium.

Mouse strains, sex and age

Whole-body iOSKM mice (*ROSA26*(*rtTA-M2*);*Col1a1*(*tetO-OSKM*)) were generated by the Jaenisch laboratory[68]. Mice were obtained from Jackson Laboratory (JAX 011004) and maintained in an in-house breeding colony to produce aging cohorts.

c+iOSKM mice were generated in-house by crossing whole-body OSKM mice (*ROSA26*(*rtTA-M2*);*Col1a1*(*tetO-OSKM*)) (JAX 011004) with a strain allowing Cre-dependent expression of rtTA (*ROSA26*(*lox*-STOP-*lox*-*rtTA*-IRES-*EGFP*)) (Fig. 3a) (JAX 005670, generated by the Nagy laboratory[86]). F_1 heterozygotes were intercrossed to generate double homozygous mutants. Double homozygous mice (*ROSA26*(*lox*-STOP-*lox*-*rtTA*-IRES-*EGFP*);*Col1a1*(*tetO-OSKM*)) were intercrossed to establish the colony. Mice were maintained in an in-house breeding colony to produce aging cohorts.

We maintained in-house aging colonies of iOSKM mice and c+iOSKM mice ranging in ages up to 28 months of age. Both male and female mice were used for this study. Old animals were assigned to control or treatment conditions such that sexes and mean body weights at the beginning of the experiment were balanced between conditions. Mice were considered young adults at 3 months of age and old after 18 months of age. Specific ages are indicated in the respective figures. Sexes of mice used in single-cell RNA-seq experiments can be found in the mouse metadata table (Supplementary Table 1). Mice that died or were euthanized before the experiment endpoint (Extended Data Figs. 1g and 6h) were excluded from the study.

In vivo doxycycline administration

Doxycycline (Fisher, ICN19895505) was dissolved in drinking water at a concentration of 1 mg ml^{-1} and provided ad libitum in amber water bottles to protect the solution from light. Mouse weight and condition were monitored three times per week, and no signs of dehydration were observed. Old mice were assigned to control or doxycycline treatment conditions such that sexes and mean body weights at the beginning of the experiment were balanced between conditions.

SVZ dissection for single-cell RNA sequencing

Live cells were isolated from the SVZ for single-cell RNA-seq as previously published[69,77]. The experimenter performing dissections was blinded to the sample condition; mice were taken in an alternating fashion to minimize impacts of sample processing order. Briefly, mice were terminally anesthetized with Avertin (0.5 mg g^{-1} mouse, Sigma-Aldrich, T48402-25G) in PBS (Corning, 21-040-CV) and then perfused transcardially with 15 ml PBS with heparin (50 U ml^{-1}, Sigma-Aldrich, H3149-50KU) to remove circulating blood cells. Brains were removed into PIPES buffer on ice and dissected in ice-cold PIPES buffer. The lateral walls of the SVZs from both hemispheres were carefully dissected under a dissecting microscope using forceps, a scalpel with a no. 22 blade and a 22.5° stab knife. The dissected tissue includes NSCs (which are within a few cell layers of the ventricle) as well as part of the striatum (evidenced by the oligodendrocyte population recovered). SVZs were minced and then digested in papain solution (14 U ml^{-1}, Worthington, LS003119) for 10 min at 37 °C. After centrifugation at 300*g* for 5 min at 4 °C, liquid was removed, and ovomucoid solution (0.7 mg ml^{-1} ovomucoid (Sigma-Aldrich, T9253-1G), 0.5 mg ml^{-1} DNase I (Sigma-Aldrich, DN25-100MG) in DMEM/F12 (Gibco, 11330057)) was added. Tissue was triturated with a P1000 pipette to obtain a single-cell suspension. Cells were then layered onto 22% (vol/vol) Percoll (Sigma-Aldrich, GE17-0891-01) in PBS and centrifuged at 700*g* for 10 min at 4 °C without brakes to remove myelin debris. The supernatant, containing myelin and debris, was removed. The cell pellet was then resuspended in FACS buffer (1% BSA (Sigma, A7979) with 0.1% glucose (Sigma, G7021) in PBS) to wash and filtered through a 40-µm strainer. Cells were centrifuged at 300*g* for 5 min at 4 °C and then resuspended in 70 µl FACS buffer with DAPI (1 µg ml^{-1}, Thermo, 62248). Live cells were isolated by flow cytometry (Extended Data Fig. 10a) on a BD Aria II sorter (BD FACSDiva software version 8.0.1) using a 100-µm nozzle at 20 psi and collected in 750 µl FACS buffer in a protein low-bind microcentrifuge tube (Eppendorf, 0030108442).

Sample multiplexing with lipid-modified oligonucleotides

Cells were labeled with lipid-modified oligonucleotides (LMOs) at 4 °C using a protocol[77] adapted from MULTI-seq[87]. Lipid anchor and co-anchor reagents were generously provided by the Gartner laboratory at the University of California, San Francisco. Custom oligonucleotides were purchased from Integrated DNA Technologies. The entirety of each sample was labeled and used. Cells from two to six mice were combined after labeling and loaded onto each lane of a 10x Genomics chip. Metadata for all mice used in single-cell RNA-seq experiments, including sequences of multiplexing oligonucleotides and distribution of mice in each 10x lane, can be found in Supplementary Table 1.

Single-cell library preparation and sequencing

The 10x Genomics Chromium Next GEM Single Cell 3′ kits were used to perform single-cell RNA-seq chip loading and library preparation according to the manufacturer's instructions. Kit version 3 was used for one experiment (Extended Data Fig. 2b–f); version 3.1 was used for all other experiments. Gene expression libraries were prepared according to the manufacturer's instructions. LMO libraries were prepared according to the MULTI-seq protocol[87]. All gene expression libraries and LMO libraries from an individual experiment were pooled and sequenced on the Illumina HiSeq (whole-body OSKM experiments 1 and 2) or the NextSeq (SVZ-specific OSKM experiment) with paired-end 150-bp reads.

Single-cell RNA-seq data processing and cell type identification

Cell Ranger (version 3.0.2 for whole-body reprogramming experiments, version 6.0.2 for SVZ-targeted reprogramming experiments) default settings were used to distinguish cells from background. Reads were mapped to a custom genome (mm10), with the following transgene sequences added as additional chromosomes: for whole-body iOSKM mice, *rtTA-M2*; for c+iOSKM, *NeoR* and *rtTA*-IRES-*EGFP*. To determine and confirm these sequences, we performed PCR amplification from genomic DNA using multiple primer sets tiling the locus, and PCR products were Sanger sequenced (see 'Genomic DNA extraction and PCR'); primer sequences are in Supplementary Table 3. *P2A*, *E2A* and *T2A* sequences were also added to the genome as separate chromosomes, but reads did not map to them, likely due to their very short length of 54–60 nucleotides. Seurat[88] (version 3.1.2) was used for quality control. Cells were filtered out if they contained more than 10% mitochondrial reads or less than 500 genes.

For LMO libraries, CITE-seq count (version 1.4.5) was used to map reads to sample barcodes. Samples were demultiplexed using

HTODemux in Seurat or the MULTI-seq strategy[87]. Cells showing strong expression of multiple sample barcodes were considered doublets and excluded from subsequent analysis, as were cells that could not be assigned to any sample barcode.

Seurat was used for SCT normalization, dimensionality reduction, clustering and marker gene identification. Cell types were manually annotated as previously described[77]. Major cell clusters were identified in Seurat using 'FindClusters()', and marker genes were identified using 'FindAllMarkers()'. Expression of marker genes was used to label cell types based on literature and PanglaoDB[89]. This analysis identified 13 clusters of cells (depending on the dataset): astrocytes and qNSCs, aNSCs and NPCs, neuroblasts, neurons, oligodendrocytes, oligodendrocyte progenitor cells, endothelial cells, microglia, monocytes and macrophages, T cells, mural cells (pericytes and vascular smooth muscle cells) and ependymal cells. Very small cell clusters (fewer than 20 cells, labeled as clusters 27–30) from the whole-body reprogramming experiment were not annotated; they likely contain T cells and potentially doublets. The top five differentially expressed marker genes for each cluster are shown in Extended Data Fig. 2j. Full lists of marker genes are in Supplementary Table 2.

Single-cell RNA-seq cell type proportion analysis

Cell type proportions for aNSCs–NPCs and neuroblasts were calculated as a fraction of the total cells within the NSC lineage (astrocytes–qNSCs, aNSCs–NPCs, neuroblasts) because small differences in SVZ microdissection could have an impact on the number of other cell types recovered (that is, oligodendrocytes). Cell type proportions as a fraction of total cells are also shown for completeness. It is possible that steps in the protocol, including tissue dissociation, live cell sorting and loading into the microfluidic chip might influence the recovery of specific cell types relative to others. The following cell types were excluded from cell type proportion analyses: (1) ependymal cells. Our single-cell RNA-seq datasets captured a small number of ependymal cells, as shown previously[69,77], even though ependymal cells are known to be more numerous in the SVZ niche. This could be because ependymal cells fall outside of the scatter gate used in flow cytometry or these cells were too big to be uploaded in droplets or were sheared in the 10x microfluidic device. Thus, ependymal cells were excluded from cell type proportion analyses. (2) Neurons. A small number of neurons were captured in the SVZ-targeted reprogramming experiments, all of which originated from old + OSKM (SVZ) mice but only in one independent experiment. In the other independent experiment (and in all other mice in both experiments), zero neurons were captured. We thus excluded neurons from cell type proportion analyses.

Single-cell RNA-seq differential expression and pathway enrichment analysis

MAST (implemented in 'FindMarkers()' in Seurat) was used for differential gene expression analysis for each cell type. Cell types with very few cells per condition (OPCs and small clusters 27–30 in the iOSKM experiment) were excluded, as were ependymal cells and neurons as above. For iOSKM experiments, these analyses were performed with cohort 2, which included young mice to compare the effects of aging and reprogramming. To identify pathways that change with aging and reprogramming, the gene list from MAST was ranked by decreasing Z score, and then pathway enrichment was performed using the R implementation of the Broad Institute's preranked GSEA algorithm (fgsea) and the pathways provided in MSigDB version 7.1. To compare trends in whole-body and SVZ-targeted partial reprogramming paradigms, pathways were clustered by k-means clustering as implemented in pheatmap.

Machine learning models to predict age from cell proportion in the SVZ niche

A cell proportion linear regression model was trained on previously acquired single-cell RNA-seq data from the SVZ neurogenic niche of 28 male C57BL/6JN mice spanning 3–29 months of age[77], using the fraction of each cell type (oligodendrocyte, endothelial, microglia, macrophage, astrocyte–qNSC, aNSC–NPC, neuroblast, mural (vascular smooth muscle cells and pericytes), ependymal, OPC) and age of the mouse of origin. For validation, models were built on 27 of the 28 mice and then tested on the remaining mouse ('leave-one-mouse-out' validation). To quantify model performance, the data were presented as a correlation between the actual chronological age of the mouse and the predicted age for that mouse (Extended Data Fig. 2k). Each mouse is represented as a dot. We fitted a linear model (blue line) through the points as well as the 95% confidence interval (light gray) using 'geom_smooth' (ggplot2). Pearson's correlation (R) is indicated on the graph. Model coefficients are as follows: microglia, 176.32; oligodendrocyte, 106.15; neuroblast, 92.69; astrocyte–qNSC, 132.32; aNSC–NPC, 49.74; endothelial, 12.34; mural, 174.44; OPC, 65.86; macrophage, 33.24 (intercept, −94.98).

Protein extraction from tissues and cells for western blotting

Mice were euthanized using CO_2 inhalation, and then tissues were immediately extracted and flash frozen in liquid nitrogen. Brains were immersed in ice-cold PBS while regions were dissected, and then dissected regions were flash frozen. For protein extraction, ice-cold RIPA buffer (50 mM Tris-HCl, pH 7.4, 150 mM NaCl, 1% NP-40, 0.5% sodium deoxycholate, 0.1% SDS) (Alfa Aesar, J62524) with protease inhibitors (Roche, 11836153001) was added to pieces of frozen tissue. Tissues were homogenized on ice with a handheld electric homogenizer (Fisher, 03-421-215) and a microtube pestle attachment (Fisher, 12-141-364). Lysates were centrifuged at 16,000g for 20 min at 4 °C to remove tissue debris and chromatin, and the pellet was discarded. Protein concentration was quantified using the BCA assay (Thermo Fisher Scientific, 23225).

For protein extraction from primary NSCs, to minimize the impact of batch effects and confluency, all NSCs for each experiment were plated on the same day and collected on the same day. The same number of cells was plated per well within each experiment (dose–response, Extended Data Fig. 1b, 300,000 cells per well in a 12-well plate; time course, Extended Data Fig. 1c, 500,000 cells per well in a 12-well plate). Cells were treated with doxycycline at the dose or time indicated in the respective figures, and then cells were rinsed with PBS and then lysed directly in the wells using 200 µl RIPA buffer with protease inhibitors and a cell scraper. Lysates were incubated with rotation for 30 min at 4 °C and then centrifuged at 16,000g for 20 min at 4 °C to remove chromatin and debris, and the pellet was discarded. Protein concentration was quantified using the BCA assay (Thermo Fisher Scientific, 23225).

Laemmli buffer (Alfa Aesar, J61337) was added to lysates, and proteins were reduced and denatured at 70 °C for 10 min. Proteins were separated by electrophoresis in MOPS buffer (Invitrogen, NP0001) on precast 4–12% Bis-Tris polyacrylamide gels (Invitrogen, NP0323BOX). For blots with all tissues (Extended Data Fig. 1a), equal protein amounts were loaded into each lane. For blots with only brain regions (Fig. 1b), an equal volume of cleared lysate was loaded in each lane to maximize signal due to the small size of dissected tissue. For blots from cell culture, an equal volume of lysate (Extended Data Fig. 1c) or the indicated protein amount (Extended Data Fig. 1b) was loaded into each lane. Proteins were transferred onto nitrocellulose membranes. Ponceau staining was used to visualize protein bands to facilitate cutting the membrane to probe for loading controls. Membranes were incubated for 1 h at room temperature in blocking buffer (PBS with 5% (wt/vol) non-fat dry milk and 0.1% Tween-20). Primary antibodies diluted in blocking buffer were incubated overnight at 4 °C. Primary antibodies used were as follows: anti-OCT3/OCT4 (1:2,500, Abcam, ab181557, clone EPR17929), anti-KPNB1 (1:2,500, Abcam, ab2811, clone 3E9), anti-SOX2 (1:1,000, R&D, AF2018, lot KOY0317071) and anti-TetR/rtTA (1:1,000, Takara Bio, 631132, clone 9G9). We tested other antibodies (R&D, AF3158; Abcam, ab106629; Santa Cruz, sc-40) that we were

unable to confidently validate in our hands. After three washes with PBS with 0.1% Tween-20, secondary antibodies diluted in blocking buffer were incubated with the membranes for 1 h at room temperature. Secondary antibodies used were as follows: goat anti-rabbit peroxidase (1:10,000, Calbiochem, 401393), goat anti-mouse peroxidase (1:10,000, Calbiochem, 401215), rabbit anti-goat peroxidase (1:10,000, Calbiochem, 401515). Membranes were washed with PBS with 0.1% Tween-20. Detection was performed using SuperSignal West Dura chemiluminescent substrate (Thermo Fisher Scientific, 34076) and film (Thermo Fisher Scientific, 34090).

Primary neural stem cell isolation and culture

Primary NSCs from adult mice (either iOSKM or c+iOSKM, see 'Mouse strains, sex and age') were isolated and cultured based on previously published protocols[63,90,91]. Briefly, mice were euthanized using CO_2 inhalation, and then brains were removed and immersed in PBS (Corning, 21-040-CV) with 1% penicillin–streptomycin–glutamine (PSQ; Gibco, 10378016) and 0.1% gentamicin (Gibco, 15710064) on ice. Both SVZs were dissected as described previously[92]. Tissue was minced and then transferred to a conical tube on ice with fresh PBS with 1% PSQ and 0.1% gentamicin. After centrifugation at 500*g* for 5 min, supernatant was removed, and 5 ml per brain of digestion buffer (HBSS (Corning, 21-021-CV), PSQ (1%), dispase II (1 U ml^{-1}, Stemcell Technologies, 07913), papain (2.5 U ml^{-1}, Worthington, LS003126), DNase I (250 U ml^{-1})) was added. Samples were incubated at 37 °C for 40 min on a rocker and then centrifuged at 300*g* for 5 min. Supernatant was removed, and samples were triturated 60× with a P1000 pipette in 1 ml Neurobasal-A (NBA; Gibco, 10888022) with 1% PSQ and 2% B-27 (minus vitamin A, Gibco, 12587010), hereafter called 'NBA/PSQ/B-27', to obtain single cells. After trituration, an additional 9 ml NBA/PSQ/B-27 was added, and then cells were centrifuged at 300*g* for 5 min. The pellet was resuspended in 5 ml of complete NSC growth medium (NBA/PSQ/B-27 with EGF (20 ng ml^{-1}, PeproTech, AF-100-15) and bFGF (20 ng ml^{-1}, PeproTech, 100-18B)) and transferred to a 6-cm dish. Cells were maintained in a humidified incubator at 37 °C with 5% CO_2. Cells were fed every 2 d by replacing half of the conditioned medium with fresh NBA/PSQ/B-27, adding EGF and bFGF to a final concentration of 20 ng ml^{-1} each. To passage, neurospheres were pelleted by centrifugation at 300*g* for 5 min and then incubated with 1 ml Accutase (Millipore, SCR005 or Stemcell Technologies, 07920) for 5 min at room temperature. Neurospheres were triturated 20× with a P1000 pipette to dissociate them into single cells, and then 5 ml PBS was added before centrifugation at 300*g* for 5 min. Cells were resuspended in 10 ml NSC growth medium (up to 50% of which can be conditioned medium; EGF and bFGF were at a final concentration of 20 ng ml^{-1} each) and then plated in a 10-cm dish. Cells were fed or passaged every 2 d. For protein extraction, RNA extraction or AAV infection (see respective sections below), neurospheres were dissociated into single cells as above, and then cells were plated in wells precoated with poly-D-lysine (0.05 mg ml^{-1} in PBS; Sigma-Aldrich, P6407) and maintained as adherent monolayer cultures.

Doxycycline treatment of primary NSCs

Doxycycline was dissolved in PBS and added to the culture medium at 2 µg ml^{-1}, unless otherwise indicated.

RNA extraction and reverse transcription followed by quantitative PCR

For RNA extraction from primary NSCs, to minimize the impact of batch effects and confluency, all cells for each experiment were plated on the same day and collected on the same day. For the doxycycline time course (Extended Data Fig. 1d), NSCs were plated at 200,000 cells per well in a six-well plate. For other experiments, NSCs were plated at 250,000 cells per well in a 12-well plate. Total RNA from cultured cells was isolated using the Qiagen RNeasy kit according to the manufacturer's instructions. Cells were washed with PBS and then lysed in the well using Buffer RLT (350 µl for 12-well plates, 600 µl for six-well plates) with β-mercaptoethanol added and a cell scraper. On-column DNase digestion was performed to remove genomic DNA. RNA concentration was determined using a NanoDrop spectrophotometer or a Varioskan LUX reader with a µDrop plate. cDNA was synthesized using the High-Capacity cDNA Reverse Transcription Kit (Applied Biosystems, 4368814) using equal input of RNA for each sample within the experiment. cDNA was diluted 1:10 in water, and qPCR was performed using iTaq Universal SYBR Green Supermix (Bio-Rad) and run on the 7900HT system or the QuantStudio 12K Flex instrument (Applied Biosystems). All reactions were performed with two to four technical replicates. Relative gene expression fold changes were calculated as 2^{-ddCt}, normalizing to the geometric mean of housekeeping genes (*Gapdh*, *Hprt1*, *Actb*). For wells where product was undetected, the maximum cycle number (40) was used for calculations. Primer sequences are listed in Supplementary Table 9.

Immunohistochemistry on brain sections

Mice were terminally anesthetized with Avertin in PBS and then transcardially perfused with PBS and heparin followed by PBS with 4% paraformaldehyde. Brains were removed, postfixed in PBS with 4% paraformaldehyde overnight at 4 °C, washed with PBS and then cryoprotected in 30% sucrose at 4 °C until they sank. Tissue was embedded in optimal cutting temperature medium (Tissue-Tek, Electron Microscopy Services, 62550-12) in cryomolds and frozen in a dry ice–ethanol bath. Coronal sections (20 µm) were cut with a Leica cryostat and collected on Superfrost Plus slides (Fisher, 12-550-15).

Coronal sections were washed with PBS, permeabilized in ice-cold methanol with 0.1% Triton X-100 for 15 min and then blocked in 5% normal donkey serum (ImmunoReagents, SP-072-VX10) with 1% BSA in PBS for 30 min. Primary antibodies were diluted in blocking buffer and incubated overnight at 4 °C. Primary antibodies used were as follows: anti-DCX (1:1,000, Cell Signaling Technology, 4604, lot 7), anti-Ki-67 (1:1,000, Invitrogen–eBioscience, clone SolA15), anti-mCherry (1:500, Invitrogen, M11217, clone 16D7), anti-Cre (1:500, Millipore-Sigma, MAB3120, clone 2D8), anti-GFAP (1:1,000, Abcam, ab53554, lot GR3402854-1), anti-SOX2 (1:500, R&D, AF2018, lot KOY0317071), anti-NeuN (1:250, MilliporeSigma, MAB377, clone A60), anti-PSA-NCAM (1:2,000, Invitrogen, 14-9118-82, clone 12E3), anti-EGFR (1:100, Millipore, 06-847, lot 3900816). After three washes with 0.1% Tween-20 in PBS, secondary antibodies and DAPI diluted in blocking buffer were incubated for 2 h at room temperature. Secondary antibodies used were as follows: donkey anti-rabbit, donkey anti-mouse, donkey anti-goat and donkey anti-rat, conjugated to AF 488, AF 568, AF 594 or AF 647 (1:500–1:1,000, Invitrogen), or donkey anti-mouse IgM AF 488 (1:500, Jackson ImmunoResearch, 715-545-020). DAPI was used at 1 µg ml^{-1}. Sections were washed three times with 0.1% Tween-20 in PBS and twice with PBS, and then a coverslip was added with ProLong Gold antifade mounting medium (Invitrogen, P36930). Images were acquired on a Zeiss LSM 900 confocal microscope using a ×20 objective and ZEN Blue 3.0 software.

Imaging and quantification of in situ neuroblast proportion in brain sections

For quantification of neuroblasts in the SVZ by immunostaining, 20-µm coronal brain sections were cut with a Leica cryostat. Every seventh section was collected onto the same slide, with five sections per slide. One slide per mouse (five coronal sections) was stained as above (see 'Immunohistochemistry on brain sections'). To quantify the number of neuroblasts in the SVZ, the entire lateral wall of each lateral ventricle was imaged on a Zeiss LSM 900 confocal microscope using a ×20 objective and automatic tiling, taking five optical sections at 2-µm intervals. Only tiles containing SVZ were imaged; note that ImageJ fills the non-imaged tiles with 0 values to make an overall rectangular image, and thus these areas appear as black boxes in the representative images

shown. Cell counting was performed in a blinded and semi-automated manner using QuPath 0.2.3. For this, a region of interest (ROI) was manually drawn (on blinded and randomized images) around the SVZ to exclude irrelevant areas (ventricle, corpus callosum, striatum) from total cell counts. Counting was then performed in an automated manner in QuPath. Nuclei were segmented based on DAPI staining, and then nuclear masks were expanded by 2 µm to define the cytoplasm. Cells were identified as DCX^+ based on a threshold for mean cytoplasmic DCX intensity and as $Ki\text{-}67^+$ based on a threshold for mean nuclear Ki-67 intensity. Cell proportion was calculated as the number of positive cells over the total number of cells. Cell density was calculated as the number of positive cells over volume (area of ROI × 8 µm, the thickness of the *z* stack). For quantification of DCX intensity, ImageJ–Fiji version 2.9.0/1.53t was used to generate maximum intensity projections for each *z*-stack image. The integrated density (intensity and area) of DCX signal above background was measured in an automated manner for each image. Images were blinded and randomized for analysis.

In vivo EdU administration

EdU (Invitrogen, A10044, E10187) was dissolved in sterile PBS to make a 5 mg ml^{-1} stock solution and administered by i.p. injection for a dose of 50 mg kg^{-1} body weight. To count newborn neurons, EdU was injected once daily for 2 d (concurrent with doxycycline administration), followed by a 5-d chase, repeated for the duration of the partial reprogramming experiment. The endpoint for analysis was 16 d after the first EdU injection and 1 d after the last EdU injection.

Imaging and quantification of newborn neurons in brain sections

For quantification of newborn neurons in the olfactory bulb by immunostaining, 20-µm coronal brain sections were cut with a Leica cryostat. Every seventh section was collected onto the same slide, with five sections per slide. One slide per mouse (five coronal sections) was stained. EdU detection was performed on brain sections after permeabilization and before blocking. Following permeabilization, sections were washed twice with PBS, and then EdU was detected using the Click-iT Plus EdU imaging kit (Invitrogen, C10637) according to the manufacturer's instructions. Blocking and antibody incubation were then performed as usual (see 'Immunohistochemistry on brain sections'). The entirety of each olfactory bulb was imaged on a Zeiss LSM 900 confocal microscope using a ×10 objective and automatic tiling, taking one optical section. Cell counting was performed manually in QuPath 0.2.3. An ROI was drawn based on DAPI signal around the central layers of the olfactory bulb, up to and including the mitral layer. $DAPI^+EdU^+NeuN^+$ cells within the ROI were counted manually using a counting grid overlay in QuPath. Images were blinded and randomized for analysis.

Generation of adeno-associated virus

Viruses were generated and purified by the Stanford Gene Vector and Virus Core using the following plasmids. The AAV serotype SCH9 packaging plasmid[79] was kindly provided by D. Schaffer at the University of California, Berkeley. pAAV-EF1a-mCherry-IRES-Cre was a gift from K. Deisseroth at Stanford University (Addgene plasmid 55632, http://n2t.net/addgene:55632 RRID Addgene_55632). pAAV-EF1a-Cre was a gift from K. Deisseroth (Addgene plasmid 55636, http://n2t.net/addgene:55636, RRID Addgene_55636). pAAV-Ef1a-mCherry was a gift from K. Deisseroth (Addgene plasmid 114470, http://n2t.net/addgene:114470, RRID Addgene_114470). Viral titers (viral genomes (vg) ml^{-1}) were as follows: AAV-SCH9 *Ef1a-Cre*, 1.66×10^{13} (Figs. 4e and 6d,e and Extended Data Fig. 5f,i,l,m) or 2.75×10^{12} (Fig. 4f and Extended Data Fig. 5h); AAV-SCH9 *Ef1a-mCherry*, 2.12×10^{13} (Figs. 4e and 6d,e and Extended Data Fig. 5f,i,l,m); AAV-SCH9 *Ef1a-mCherry*-IRES-*Cre*, 1.38×10^{13} (Extended Data Fig. 5i) or 1.07×10^{12} (Fig. 4b–d and Extended Data Fig. 5h,j,k,m).

Stereotaxic injection of viral vector

To target reprogramming to the SVZ, stereotaxic surgery was performed on c+iOSKM mice (see 'Mouse strains, sex and age') to inject virus into the right lateral ventricle according to published protocols[93]. Mice were anesthetized with isoflurane and positioned on heating pads in a Kopf (model 940) stereotaxic frame set up with a World Precision Instruments (UMP3T-1) UltraMicroPump3 and a Hamilton 1710RN 100-µl syringe with a 30G Small Hub RN needle with a point 2 beveled end. Injections were made into the right lateral ventricles at the following coordinates relative to the bregma: lateral, 1.0 mm; anterior, 0.3 mm; ventral depth, 3.0 mm from the skull surface. After drilling the skull and inserting the needle into position, we waited 5 min before injecting virus. We injected 3 µl of virus (AAV-Cre, 2.75×10^{12} vg ml^{-1}; AAV-mCherry-IRES-Cre, 1.07×10^{12} vg ml^{-1}) at a rate of 10 nl s^{-1} and then waited 7 min before removing the needle and suturing the skin. A single dose of buprenorphine SR (0.5 mg kg^{-1}) was administered subcutaneously for postoperative pain management, and animals were monitored daily until full recovery.

AAV infection of primary neural stem cells in culture

Primary NSCs were plated at 250,000 cells per well in a 12-well plate precoated with poly-D-lysine. After 24 h, virus was added to the cells (1 µl of virus, unless otherwise indicated). After overnight incubation, medium was replaced with fresh NSC growth medium. After 48 h, cells were fixed for immunocytochemistry, lysed for genomic DNA extraction, processed for flow cytometry or dissociated for passaging.

For immunocytochemistry, 8-mm German glass coverslips (Electron Microscopy Services, 72296-08) were sterilized in 70% ethanol, air dried and then placed into each well and precoated with poly-D-lysine. Primary NSCs were plated onto the coverslips and infected with AAV as above, and then cells were fixed in 4% PFA in PBS for 15 min at room temperature and washed twice with PBS before immunostaining.

For AAV infection followed by passaging, primary NSCs were plated and infected with AAV as above, targeting 95% infection. Cells were then dissociated using Accutase, washed and replated in suspension in six-well plates. Neurospheres were then cultured and passaged as usual for 1–2 weeks to allow for recovery from virus and then plated for RT–qPCR (see 'RNA extraction and reverse transcription followed by quantitative PCR').

Immunocytochemistry of primary neural stem cell cultures

To detect AAV infection of primary NSCs or to test NSC identity and differentiation by immunostaining, cells were grown on coverslips and fixed (see 'AAV infection of primary neural stem cells in culture' and 'In vitro differentiation of primary neural stem cells'). Coverslips were permeabilized with 0.1% Triton X-100 in PBS for 10 min and then blocked in 2% BSA with 0.2% Tween-20 in PBS (PBST) for 30 min (for staining using anti-O4 or anti-PSA-NCAM antibody, cells were not permeabilized and detergent was omitted from all steps). Primary antibodies were diluted in blocking buffer and incubated for 1 h at room temperature or overnight at 4 °C. Primary antibodies used were as follows: anti-DCX (1:1,000, Cell Signaling Technology, 4604), anti-DCX (1:500, MilliporeSigma, AB2253, lot 3777998), anti-GFAP (1:1,000, Abcam, ab53554), anti-Ki-67 (1:1,000, Invitrogen–eBioscience, clone SolA15), anti-mCherry (1:1,000, Invitrogen, clone 16D7), anti-GFP (1:500, Abcam, ab13970, lot GR3361051-14), anti-Cre (1:500, MilliporeSigma, MAB3120, clone 2D8), anti-TUJ1 (1:500, BioLegend, 802001), anti-O4 (1:500, R&D, MAB1326, clone O4), anti-EGFR (1:500, Millipore, 06-847, lot 3173794), anti-nestin (1:250, BD Pharmingen, 556309, lot 6084618), anti-PSA-NCAM (1:2,000, Invitrogen, 14-9118-82, clone 12E3). After three rinses with PBST, secondary antibodies and DAPI diluted in PBS were incubated for 30 min at room temperature. Secondary antibodies used were as follows: donkey anti-rabbit,

donkey anti-mouse, donkey anti-goat, donkey anti-rat, conjugated to Alexa Fluor (AF) 488, 568, 594 or 647 (1:1,000, Invitrogen, A-21206, A-31573, A10042, A-21202, A-31571, A-21447, A-21208, A-21209, A21247); donkey anti-mouse IgM AF 488 (1:1,000, Jackson ImmunoResearch, 715-545-020); goat anti-chicken IgY AF 488 (1:1,000, Invitrogen, A-11039); donkey anti-chicken IgY AF 488 (1:1,000, Jackson ImmunoResearch, 703-545-155); donkey anti-guinea pig AF 594 (1:250, Jackson ImmunoResearch, 706-585-148). DAPI was used at 1 μg ml^{-1}. Coverslips were rinsed three times with PBST, twice with PBS and once with water before mounting onto glass slides with ProLong Gold antifade mounting medium.

In vitro EdU treatment and detection

EdU was dissolved in sterile PBS to make a 10 mg ml^{-1} stock solution. EdU was added to prewarmed complete NSC growth medium (see 'Primary neural stem cell isolation and culture'), and then one volume of this mixture was added to the existing medium in each well for a final EdU concentration of 10 μg ml^{-1}. Cells were incubated for 1 h before fixation for immunostaining. Following permeabilization, EdU was detected using the Click-iT Plus EdU imaging kit (Invitrogen, C10639) according to the manufacturer's instructions. After EdU detection, primary and secondary antibody incubations were performed as usual (see 'Immunocytochemistry of primary neural stem cell cultures').

Imaging and quantification of immunocytochemistry

Samples were imaged using a ×20 objective on a Zeiss LSM 900 confocal microscope, taking three optical sections at 1-μm intervals. Eight fields of view were imaged for each coverslip. Maximum intensity projections were generated in ImageJ–Fiji version 2.9.0/1.53t, and then cell counting was performed in an automated manner in QuPath. Nuclei were segmented based on DAPI, and then nuclear masks were expanded by 2 μm to define the cytoplasm. Dead cells were excluded based on nuclear size and DAPI intensity, and then cells were classified as positive or negative based on signal intensity thresholds for each antibody. Images were blinded and randomized for analysis.

Flow cytometry of primary neural stem cells in culture

Primary NSCs were dissociated using Accutase into a single-cell suspension and washed with FACS buffer (PBS with 1% BSA and 0.1% glucose). Cells were resuspended in FACS buffer with DAPI (1 μg ml^{-1}) and filtered through a filter-cap 5-ml FACS tube before running on a BD LSR II flow cytometer. Debris and doublets were excluded based on scatter, and dead cells were excluded based on DAPI (Extended Data Fig. 10b–d). Analysis was performed using FlowJo version 10.

Genomic DNA extraction and PCR

To confirm AAV-Cre-mediated excision of the *lox*-STOP-*lox* cassette in c+iOSKM cells, genomic DNA was extracted from primary NSCs in culture. NSCs were lysed in DirectPCR lysis reagent (Viagen, 101-T) with proteinase K added (1:100, Invitrogen, 25530049) and then incubated at 65 °C for 25 min and 95 °C for 15 min. For PCR, 0.5 μl of crude genomic DNA extract was used per 25-μl reaction, with 2× Phusion Master Mix with GC Buffer (Thermo, F-532), 1 μM each primer and 2.5% DMSO. Primer sequences are listed in Supplementary Table 9. Cycling was performed on a preheated block as follows: 98 °C for 3 min, 35 cycles (98 °C for 15 s, 65.5 °C for 30 s, 72 °C for 2 min 30 s), 72 °C for 10 min. The PCR product was mixed with 6× purple loading dye (NEB) and run alongside the 1 kb Plus ladder (NEB) on a 1% agarose gel with SYBR Safe. Images were acquired on a UV gel imaging station (Analytik Jena UVP UVsolo Touch). To confirm the sequence of transgenes for single-cell RNA-seq read mapping, portions of the *ROSA26* locus and transgene were amplified by PCR as above, followed by Sanger sequencing using primers tiling the locus. All primer sequences are listed in Supplementary Table 9.

Induction of quiescence in primary neural stem cell culture

Primary NSCs were plated at a density of 250,000 cells per well in a 12-well plate precoated with poly-D-lysine. Two days later, the medium was replaced with quiescence medium (NBA/PSQ/B-27 with bFGF (20 ng ml^{-1}) and BMP4 (50 ng ml^{-1}, BioLegend)) to induce quiescence[90]. Cells were maintained in quiescence medium for at least 5 d before AAV infection, replacing the medium every 2 d.

In vitro differentiation of primary neural stem cells

Primary NSCs were freshly isolated from the SVZ and cultured as above and used at low passage (passages 3–5), with the exception of the experiment in Fig. 4e (used at passages 9–10 due to passaging of cells after AAV infection to allow recovery from virus). To assess differentiation by immunostaining and microscopy, 8-mm German glass coverslips (Electron Microscopy Services, 72296-08) were sterilized in 70% ethanol, air dried and then placed into 12-well plates (four to five per well, arranged to not overlap). Coverslips were coated with laminin (5 μg ml^{-1}, Gibco, 23017015) and poly-D-lysine (50 μg ml^{-1}) in PBS, for 4 h to overnight at 37 °C. Wells were washed twice with PBS before plating cells. NSCs were plated into prepared wells at a density of 500,000 cells per well in NSC growth medium with or without doxycycline and incubated overnight. Next, wells were gently washed once with differentiation medium (NBA with 1% PSQ and 2% B-27, no growth factors), and then fresh differentiation medium with or without doxycycline was added to each well. Half of the medium was replaced with fresh differentiation medium with or without doxycycline every 2 d, avoiding exposure of cells to air. To fix cells for immunostaining, one volume of 4% PFA in PBS was added to the existing culture medium in each well, and plates were incubated for 5 min at room temperature. Liquid was then removed and replaced with 4% PFA in PBS for 10 min at room temperature. Wells were washed with PBS, and plates were stored at 4 °C before immunocytochemistry.

Sample preparation for bulk RNA sequencing

Primary NSCs were freshly isolated from the SVZ and cultured as above and used at passage 3. Twelve-well plates were coated with laminin (5 μg ml^{-1}, Gibco, 23017015) and poly-D-lysine (50 μg ml^{-1}) in PBS. Wells were washed twice with PBS before plating cells. Primary NSCs were plated into prepared wells at a density of 500,000 cells per well in NSC growth medium with or without doxycycline, except for the NSC 48-h time point, for which cells were plated at a density of 250,000 cells per well to prevent overgrowth during the experiment. For differentiation time points, cells were incubated overnight in NSC growth medium before switching to differentiation medium (see 'In vitro differentiation of primary neural stem cells'). One culture isolated from an old mouse did not expand sufficiently by passage 3 and was thus excluded from the experiment.

At the appropriate time point, cells were lysed in the well using 350 μl Buffer RLT with β-mercaptoethanol added and a cell scraper. Lysates were transferred to microcentrifuge tubes, flash frozen in liquid nitrogen and stored at −80 °C until all samples were collected. Total RNA was isolated using the Qiagen RNeasy kit according to the manufacturer's instructions, with on-column DNase digestion. RNA concentration and purity were determined using a Varioskan LUX with a μDrop plate. For samples with $A_{260}/A_{230} < 1.7$, RNA cleanup was performed using the Qiagen RNeasy kit according to the manufacturer's instructions. RNA integrity analysis was performed using the Bioanalyzer for 16 randomly chosen samples.

Library construction was performed using 500 ng of each sample as input and the Illumina Stranded mRNA Prep (ligation) kit (20040534) and IDT for Illumina DNA/RNA UD Indexes, plate A index adaptors, according to the manufacturer's instructions. Insert sizes were verified using the Bioanalyzer for a random selection of samples. Concentrations of all individual libraries were determined using a Qubit, and then samples were combined into a single pooled library. A final AMPure

cleanup was performed on the pooled library before quality control and sequencing. The pooled library was sequenced across three lanes of an Illumina NovaSeq X Plus with paired-end 150-bp reads.

Bulk RNA sequencing data processing and analysis

Clipping of 5′ T overhangs, quality trimming and adaptor trimming were performed using Trim Galore (version 0.6.6). Trimmed reads were mapped to a custom genome (mm10 with *rtTA* and each 2A sequence added as chromosomes) using STAR (2.7.10b), allowing for chimeric mapping (minimum length of 25). Multimapped reads were removed with SAMtools, and then features were counted with Subread.

The count matrix was used to analyze gene expression using DESeq2 (1.40.1) with a single design variable incorporating time point, age and treatment. Differentially expressed genes were identified for pairwise comparisons with Wald test *P* values as implemented in DESeq2. Genes were considered significantly differentially expressed if $P_{adj} < 0.1$. Heatmaps, hierarchical clustering and PCA were performed on VST-transformed values (implemented in DESeq2). To identify pathways that change with reprogramming, the complete gene list was ranked by decreasing *Z* score (calculated using $\log_2$ (fold change) and *P* values from DESeq2), and then pathway enrichment was performed using the R implementation of the Broad Institute's preranked GSEA algorithm (fgsea) and the GO pathways provided in MSigDB version 7.1.

Statistics and reproducibility

No statistical methods were used to predetermine sample sizes. Data distribution was not formally tested for normality. Two-sided Kruskal–Wallis rank-sum test was used to compare more than two groups, and two-sided Wilcoxon rank-sum test was used for comparison between specific groups, unless otherwise stated in figure legends. Statistical tests were performed in R (version 4.0.2) or in GraphPad Prism (version 9.3.1). Plots were generated in R (ggplot2, Seurat or UpSetR[94]) or Prism. For sequencing experiments and representative images of immunostaining with quantification, the number of independent experiments is listed in the figure legend and all data points are shown in the figures. For other panels, the numbers of independent experiments are as follows: Fig. 1b, 1; Fig. 4b–d, 2; Fig. 8d–g, 1; Extended Data Fig. 1a,b, 1; Extended Data Fig. 4f,g, 1; Extended Data Fig. 5d, 1; Extended Data Fig. 5h, 1 for each batch of virus; Extended Data Fig. 5n, 1; Extended Data Fig. 8a,b, 2. For in vivo experiments, group allocation was not randomized; rather, animals were assigned to experimental versus control groups based on starting weight and sex to minimize the impact of these differences. For in vitro experiments, randomization was not performed, as each culture was split into both experimental and control groups. Randomization and blinding were performed to minimize bias from sample preparation for single-cell RNA-seq and image quantification. For single-cell RNA-seq, the experimenter performing dissections was blinded to the sample condition; mice were taken in an alternating fashion to minimize impacts of sample processing order. For image quantification, images were blinded and randomized for analysis.

Reporting summary

Further information on research design is available in the Nature Portfolio Reporting Summary linked to this article.

Data availability

Raw sequencing reads and processed files for single-cell RNA-seq are available at the Gene Expression Omnibus under accession number GSE224438. Processed Seurat objects are available on Zenodo (https://doi.org/10.5281/zenodo.10626910)[95]. Raw sequencing reads and count files for bulk RNA-seq are available at the Gene Expression Omnibus under accession number GSE245385. Gene mapping was based on the mm10 mouse genome. Source data are provided with this paper. All other data supporting the conclusions of this study are available from the corresponding author upon request.

Code availability

Code used to process and analyze single-cell RNA-seq data and bulk RNA-seq data are available on GitHub (https://github.com/gitlucyxu/SVZreprogramming)[96].

References

1. Kenyon, C. J. The genetics of ageing. *Nature* **464**, 504–512 (2010).
2. de Cabo, R., Carmona-Gutierrez, D., Bernier, M., Hall, M. N. & Madeo, F. The search for antiaging interventions: from elixirs to fasting regimens. *Cell* **157**, 1515–1526 (2014).
3. Barzilai, N., Crandall, J. P., Kritchevsky, S. B. & Espeland, M. A. Metformin as a tool to target aging. *Cell Metab.* **23**, 1060–1065 (2016).
4. Bonkowski, M. S. & Sinclair, D. A. Slowing ageing by design: the rise of NAD^+ and sirtuin-activating compounds. *Nat. Rev. Mol. Cell Biol.* **17**, 679–690 (2016).
5. Lopez-Otin, C., Galluzzi, L., Freije, J. M. P., Madeo, F. & Kroemer, G. Metabolic control of longevity. *Cell* **166**, 802–821 (2016).
6. Mahmoudi, S., Xu, L. & Brunet, A. Turning back time with emerging rejuvenation strategies. *Nat. Cell Biol.* **21**, 32–43 (2019).
7. Campisi, J. et al. From discoveries in ageing research to therapeutics for healthy ageing. *Nature* **571**, 183–192 (2019).
8. Fan, X., Wheatley, E. G. & Villeda, S. A. Mechanisms of hippocampal aging and the potential for rejuvenation. *Annu. Rev. Neurosci.* **40**, 251–272 (2017).
9. Ocampo, A., Reddy, P. & Belmonte, J. C. I. Anti-aging strategies based on cellular reprogramming. *Trends Mol. Med.* **22**, 725–738 (2016).
10. Rando, T. A. & Chang, H. Y. Aging, rejuvenation, and epigenetic reprogramming: resetting the aging clock. *Cell* **148**, 46–57 (2012).
11. Miller, J. D. et al. Human iPSC-based modeling of late-onset disease via progerin-induced aging. *Cell Stem Cell* **13**, 691–705 (2013).
12. Lapasset, L. et al. Rejuvenating senescent and centenarian human cells by reprogramming through the pluripotent state. *Genes Dev.* **25**, 2248–2253 (2011).
13. Suhr, S. T. et al. Mitochondrial rejuvenation after induced pluripotency. *PLoS ONE* **5**, e14095 (2010).
14. Lo Sardo, V. et al. Influence of donor age on induced pluripotent stem cells. *Nat. Biotechnol.* **35**, 69–74 (2017).
15. Mahmoudi, S. et al. Heterogeneity in old fibroblasts is linked to variability in reprogramming and wound healing. *Nature* **574**, 553–558 (2019).
16. Ohnishi, K. et al. Premature termination of reprogramming in vivo leads to cancer development through altered epigenetic regulation. *Cell* **156**, 663–677 (2014).
17. Abad, M. et al. Reprogramming in vivo produces teratomas and iPS cells with totipotency features. *Nature* **502**, 340–345 (2013).
18. Mosteiro, L. et al. Tissue damage and senescence provide critical signals for cellular reprogramming in vivo. *Science* **354**, aaf4445 (2016).
19. Ocampo, A. et al. In vivo amelioration of age-associated hallmarks by partial reprogramming. *Cell* **167**, 1719–1733 (2016).
20. Neumann, B. et al. Myc determines the functional age state of oligodendrocyte progenitor cells. *Nat. Aging* **1**, 826–837 (2021).
21. Gill, D. et al. Multi-omic rejuvenation of human cells by maturation phase transient reprogramming. *eLife* **11**, e71624 (2022).
22. Browder, K. C. et al. In vivo partial reprogramming alters age-associated molecular changes during physiological aging in mice. *Nat. Aging* **2**, 243–253 (2022).
23. Chen, Y. et al. Reversible reprogramming of cardiomyocytes to a fetal state drives heart regeneration in mice. *Science* **373**, 1537–1540 (2021).
24. Cheng, F. et al. Partial reprogramming strategy for intervertebral disc rejuvenation by activating energy switch. *Aging Cell* **21**, e13577 (2022).

25. Olova, N., Simpson, D. J., Marioni, R. E. & Chandra, T. Partial reprogramming induces a steady decline in epigenetic age before loss of somatic identity. *Aging Cell* **18**, e12877 (2019).
26. Rodriguez-Matellan, A., Alcazar, N., Hernandez, F., Serrano, M. & Avila, J. In vivo reprogramming ameliorates aging features in dentate gyrus cells and improves memory in mice. *Stem Cell Reports* **15**, 1056–1066 (2020).
27. Roux, A. E. et al. Diverse partial reprogramming strategies restore youthful gene expression and transiently suppress cell identity. *Cell Syst.* **13**, 574–587 (2022).
28. Wang, C. et al. In vivo partial reprogramming of myofibers promotes muscle regeneration by remodeling the stem cell niche. *Nat. Commun.* **12**, 3094 (2021).
29. Sarkar, T. J. et al. Transient non-integrative expression of nuclear reprogramming factors promotes multifaceted amelioration of aging in human cells. *Nat. Commun.* **11**, 1545 (2020).
30. Lu, Y. et al. Reprogramming to recover youthful epigenetic information and restore vision. *Nature* **588**, 124–129 (2020).
31. Chondronasiou, D. et al. Multi-omic rejuvenation of naturally aged tissues by a single cycle of transient reprogramming. *Aging Cell* **21**, e13578 (2022).
32. Hishida, T. et al. In vivo partial cellular reprogramming enhances liver plasticity and regeneration. *Cell Rep.* **39**, 110730 (2022).
33. Shen, Y. et al. Expansion of the neocortex and protection from neurodegeneration by in vivo transient reprogramming. Preprint at *bioRxiv* https://doi.org/10.1101/2023.11.27.568858 (2023).
34. Seo, J. H. et al. In situ pluripotency factor expression promotes functional recovery from cerebral ischemia. *Mol. Ther.* **24**, 1538–1549 (2016).
35. van Wijngaarden, P. & Franklin, R. J. Ageing stem and progenitor cells: implications for rejuvenation of the central nervous system. *Development* **140**, 2562–2575 (2013).
36. Katsimpardi, L. & Lledo, P. M. Regulation of neurogenesis in the adult and aging brain. *Curr. Opin. Neurobiol.* **53**, 131–138 (2018).
37. DeCarolis, N. A., Kirby, E. D., Wyss-Coray, T. & Palmer, T. D. The role of the microenvironmental niche in declining stem-cell functions associated with biological aging. *Cold Spring Harb. Perspect. Med.* **5**, a025874 (2015).
38. Ming, G. L. & Song, H. Adult neurogenesis in the mammalian brain: significant answers and significant questions. *Neuron* **70**, 687–702 (2011).
39. McAvoy, K. M. & Sahay, A. Targeting adult neurogenesis to optimize hippocampal circuits in aging. *Neurotherapeutics* **14**, 630–645 (2017).
40. Babcock, K. R., Page, J. S., Fallon, J. R. & Webb, A. E. Adult hippocampal neurogenesis in aging and Alzheimer's disease. *Stem Cell Reports* **16**, 681–693 (2021).
41. Bond, A. M., Ming, G. L. & Song, H. Adult mammalian neural stem cells and neurogenesis: five decades later. *Cell Stem Cell* **17**, 385–395 (2015).
42. Zhao, C., Deng, W. & Gage, F. H. Mechanisms and functional implications of adult neurogenesis. *Cell* **132**, 645–660 (2008).
43. Lois, C. & Alvarez-Buylla, A. Proliferating subventricular zone cells in the adult mammalian forebrain can differentiate into neurons and glia. *Proc. Natl Acad. Sci. USA* **90**, 2074–2077 (1993).
44. Shen, Q. et al. Adult SVZ stem cells lie in a vascular niche: a quantitative analysis of niche cell–cell interactions. *Cell Stem Cell* **3**, 289–300 (2008).
45. Silva-Vargas, V., Crouch, E. E. & Doetsch, F. Adult neural stem cells and their niche: a dynamic duo during homeostasis, regeneration, and aging. *Curr. Opin. Neurobiol.* **23**, 935–942 (2013).
46. Obernier, K. & Alvarez-Buylla, A. Neural stem cells: origin, heterogeneity and regulation in the adult mammalian brain. *Development* **146**, dev156059 (2019).
47. Urban, N., Blomfield, I. M. & Guillemot, F. Quiescence of adult mammalian neural stem cells: a highly regulated rest. *Neuron* **104**, 834–848 (2019).
48. Doetsch, F., Garcia-Verdugo, J. M. & Alvarez-Buylla, A. Cellular composition and three-dimensional organization of the subventricular germinal zone in the adult mammalian brain. *J. Neurosci.* **17**, 5046–5061 (1997).
49. Li, W. L. et al. Adult-born neurons facilitate olfactory bulb pattern separation during task engagement. *eLife* **7**, e33006 (2018).
50. Lois, C., García-Verdugo, J. M. & Alvarez-Buylla, A. Chain migration of neuronal precursors. *Science* **271**, 978–981 (1996).
51. Gheusi, G. et al. Importance of newly generated neurons in the adult olfactory bulb for odor discrimination. *Proc. Natl Acad. Sci. USA* **97**, 1823–1828 (2000).
52. Kernie, S. G. & Parent, J. M. Forebrain neurogenesis after focal ischemic and traumatic brain injury. *Neurobiol. Dis.* **37**, 267–274 (2010).
53. Faiz, M. et al. Adult neural stem cells from the subventricular zone give rise to reactive astrocytes in the cortex after stroke. *Cell Stem Cell* **17**, 624–634 (2015).
54. Llorens-Bobadilla, E. et al. Single-cell transcriptomics reveals a population of dormant neural stem cells that become activated upon brain injury. *Cell Stem Cell* **17**, 329–340 (2015).
55. Enwere, E. et al. Aging results in reduced epidermal growth factor receptor signaling, diminished olfactory neurogenesis, and deficits in fine olfactory discrimination. *J. Neurosci.* **24**, 8354–8365 (2004).
56. Luo, J., Daniels, S. B., Lennington, J. B., Notti, R. Q. & Conover, J. C. The aging neurogenic subventricular zone. *Aging Cell* **5**, 139–152 (2006).
57. Maslov, A. Y., Barone, T. A., Plunkett, R. J. & Pruitt, S. C. Neural stem cell detection, characterization, and age-related changes in the subventricular zone of mice. *J. Neurosci.* **24**, 1726–1733 (2004).
58. Jin, K. et al. Neurogenesis and aging: FGF-2 and HB-EGF restore neurogenesis in hippocampus and subventricular zone of aged mice. *Aging Cell* **2**, 175–183 (2003).
59. Molofsky, A. V. et al. Increasing p16INK4a expression decreases forebrain progenitors and neurogenesis during ageing. *Nature* **443**, 448–452 (2006).
60. Tropepe, V., Craig, C. G., Morshead, C. M. & van der Kooy, D. Transforming growth factor-α null and senescent mice show decreased neural progenitor cell proliferation in the forebrain subependyma. *J. Neurosci.* **17**, 7850–7859 (1997).
61. van Praag, H., Shubert, T., Zhao, C. & Gage, F. H. Exercise enhances learning and hippocampal neurogenesis in aged mice. *J. Neurosci.* **25**, 8680–8685 (2005).
62. Katsimpardi, L. et al. Vascular and neurogenic rejuvenation of the aging mouse brain by young systemic factors. *Science* **344**, 630–634 (2014).
63. Leeman, D. S. et al. Lysosome activation clears aggregates and enhances quiescent neural stem cell activation during aging. *Science* **359**, 1277–1283 (2018).
64. Bondolfi, L., Ermini, F., Long, J. M., Ingram, D. K. & Jucker, M. Impact of age and caloric restriction on neurogenesis in the dentate gyrus of C57BL/6 mice. *Neurobiol. Aging* **25**, 333–340 (2004).
65. Navarro Negredo, P., Yeo, R. W. & Brunet, A. Aging and rejuvenation of neural stem cells and their niches. *Cell Stem Cell* **27**, 202–223 (2020).
66. Horowitz, A. M. et al. Blood factors transfer beneficial effects of exercise on neurogenesis and cognition to the aged brain. *Science* **369**, 167–173 (2020).
67. Wyss-Coray, T. Ageing, neurodegeneration and brain rejuvenation. *Nature* **539**, 180–186 (2016).

68. Carey, B. W., Markoulaki, S., Beard, C., Hanna, J. & Jaenisch, R. Single-gene transgenic mouse strains for reprogramming adult somatic cells. *Nat. Methods* **7**, 56–59 (2010).
69. Dulken, B. W. et al. Single-cell analysis reveals T cell infiltration in old neurogenic niches. *Nature* **571**, 205–210 (2019).
70. Zywitza, V., Misios, A., Bunatyan, L., Willnow, T. E. & Rajewsky, N. Single-cell transcriptomics characterizes cell types in the subventricular zone and uncovers molecular defects impairing adult neurogenesis. *Cell Rep.* **25**, 2457–2469 (2018).
71. Mizrak, D. et al. Single-cell analysis of regional differences in adult V-SVZ neural stem cell lineages. *Cell Rep.* **26**, 394–406 (2019).
72. Cebrian-Silla, A. et al. Single-cell analysis of the ventricular–subventricular zone reveals signatures of dorsal and ventral adult neurogenesis. *eLife* **10**, e67436 (2021).
73. Xie, X. P. et al. High-resolution mouse subventricular zone stem-cell niche transcriptome reveals features of lineage, anatomy, and aging. *Proc. Natl Acad. Sci. USA* **117**, 31448–31458 (2020).
74. Kalamakis, G. et al. Quiescence modulates stem cell maintenance and regenerative capacity in the aging brain. *Cell* **176**, 1407–1419 (2019).
75. Shi, Z. et al. Single-cell transcriptomics reveals gene signatures and alterations associated with aging in distinct neural stem/progenitor cell subpopulations. *Protein Cell* **9**, 351–364 (2017).
76. Ximerakis, M. et al. Single-cell transcriptomic profiling of the aging mouse brain. *Nat. Neurosci.* **22**, 1696–1708 (2019).
77. Buckley, M. T. et al. Cell-type-specific aging clocks to quantify aging and rejuvenation in neurogenic regions of the brain. *Nat. Aging* **3**, 121–137 (2022).
78. Zhao, X. et al. 4D imaging analysis of the aging mouse neural stem cell niche reveals a dramatic loss of progenitor cell dynamism regulated by the RHO–ROCK pathway. *Stem Cell Reports* **17**, 245–258 (2022).
79. Ojala, D. S. et al. In vivo selection of a computationally designed SCHEMA AAV library yields a novel variant for infection of adult neural stem cells in the SVZ. *Mol. Ther.* **26**, 304–319 (2018).
80. Parras, A. et al. In vivo reprogramming leads to premature death linked to hepatic and intestinal failure. *Nat. Aging* **3**, 1509–1520 (2023).
81. Conti, L. et al. Niche-independent symmetrical self-renewal of a mammalian tissue stem cell. *PLoS Biol.* **3**, e283 (2005).
82. White, C. W. 3rd et al. Age-related loss of neural stem cell *O*-GlcNAc promotes a glial fate switch through STAT3 activation. *Proc. Natl Acad. Sci. USA* **117**, 22214–22224 (2020).
83. Lledo, P. M., Alonso, M. & Grubb, M. S. Adult neurogenesis and functional plasticity in neuronal circuits. *Nat. Rev. Neurosci.* **7**, 179–193 (2006).
84. Tsunemoto, R. et al. Diverse reprogramming codes for neuronal identity. *Nature* **557**, 375–380 (2018).
85. Ximerakis, M. et al. Heterochronic parabiosis reprograms the mouse brain transcriptome by shifting aging signatures in multiple cell types. *Nat. Aging* **3**, 327–345 (2023).
86. Belteki, G. et al. Conditional and inducible transgene expression in mice through the combinatorial use of Cre-mediated recombination and tetracycline induction. *Nucleic Acids Res.* **33**, e51 (2005).
87. McGinnis, C. S. et al. MULTI-seq: sample multiplexing for single-cell RNA sequencing using lipid-tagged indices. *Nat. Methods* **16**, 619–626 (2019).
88. Stuart, T. et al. Comprehensive integration of single-cell data. *Cell* **177**, 1888–1902 (2019).
89. Franzén, O., Gan, L.-M. & Björkegren, J. L. M. PanglaoDB: a web server for exploration of mouse and human single-cell RNA sequencing data. *Database* **2019**, baz046 (2019).
90. Martynoga, B. et al. Epigenomic enhancer annotation reveals a key role for NFIX in neural stem cell quiescence. *Genes Dev.* **27**, 1769–1786 (2013).
91. Yeo, R. W. et al. Chromatin accessibility dynamics of neurogenic niche cells reveal defects in neural stem cell adhesion and migration during aging. *Nat. Aging* **3**, 866–893 (2023).
92. Mirzadeh, Z., Doetsch, F., Sawamoto, K., Wichterle, H. & Alvarez-Buylla, A. The subventricular zone en-face: wholemount staining and ependymal flow. *J. Vis. Exp.* **39**, e1938 (2010).
93. Ruetz, T. J. et al. In vitro and in vivo CRISPR–Cas9 screens reveal drivers of aging in neural stem cells of the brain. Preprint at *bioRxiv* https://doi.org/10.1101/2021.11.23.469762 (2021).
94. Conway, J. R., Lex, A. & Gehlenborg, N. UpSetR: an R package for the visualization of intersecting sets and their properties. *Bioinformatics* **33**, 2938–2940 (2017).
95. Xu, L. Processed Seurat objects from scRNA-seq data of the aging subventricular zone (SVZ) neurogenic niche with partial reprogramming. *Zenodo* https://doi.org/10.5281/zenodo.10626909 (2024).
96. Xu, L. SVZ reprogramming. *GitHub* https://github.com/gitlucyxu/SVZreprogramming (2024).

Acknowledgements

We thank T. Ruetz, P. Navarro and O. Zhou for assistance with surgeries and sample processing; F. Boos for independent code checking; J. Butterfield for help with mouse husbandry and genotyping; J. Na for help with pilot experiments; the entire Brunet laboratory and in particular X. Zhao, C. Bedbrook, K. Papsdorf, P. Navarro and J. Chen for discussion and feedback on the manuscript; M. Abu-Remaileh for use of equipment; D. Schaffer for the AAV-SCH9 plasmid; and K. Shen, S. Dixon, H. Nakauchi and T. Wyss-Coray for guidance. Some illustrations were created with https://www.biorender.com. Cell sorting and flow cytometry analysis were performed on instruments in the Stanford Shared FACS Facility, including those obtained using NIH S10 Shared Instrument Grants S10RR025518-01 and S10RR027431-01. This work was supported by NIH P01 AG036695 (A.B.), the Milky Way Research Foundation (A.B.), NSF Graduate Research Fellowships (L.X. and M.T.B.) and a Stanford Graduate Fellowship (L.X.).

Author contributions

This study was conceived by L.X. and A.B. L.X. designed and performed all experiments and analyses unless noted. J.R.-M. helped with immunofluorescence of brain sections, surgeries and sample processing for single-cell RNA-seq and performed mouse husbandry and genotyping. M.H. helped with immunofluorescence of brain sections and RT–qPCR and performed mouse husbandry and genotyping and independent code checking. E.D.S. performed analyses with transcriptomic clocks and provided independent code checking. J.C.L. helped with RT–qPCR and AAV experiments. M.T.B. helped with sample processing and analysis for single-cell RNA-seq. The manuscript was written by L.X. and A.B., and all authors provided comments.

Competing interests

M.T.B. is a cofounder of Retro Biosciences. The other authors declare no competing interests.

Additional information

Extended data is available for this paper at https://doi.org/10.1038/s43587-024-00594-3.

Supplementary information The online version contains supplementary material available at https://doi.org/10.1038/s43587-024-00594-3.

Correspondence and requests for materials should be addressed to Anne Brunet.

Peer review information *Nature Aging* thanks Alejandro Ocampo, Juan Song and the other, anonymous, reviewer(s) for their contribution to the peer review of this work.

https://doi.org/10.1038/s43587-024-00594-3

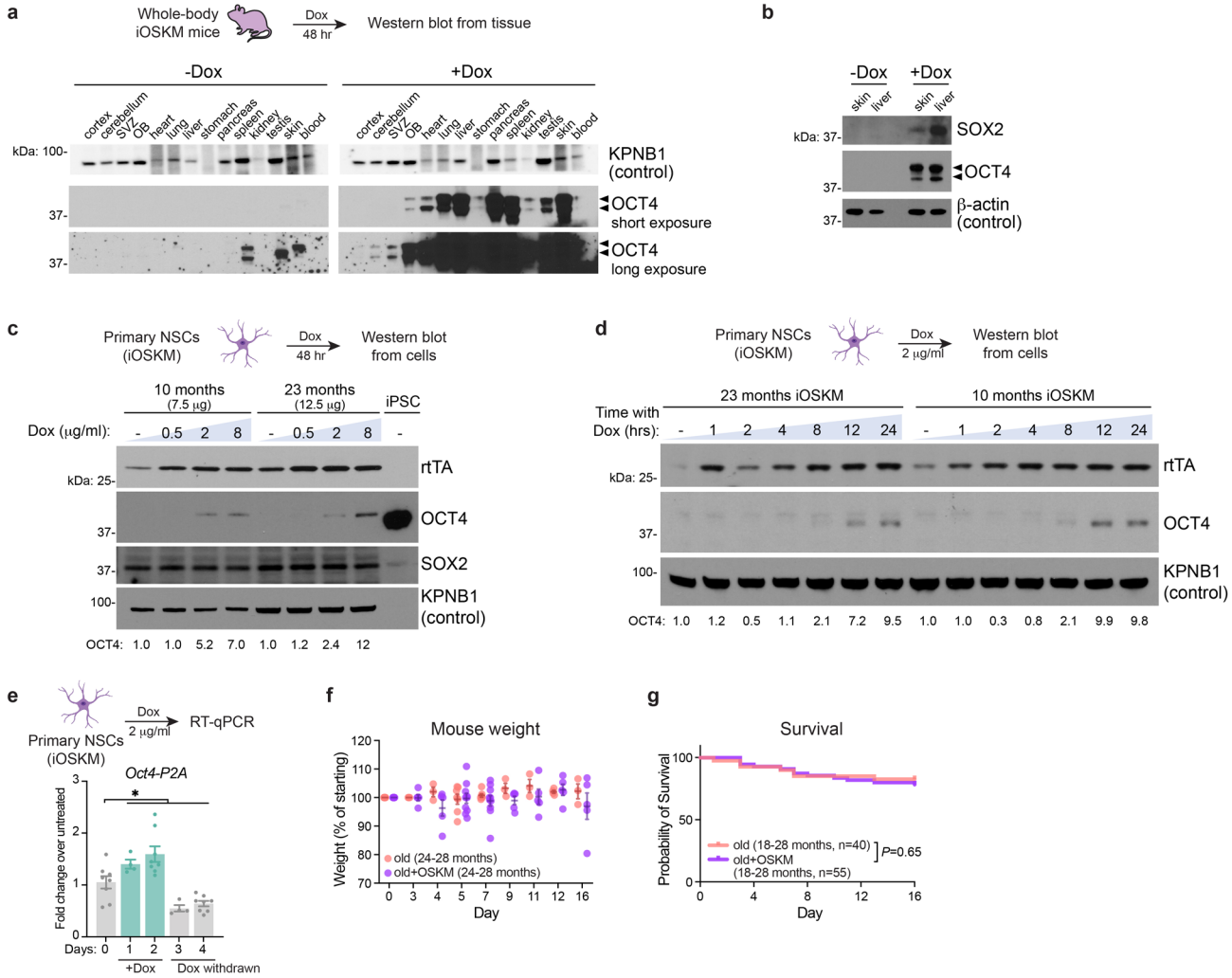

Extended Data Fig. 1 | Characterization of whole-body inducible iOSKM mice and NSCs. a-b, Western blot of tissues from whole-body reprogramming iOSKM mice after treatment with doxycycline. Two different exposures of the same OCT4 blot are shown due to varying levels of transgene expression across tissues. Size in kDa is indicated on the left. Arrowheads indicate OCT4 bands. Expression differences between tissues may be due to differences in accessibility of the *Col1a1* genomic locus and doxycycline bioavailability. **c**, Western blot of primary NSCs from iOSKM mice (n = 2 cultures, each from one mouse) treated in culture with doxycycline at different doses. For NSCs, protein concentration was equalized within each culture; total amount of protein loaded is indicated in parentheses. iPSC: induced pluripotent stem cell, as a positive control for OCT4 expression. Size in kDa is indicated on the left. Normalized densitometry quantification of OCT4 is indicated below each lane. KPNB1 is a loading control for OCT4 and a sample processing control for SOX2 and rtTA. **d**, Western blot of primary NSCs from iOSKM mice (n = 2 cultures, each from one mouse) treated in culture with doxycycline for the indicated amount of time. Normalized densitometry quantification of OCT4 is indicated below each lane. KPNB1 is a loading control. **e**, RT-qPCR of OSKM transgene expression in primary NSCs from iOSKM mice (n = 8 cultures (Days 0, 2, 4) or 4 cultures (Days 1, 3), each culture from one mouse, over 2 independent experiments) during doxycycline treatment (green bars) and withdrawal (gray bars). Each dot represents expression level from one culture. Bar plot indicates mean +/− SEM. FDR-corrected *P*-values are as follows, using Welch's ANOVA with multiple comparisons, for Day 1–4 vs. Day 0: *P* = 0.041, 0.019, 0.017, 0.019. **f**, Body weight of old (24–28 months) mice during partial reprogramming. n = 10 old (5 males and 5 females) and 15 old+OSKM (6 males and 9 females) mice. Note that not every mouse was weighed at every time point. Each dot represents weight for one mouse, normalized to starting weight. Data are mean +/− SEM. All *P*-values > 0.2 by two-sided Wilcoxon rank sum test. **g**, Survival of old (18–28 months) mice during partial reprogramming. n = 40 old (25 males and 15 females) and 55 old+OSKM (36 males and 19 females) mice. *P*-value: Mantel-Cox test.

https://doi.org/10.1038/s43587-024-00594-3

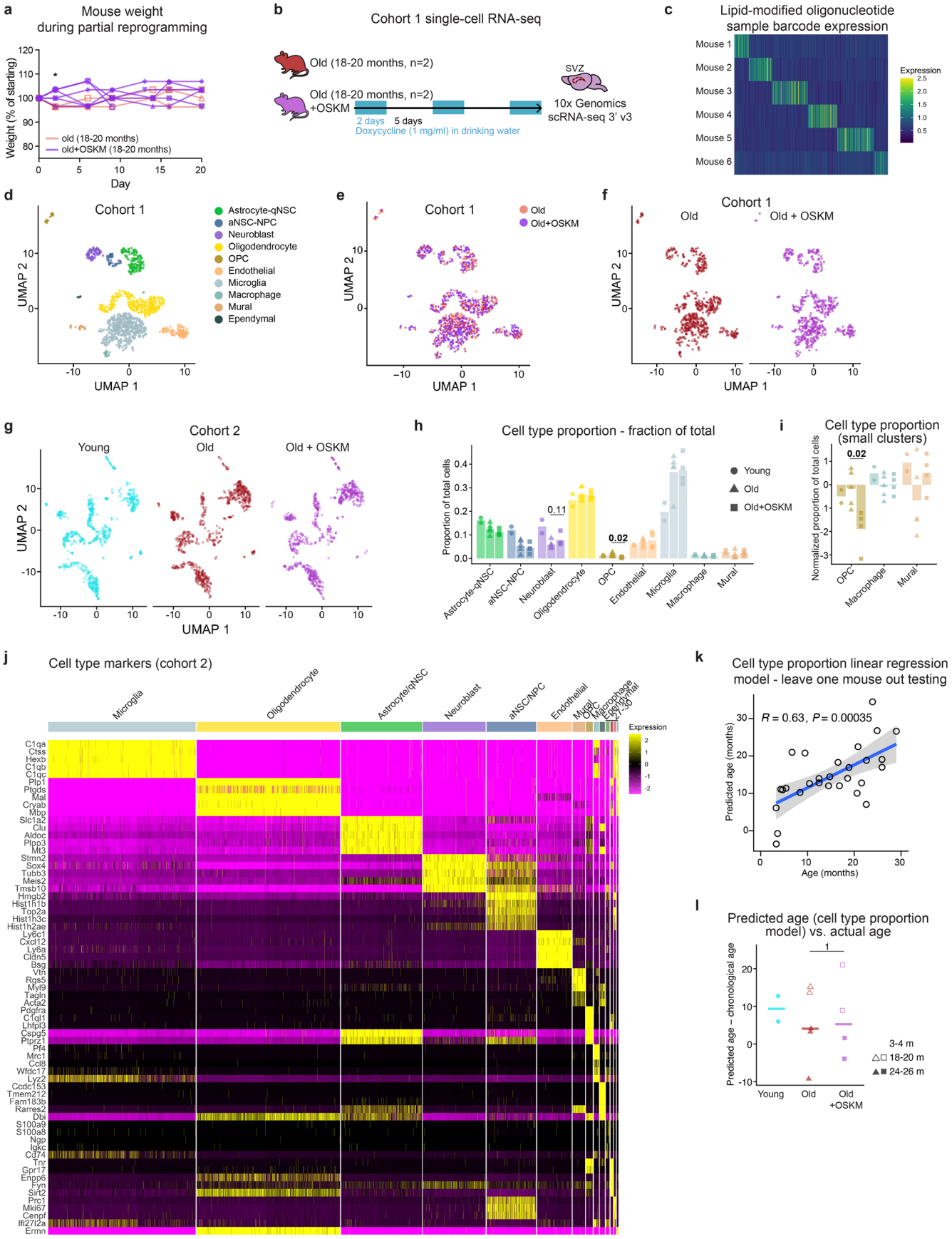

Extended Data Fig. 2 | See next page for caption.

https://doi.org/10.1038/s43587-024-00594-3

Extended Data Fig. 2 | Single-cell transcriptomics after whole-body partial reprogramming. a, Body weight of mice during doxycycline treatment. n = 3 old and 6 old+OSKM, all old (18–20 months) males. **b**, Experimental design for first single-cell RNA-sequencing experiment with old (18–20 months) whole-body iOSKM mice using 10x Genomics v3 kit. n = 2 male mice per condition. **c**, Example of expression of the lipid-modified oligonucleotides used for sample multiplexing of cells from six mice into one lane of a 10x Genomics chip. **d-e**, Dimensionality reduction of 1194 high-quality cells from single-cell RNA-seq of cohort 1, colored by celltype (d) or condition (e). **f**, Dimensionality reduction from single-cell RNA-seq of cohort 1, split by condition. Cell number is downsampled to 550 cells per condition. **g**, Dimensionality reduction from single-cell RNA-seq of cohort 2, split by condition. Cell number is downsampled to 732 cells per condition. **h**, Cell type proportions by single-cell RNA-seq, as a proportion of total cells recovered per mouse. Each dot represents cell proportion for one mouse. Bar plot indicates mean. Mice from both independent cohorts are combined: n = 2 young (3-4 months; 2 males), 5 old (18–20 months or 24–26 months; 4 males and 1 female), 4 old+OSKM (18–20 months or 24–26 months; 3 males and 1 female), over 2 independent experiments (see Fig. 1d, Extended Data Fig. 2b, Supplementary Table 1). *P*-values: two-sided Wilcoxon rank sum test. **i**, Cell type proportions for clusters with very few cells, as a proportion of total cells per mouse, and normalized as log2 fold change over the mean of old untreated mice within each experiment. Bar is mean, each dot is one mouse. n = 2 young, 5 old, 4 old+OSKM, over 2 independent experiments, as in (h). *P*-values: two-sided Wilcoxon rank sum test. **j**, Heatmap of the expression of the top 5 differentially expressed genes in each cell type cluster. Annotation of cell types is indicated on top. Full list of marker genes is in Supplementary Table 2. **k**, Performance of linear regression model trained to predict age based on cell type proportions in the SVZ from single-cell RNA-seq of 28 mice from 3–29 months old (see Methods). Scatter plot shows correlation between predicted age from using leave-one-mouse-out testing vs. actual chronological age of the mouse. Each point represents one mouse. *R* is Pearson's correlation coefficient. *P*-value: two-sided. Blue line is linear model, gray band is 95% confidence interval. **l**, Difference between predicted age from cell type proportion model and actual chronological age for each mouse. Line represents median. n = 2 young, 5 old, 4 old+OSKM, over 2 independent experiments, as in (h). *P*-value: two-sided Wilcoxon rank sum test.

https://doi.org/10.1038/s43587-024-00594-3

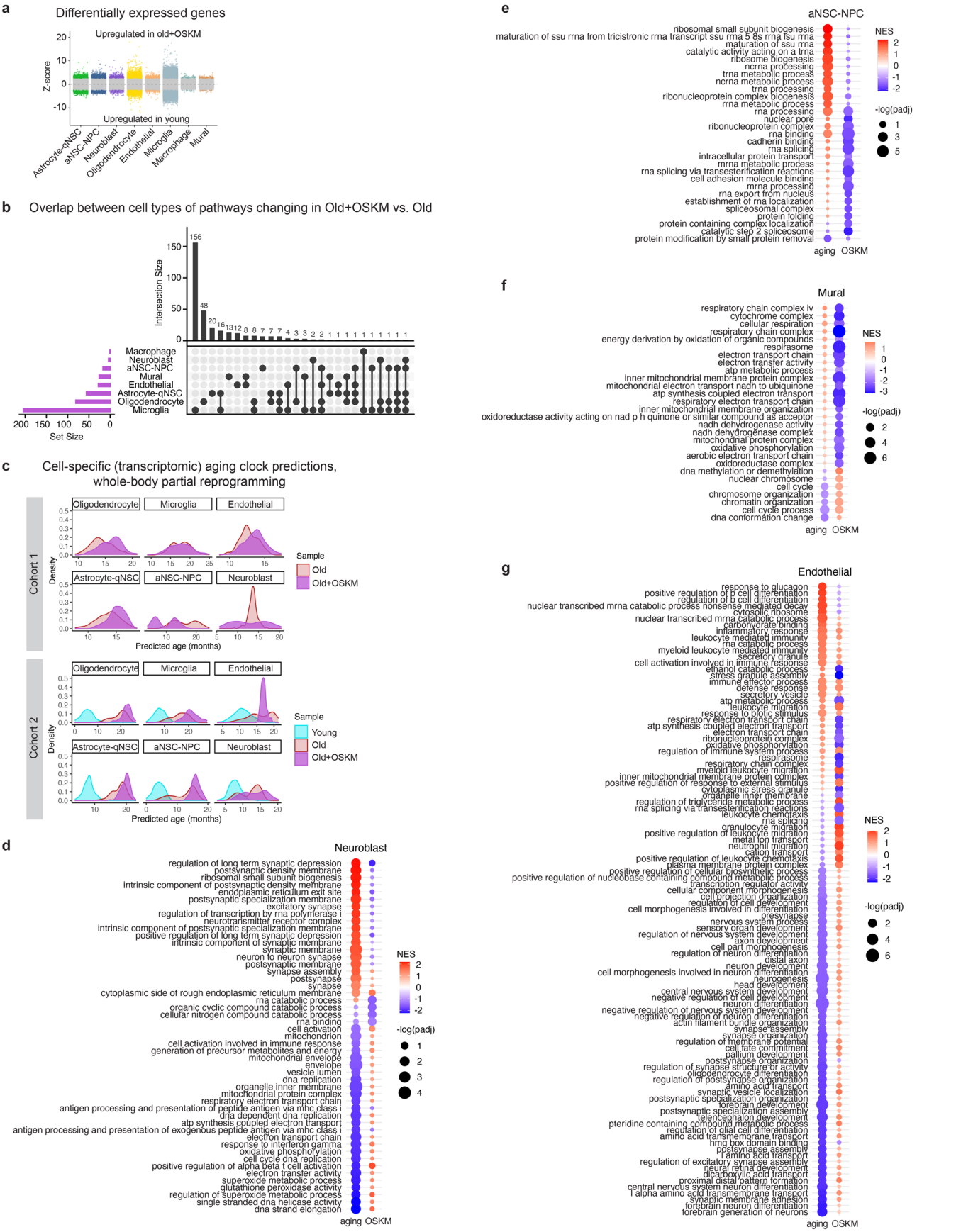

Extended Data Fig. 3 | See next page for caption.

https://doi.org/10.1038/s43587-024-00594-3

Extended Data Fig. 3 | Pathways and transcriptomic clocks after whole-body partial reprogramming. a, Differential gene expression by MAST for each cell type from single-cell RNA-seq, comparing old+OSKM vs. young untreated iOSKM mice. Each dot represents the Z-score for one gene. Positive Z-score indicates upregulation in old+OSKM. Color indicates FDR < 0.2. **b**, UpSet plot showing overlap between significantly changing pathways (BH-adjusted two-sided FGSEA *P*-value, padj < 0.05) after whole-body partial reprogramming across cell types. Purple bars at lower left indicate total number of significant pathways for each cell type. Main bar plot shows number of pathways shared between the cell types indicated in the matrix below (note that direction of change may be different). **c**, Cell type-specific transcriptomic aging clocks previously trained to predict chronological age using single-cell RNA-seq of the SVZ of 28 mice from 3–29 months old were applied to each cell type after partial reprogramming. Density plots show the distribution of predicted ages of each cell type from each condition. The 2 independent experiments (Fig. 1d, Extended Data Fig. 2b) are shown separately. **d-g**, Dot plot of gene set enrichment analysis comparing the effects of aging and reprogramming in neuroblasts (d), aNSCs-NPCs (e), mural cells (f), and endothelial cells (g). Names of gene ontology (GO) pathways are listed on the left. padj: BH-adjusted two-sided FGSEA *P*-value. Pathways that are significantly enriched (padj < 0.05) in at least one comparison are shown. Size of dot reflects adjusted *P*-value (padj). Color indicates normalized effect size (NES), where positive values (red) indicate increase with age ('aging') or increase with partial reprogramming ('OSKM').

https://doi.org/10.1038/s43587-024-00594-3

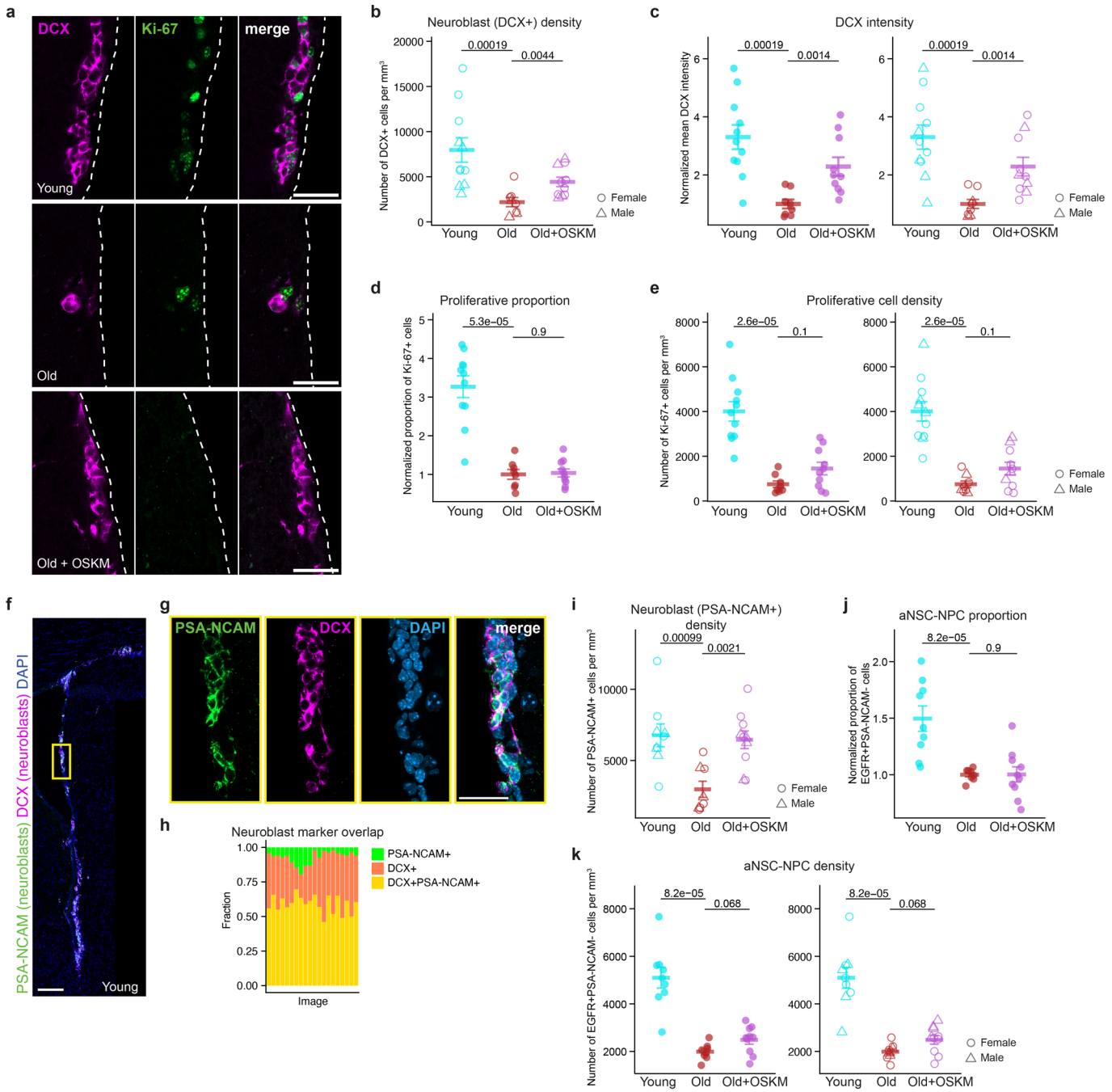

Extended Data Fig. 4 | See next page for caption.

https://doi.org/10.1038/s43587-024-00594-3

Extended Data Fig. 4 | Neuroblasts and proliferation in the intact SVZ after whole-body partial reprogramming. a, High-magnification images of Fig. 3a. Immunofluorescence staining of the SVZ in coronal sections of brains after *in vivo* partial reprogramming. Dorsal is up, lateral is left. Magenta, DCX (neuroblasts); green, Ki-67 (proliferative cells). Dashed line indicates border of ventricle. One optical section (1.0 µm thick) of a confocal image acquired using 63x objective. Scale bars are 25 µm. **b-e**, Quantification of immunofluorescence of the SVZ in coronal brain sections, related to Fig. 3. Multiple optical sections totaling 8 µm thick were acquired for each SVZ, and both hemispheres in five coronal sections at 120 µm intervals were quantified per mouse (see Methods). n = 11 young (3-4 months; 5 males and 6 females), 8 old (20–26 months; 3 males and 5 females), and 10 old+OSKM (20–26 months; 4 males and 6 females) mice, over 3 independent experiments (for individual experiments, see Source Data Table). Each dot represents value for one mouse. Data are mean +/− SEM. *P*-values: two-sided Wilcoxon rank sum test. **b**, Same as Fig. 3e, but symbols represent sex. Neuroblast density (number of DCX^+ cells per mm^3) in the SVZ per mouse. **c**, Total DCX fluorescence intensity (intensity x area) per mouse, normalized to the mean of old control mice. **d**, Proportion of proliferative cells ($Ki\text{-}67^+$ over $DAPI^+$) in the SVZ per mouse, normalized to the mean of old control mice. **e**, Density of proliferative cells (number of $Ki\text{-}67^+$ cells per mm^3) in the SVZ per mouse. Right, symbols represent sex. **f**, Representative images for immunofluorescence staining of the SVZ. Magenta, DCX (neuroblasts); green, PSA-NCAM (neuroblasts); blue, DAPI (nuclei). Dorsal is up, lateral is right. Yellow rectangle is region shown in insets in (g). Scale bar is 100 µm. **g**, High-magnification images of inset region from (f). One optical section of a confocal image acquired using 63x objective. Scale bars are 25 µm. **h**, Quantification of immunofluorescence. Fraction of cells expressing DCX or PSA-NCAM that are positive for one or both markers. Each bar is one image of an SVZ (as shown in i), n = 20 images across 2 young mice. **i-k**, Quantification of immunofluorescence of the SVZ in coronal brain sections, related to Fig. 3. Multiple optical sections totaling 8 µm thick were acquired for each SVZ, and both hemispheres in five coronal sections at 120 µm intervals were quantified per mouse (see Methods). n = 9 young (3-4 months; 4 males and 5 females), 8 old (20–26 months; 3 males and 5 females), and 10 old+OSKM (20–26 months; 4 males and 6 females) mice, over 3 independent experiments (for individual experiments, see Source Data Table). Each dot represents value for one mouse. Data are mean +/− SEM. *P*-values: two-sided Wilcoxon rank sum test. **i**, Same as Fig. 3h, but symbols represent sex. Neuroblast density (number of $PSA\text{-}NCAM^+$ cells per mm^3) in the SVZ per mouse. **j**, Proportion of aNSCs/NPCs ($EGFR^+PSA\text{-}NCAM^-$ over $DAPI^+$) in the SVZ per mouse, normalized to the mean of old control mice. **k**, Density of aNSCs/NPCs (number of $EGFR^+PSA\text{-}NCAM^-$ per mm^3) in the SVZ per mouse. Right, symbols represent sex.

https://doi.org/10.1038/s43587-024-00594-3

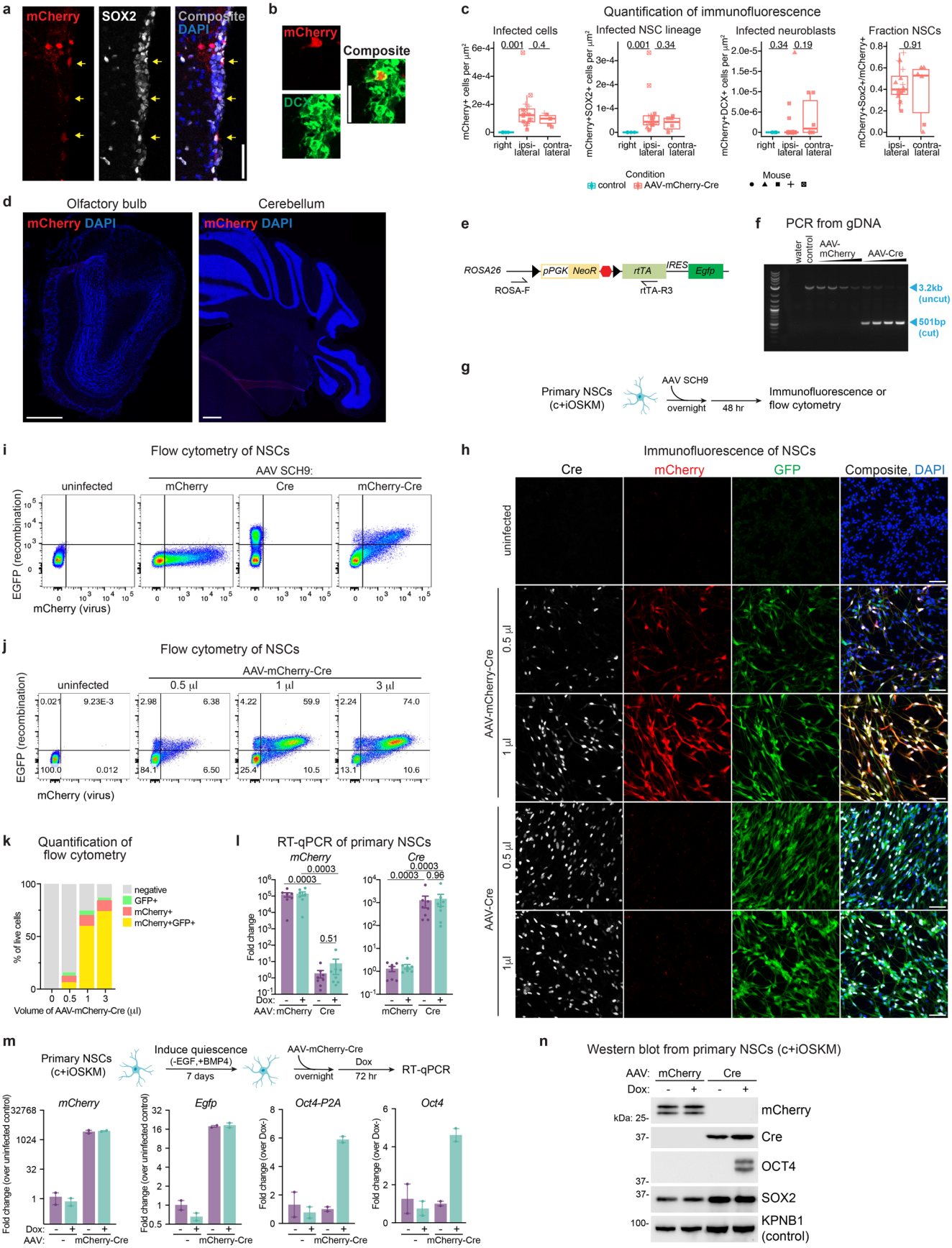

Extended Data Fig. 5 | See next page for caption.

https://doi.org/10.1038/s43587-024-00594-3

Extended Data Fig. 5 | Characterization of Cre-dependent and inducible c+iOSKM mice and AAV-SCH9. a-c, Representative images (a-b) and quantification (c) of immunofluorescence staining to detect mCherry (virus), SOX2 (NSC marker), and DCX (neuroblasts) in the SVZ, 7 days post injection of AAV into the lateral ventricle. Scale bars are 50 µm (a) and 25 µm (b). AAV-mCherry-Cre (AAV SCH9 *Ef1a-mCherry-IRES-Cre*) was injected into the lateral ventricle of the right hemisphere for experimental animals (pink, n = 4 mice), and ipsilateral and contralateral hemispheres relative to injection site were quantified separately. The right hemisphere was counted for uninjected control (n = 1 mouse). In (a), yellow arrows indicate mCherry+SOX2+ cells; mCherry+ population includes both NSCs (SOX2+) and non-NSC cells (SOX2-). Each dot represents cell counts for one image, shape denotes an individual mouse. Box plot indicates median (center line), upper and lower quartiles (box limits), and 1.5x interquartile range (whiskers). *P*-values: two-sided Wilcoxon rank sum test. **d**, Representative images of immunofluorescence of the olfactory bulb and cerebellum using an antibody against mCherry (virus), 4–6 days post injection of AAV-mCherry-Cre (AAV SCH9 *Ef1a-mCherry-IRES-Cre*) into the lateral ventricle. No mCherry signal was detected. Scale bars are 500 µm. **e**, Primer sites for PCR from genomic DNA to detect Cre-mediated recombination of lox-STOP-lox cassette in c+iOSKM cells. **f**, PCR from genomic DNA of NSCs after infection with AAV (0.125 µl to 1µl, 2-fold dilutions). AAV-mCherry: AAV SCH9 *Ef1a-mCherry*. AAV-Cre: AAV SCH9 *Ef1a-Cre*. Colored arrows indicate expected size of products with and without recombination. Equal numbers of cells were plated before infection; note that we observed a correlation between cell death and high virus doses that is reflected in the amount of PCR product (for example, see 3.2 kb band in mCherry-infected cells). Representative of n = 2 cultures. **g**, Scheme for *in vitro* AAV infection of primary NSCs isolated from c+iOSKM mice. All lots of virus were tested for infectivity/recombination in primary NSC culture by flow cytometry and/or immunofluorescence. **h**, Immunofluorescence staining of NSCs after infection with the indicated AAVs, showing efficient infection (Cre, mCherry) and recombination (GFP). Composite includes DAPI (blue). Scale bars are 50 µm. **i**, Flow cytometry of primary NSCs after infection with AAV carrying mCherry only, Cre only, or mCherry-IRES-Cre. **j-k**, Flow cytometry of NSCs after infection with increasing doses of AAV mCherry-IRES-Cre **(j)** and quantification of populations **(k)**. **l**, Related to Fig. 4e. RT-qPCR in primary c+iOSKM NSCs after infection with AAV-mCherry or AAV-Cre, showing expression of the respective viral genes. n = 4 young (3-4 months; 3 males and 1 female) and 4 old (20–23 months; 3 males and 1 female) cultures for Cre, n = 3 young (3-4 months; 2 males and 1 female) and 4 old (20–23 months; 3 males and 1 female) cultures for mCherry, over 1 independent experiment. Each dot represents expression level in one culture; each culture was isolated from one mouse. Bar plot indicates mean +/− SEM. *P*-values: two-sided Wilcoxon rank sum test. **m**, RT-qPCR in quiescent NSCs, showing AAV-SCH9 infection (*mCherry*), Cre-mediated recombination (*Egfp*), OSKM transgene induction (*Oct4-P2A*), and total Oct4 expression (*Oct4*). n = 2 cultures; one independent experiment. Each dot represents expression level in one culture; each culture was isolated from one mouse. Bar plot indicates mean +/− SEM. **n**, Western blot of primary NSCs from c+iOSKM mice, infected in culture with AAV-mCherry (control) or AAV-Cre, then treated with doxycycline. Size in kDa is indicated on the left.

https://doi.org/10.1038/s43587-024-00594-3

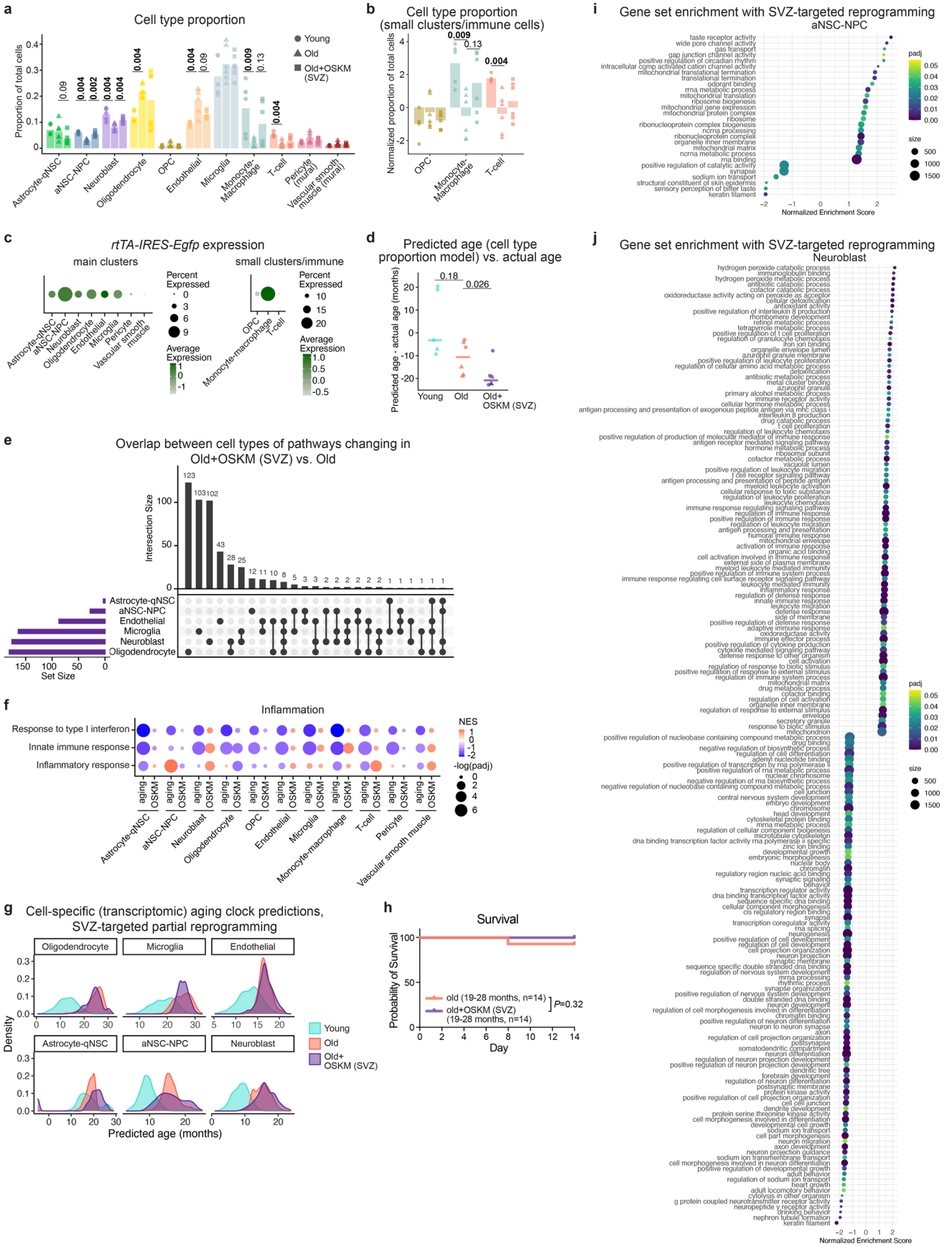

Extended Data Fig. 6 | See next page for caption.

https://doi.org/10.1038/s43587-024-00594-3

Extended Data Fig. 6 | Single-cell transcriptomics after SVZ-targeted reprogramming. a, Cell type proportions by single-cell RNA-seq, as a proportion of total cells recovered per mouse. Each dot represents cell proportion for one mouse. Bar plot indicates mean. n = 5 young, 6 old, 6 old+OSKM (SVZ), over 2 independent experiments. *P*-values: two-sided Wilcoxon rank sum test. **b**, Cell type proportions for small clusters and immune cells, as a proportion of total cells per mouse, and normalized as log2 fold change over the mean of old untreated mice. Each dot represents cell proportion for one mouse. Bar plot indicates mean. n = 5 young, 6 old, 6 old+OSKM (SVZ), over 2 independent experiments. *P*-values: two-sided Wilcoxon rank sum test. **c**, Dot plot of *rtTA-IRES-Egfp* expression by cell type from single-cell RNA-seq. Size of dot reflects percentage of cells within cluster with non-zero expression. Color indicates average expression level. **d**, Difference between predicted age from cell type proportion model and actual chronological age for each mouse. Line represents median. n = 5 young, 6 old, 6 old+OSKM (SVZ), over 2 independent experiments. *P*-value: two-sided Wilcoxon rank sum test. **e**, UpSet plot showing overlap between significantly changing pathways (BH-adjusted two-sided FGSEA *P*-value, padj < 0.05) after SVZ-targeted partial reprogramming across the six most abundant cell types. Purple bars at lower left indicate total number of significant pathways for each cell type. Main bar plot shows number of pathways shared between the cell types indicated in the matrix below (note that direction of change may be different). **f**, Dot plot of gene set enrichment analysis comparing the effects of aging and SVZ-targeted reprogramming on expression of inflammation pathways across cell types. Names of gene ontology (GO) pathways are listed on the left. padj: BH-adjusted two-sided FGSEA *P*-value. Size of dot reflects adjusted *P*-value (padj). Color indicates normalized effect size (NES), where positive values (red) indicate increase with age ('aging') or increase with SVZ-targeted reprogramming ('OSKM'). **g**, Cell type-specific transcriptomic aging clocks previously trained to predict chronological age using single-cell RNA-seq of the SVZ of 28 mice from 3–29 months old were applied to each cell type after SVZ-targeted reprogramming. Density plots show the distribution of predicted ages of each cell type from each condition. **h**, Survival of old (19–28 months) mice during SVZ-targeted partial reprogramming. n = 14 old (8 males and 6 females) and 14 old+OSKM (SVZ) (7 males and 7 females) mice. *P*-value: Mantel-Cox test. **i-j**, Dot plot showing normalized enrichment score from gene set enrichment analysis in aNSCs-NPCs (f) or neuroblasts (g) after SVZ-targeted reprogramming (old+OSKM (SVZ) vs. old control). GO pathway names are listed on the left. padj: BH-adjusted two-sided FGSEA *P*-value. Color reflects adjusted *P*-value (padj). Size of dot reflects number of genes in set. Significantly enriched pathways (padj < 0.05) are shown.

https://doi.org/10.1038/s43587-024-00594-3

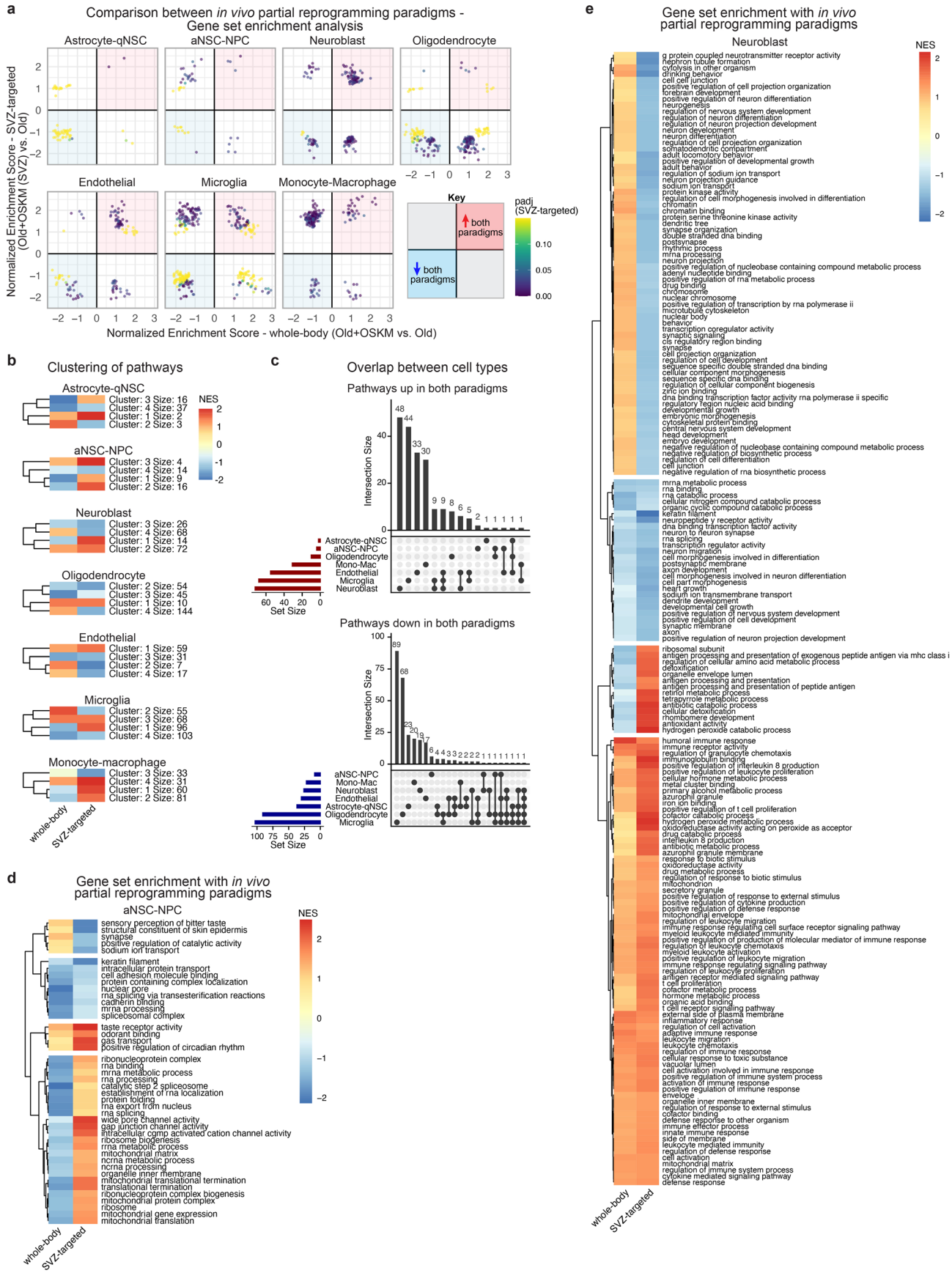

Extended Data Fig. 7 | See next page for caption.

https://doi.org/10.1038/s43587-024-00594-3

Extended Data Fig. 7 | Comparison of whole-body and SVZ-targeted reprogramming. a, Scatter plots showing normalized enrichment scores from gene set enrichment analysis, comparing SVZ-targeted reprogramming (old+OSKM (SVZ) vs. old) vs. whole-body partial reprogramming (old+OSKM vs. old) for common cell types. Each point represents the normalized enrichment scores for one pathway. For all panels, padj: BH-adjusted two-sided FGSEA *P*-value. Pathways where adjusted *P*-value (padj) < 0.05 for at least one comparison are shown. Color indicates padj for SVZ-targeted reprogramming. Pathways in the upper right quadrant and lower left quadrant change in the same direction in both partial reprogramming paradigms. **b**, Heatmap of pathway enrichment for each cell type, comparing normalized enrichment score (NES) in whole-body (old+OSKM vs. old) and SVZ-targeted (old+OSKM (SVZ) vs. old) reprogramming. Pathways where padj < 0.05 for at least one paradigm are included. Pathways are divided into 4 clusters by k-means clustering. Color reflects NES. Size is number of pathways falling into each cluster. **c**, UpSet plot showing overlap between cell types of pathways increasing (top) or decreasing (bottom) in both whole-body and SVZ-targeted partial reprogramming (padj < 0.05 for at least one paradigm). Bars at lower left indicate total number of pathways meeting these criteria for each cell type. Main bar plot shows number of pathways shared between the cell types indicated in the matrix below. **d-e**, Heatmap showing normalized enrichment score (NES) from gene set enrichment analysis in aNSCs-NPCs (d) and neuroblasts (e), comparing whole-body and SVZ-targeted partial reprogramming. GO pathway names are listed on the right. Pathways are divided into 4 clusters by k-means clustering. Color reflects NES. Pathways where padj < 0.05 for at least one comparison are included.

https://doi.org/10.1038/s43587-024-00594-3

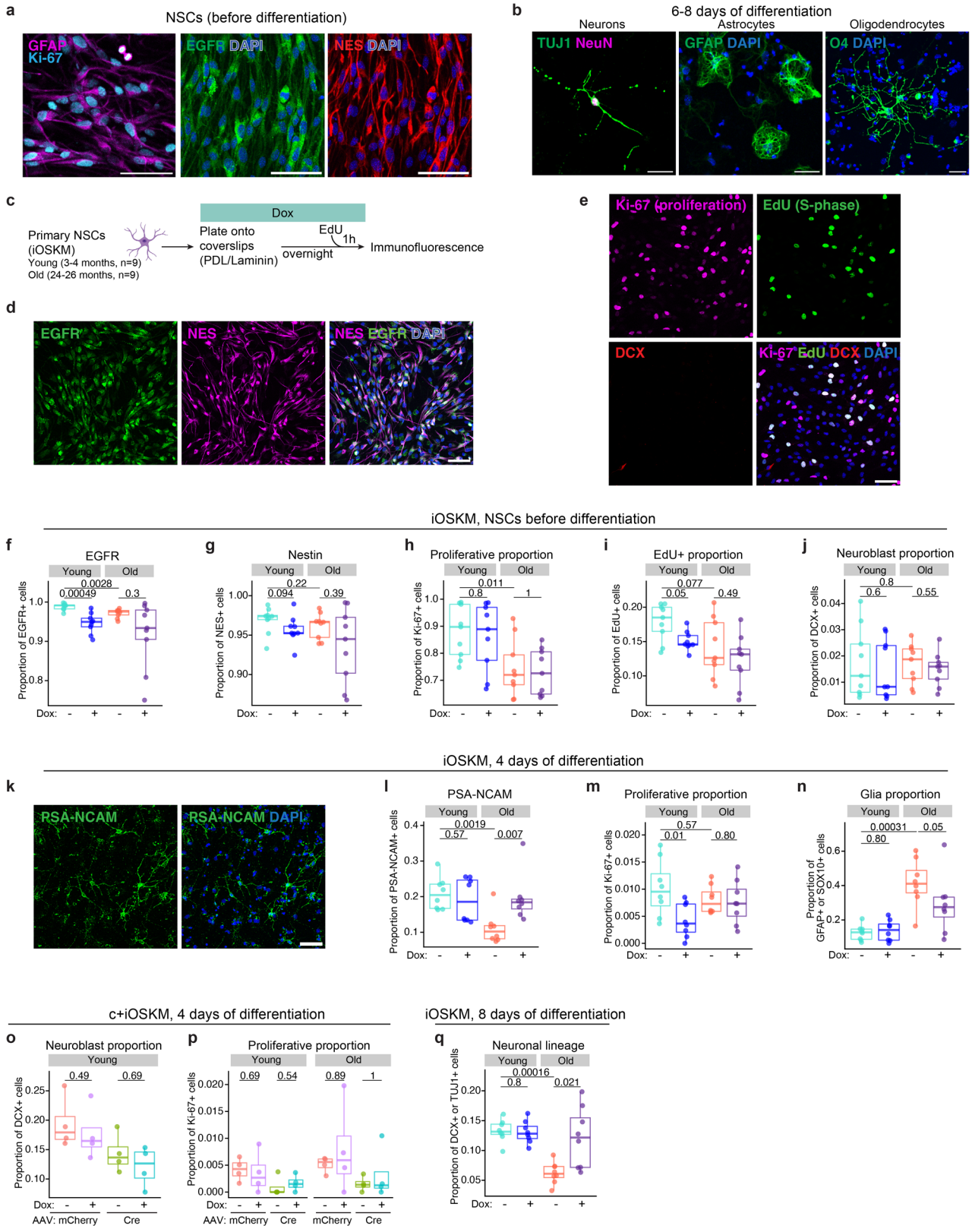

Extended Data Fig. 8 | See next page for caption.

https://doi.org/10.1038/s43587-024-00594-3

Extended Data Fig. 8 | Differentiation of primary NSCs in culture. **a**, Representative images of immunofluorescence staining of primary NSC cultures. Primary NSCs express markers of activated NSCs (Ki-67, GFAP, EGFR, and Nestin). Scale bar is 50 µm. **b**, Representative images of immunofluorescence staining after *in vitro* differentiation of primary NSCs using markers for neurons (TUJ1, NeuN), astrocytes (GFAP), and oligodendrocytes (O4). Scale bar is 25 µm. **c**, Experimental schematic for immunofluorescence of primary NSC cultures from iOSKM mice with partial reprogramming, used in panels d-j. PDL: poly-D-lysine. n = 9 young (3-4 months; 4 males and 5 females) and 9 old (24–26 months; 4 males and 5 females), over 2 independent experiments. Each culture was isolated from one mouse. **d-e**, Representative images of immunofluorescence staining for NSC markers (panel d: EGFR, green; Nestin, magenta), proliferation markers (panel e: Ki-67, magenta; EdU, green) and neuroblast markers (panel e: DCX, red) in primary NSCs from young mice before differentiation. Scale bar is 50 µm. **f-j**, Quantification of immunofluorescence in primary NSCs. n = 9 young (3-4 months; 4 males and 5 females) and 9 old (24–26 months; 4 males and 5 females), over 2 independent experiments. Each dot represents the proportion of cells positive for the indicated marker in one culture, where each culture was isolated from one iOSKM mouse. Box plot indicates median (center line), upper and lower quartiles (box limits), and 1.5x interquartile range (whiskers). *P*-values: two-sided Wilcoxon rank sum test. **k**, Representative image of immunofluorescence staining for neuroblasts (PSA-NCAM, green) after *in vitro* differentiation for 4 days. Scale bar is 50 µm. **l**, Quantification of immunofluorescence staining for neuroblasts (PSA-NCAM$^+$ over DAPI$^+$). n = 8 young (3-4 months; 4 males and 4 females) and 8 old (24–26 months; 4 males and 4 females), over 2 independent experiments. Each dot represents neuroblast proportion for one culture, where each culture was isolated from one iOSKM mouse. Box plot indicates median (center line), upper and lower quartiles (box limits), and 1.5x interquartile range (whiskers). *P*-values: two-sided Wilcoxon rank sum test. **m-n**, Related to Fig. 6a–f. Quantification of immunofluorescence for proliferative cells (Ki-67$^+$, m) and glia (sum of GFAP$^+$ cells and SOX10$^+$ cells, n) after 4 days of differentiation with partial reprogramming. n = 8 young (3-4 months; 4 males and 4 females) and 8 old (24–26 months; 4 males and 4 females), over 2 independent experiments. Each dot represents proliferative proportion for one culture, where each culture was isolated from one iOSKM mouse. Box plot indicates median (center line), upper and lower quartiles (box limits), and 1.5x interquartile range (whiskers). *P*-values: two-sided Wilcoxon rank sum test. **o-p**, Related to Fig. 6d,e. Quantification of immunofluorescence for neuroblasts (DCX$^+$) and proliferative cells (Ki-67$^+$) after AAV infection and 4 days of differentiation with partial reprogramming. n = 4 young (3-4 months; 3 males and 1 female) and 4 old (20–23 months; 3 males and 1 female), over 1 independent experiment. Each dot represents proliferative proportion for one culture, where each culture was isolated from one c+iOSKM mouse. Box plot indicates median (center line), upper and lower quartiles (box limits), and 1.5x interquartile range (whiskers). *P*-values: two-sided Wilcoxon rank sum test. **q**, Related to Fig. 8a–c. Quantification of immunofluorescence for total neuronal cells (sum of DCX$^+$ cells and TUJ1$^+$ cells, representing neuroblasts and neurons) after 8 days of differentiation with partial reprogramming. n = 8 young (3-4 months; 4 males and 4 females) and 8 old (24–26 months; 4 males and 4 females), over 2 independent experiments. Each dot represents total neuronal proportion for one culture, where each culture was isolated from one iOSKM mouse. Box plot indicates median (center line), upper and lower quartiles (box limits), and 1.5x interquartile range (whiskers). *P*-values: two-sided Wilcoxon rank sum test.

https://doi.org/10.1038/s43587-024-00594-3

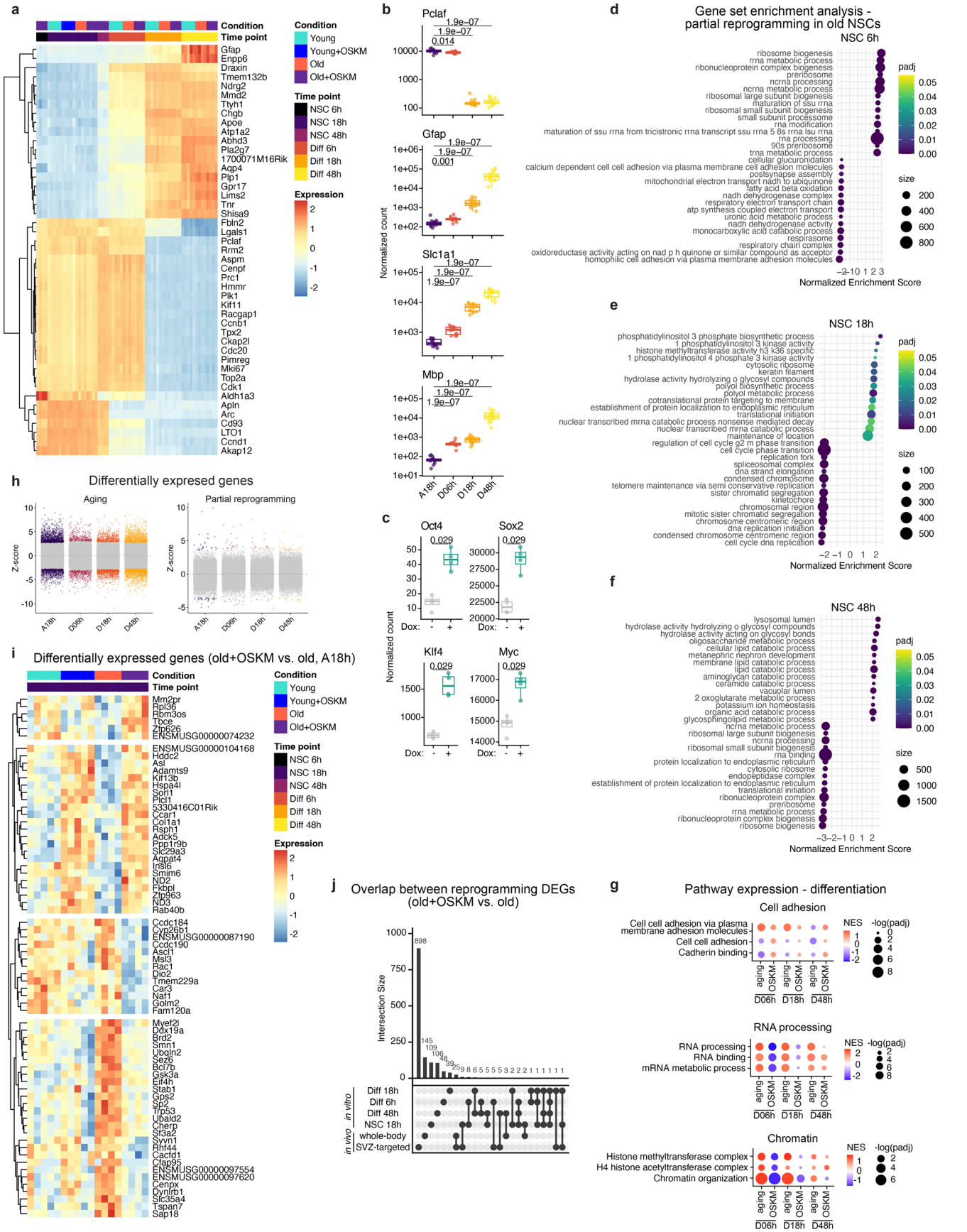

Extended Data Fig. 9 | See next page for caption.

https://doi.org/10.1038/s43587-024-00594-3

Extended Data Fig. 9 | Bulk RNA-seq of primary NSCs with partial reprogramming and differentiation. a, Heatmap of expression of the top variable genes across all samples from bulk RNA-seq of NSCs with reprogramming and differentiation. Color indicates expression, scaled by row. Condition and time point are indicated at the top. Sex-related genes are removed for visualization. **b**, Expression of selected genes that change across differentiation. Each dot represents normalized count for one culture, where each culture was isolated from one iOSKM mouse. n = 5 young (3-4 months; 2 male and 3 female) and 4 old (25 months; 2 male and 2 female) cultures. Box plot indicates median (center line), upper and lower quartiles (box limits), and 1.5x interquartile range (whiskers). *P*-values: two-sided Wilcoxon rank sum test. **c**, Expression of the reprogramming factors in old control and old+OSKM NSCs (6h time point). Each dot represents normalized count for one culture, where each culture was isolated from one iOSKM mouse. n = 4 cultures (25 months; 2 male and 2 female). Box plot indicates median (center line), upper and lower quartiles (box limits), and 1.5x interquartile range (whiskers). *P*-values: two-sided Wilcoxon rank sum test. **d-f**, Dot plot showing normalized enrichment score from gene set enrichment analysis after partial reprogramming in NSCs (old+OSKM vs. old control) at 6h (d), 18h (e), and 48h (f) time points. GO pathway names are listed on the left. padj: BH-adjusted two-sided FGSEA *P*-value. Color reflects padj. Size of dot reflects number of genes in set. Top and bottom 15 (by NES) significantly enriched pathways (padj < 0.05) are shown. **g**, Dotplots of gene set enrichment analysis comparing the effects of aging and reprogramming at each differentiation time point. Names of gene ontology (GO) pathways are listed on the left. padj: BH-adjusted two-sided FGSEA *P*-value. Size of dot reflects padj. Color indicates normalized effect size (NES). **h**, Differential gene expression by DESeq2 for each time point, comparing old vs. young (left) or old+OSKM vs. old (right). Each dot represents the Z-score for one gene. Positive Z-score indicates upregulation. Color indicates FDR < 0.1. **i**, Heatmap of expression of genes that are significantly differentially expressed in NSCs between old and old+OSKM cultures at the 18h time point. Color indicates expression, scaled by row. Condition and time point are indicated at the top. Genes are separated into 4 clusters by k-means clustering. **j**, UpSet plot showing overlap between differentially expressed genes (DEGs) after partial reprogramming (old+OSKM vs. old control) in *in vitro* time points (adjusted *P*-value < 0.2 by DESeq) and *in vivo* paradigms (adjusted *P*-value < 0.3 by MAST in aNSC-NPC, neuroblast, or astrocyte-qNSC clusters).

https://doi.org/10.1038/s43587-024-00594-3

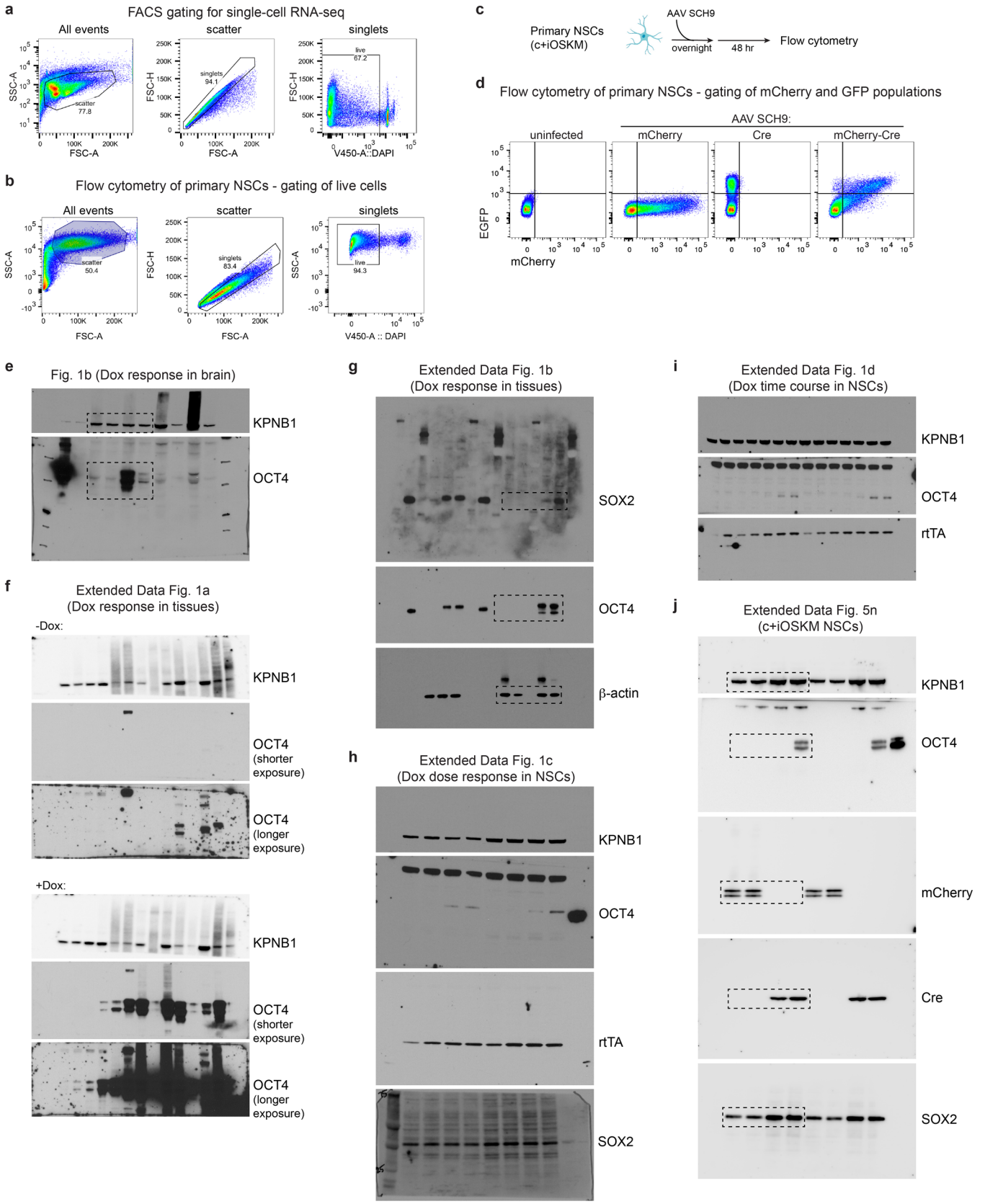

Extended Data Fig. 10 | FACS gating and Western blots. a, Representative gating for FACS sorting of live cells from the SVZ for single-cell RNA-seq. Population shown is listed above each plot. **b**, Representative gating strategy to identify live cells from primary NSCs in culture. Population shown is listed above each plot. **c**, Experimental schematic for flow cytometry analysis of AAV infection of primary NSCs in culture. **d**, Representative gating strategy for analysis of mCherry (virus) and EGFP (recombination marker). Live cells (see b) are shown. Each plot is a culture treated with the virus listed above the plot. Note that these plots are also shown in Extended Data Fig. 5i. **e-j**, Full Western blots. Corresponding figure panels are indicated above the blots. Dotted rectangles indicate cropped area shown in corresponding figure.

nature portfolio

Corresponding author(s): Anne Brunet

Last updated by author(s): Feb 4, 2024

Reporting Summary

Nature Portfolio wishes to improve the reproducibility of the work that we publish. This form provides structure for consistency and transparency in reporting. For further information on Nature Portfolio policies, see our Editorial Policies and the Editorial Policy Checklist.

Statistics

For all statistical analyses, confirm that the following items are present in the figure legend, table legend, main text, or Methods section.

n/a	Confirmed	
☐	☒	The exact sample size (*n*) for each experimental group/condition, given as a discrete number and unit of measurement
☐	☒	A statement on whether measurements were taken from distinct samples or whether the same sample was measured repeatedly
☐	☒	The statistical test(s) used AND whether they are one- or two-sided *Only common tests should be described solely by name; describe more complex techniques in the Methods section.*
☒	☐	A description of all covariates tested
☐	☒	A description of any assumptions or corrections, such as tests of normality and adjustment for multiple comparisons
☐	☒	A full description of the statistical parameters including central tendency (e.g. means) or other basic estimates (e.g. regression coefficient) AND variation (e.g. standard deviation) or associated estimates of uncertainty (e.g. confidence intervals)
☐	☒	For null hypothesis testing, the test statistic (e.g. *F*, *t*, *r*) with confidence intervals, effect sizes, degrees of freedom and *P* value noted *Give P values as exact values whenever suitable.*
☒	☐	For Bayesian analysis, information on the choice of priors and Markov chain Monte Carlo settings
☒	☐	For hierarchical and complex designs, identification of the appropriate level for tests and full reporting of outcomes
☐	☒	Estimates of effect sizes (e.g. Cohen's *d*, Pearson's *r*), indicating how they were calculated

Our web collection on statistics for biologists contains articles on many of the points above.

Software and code

Policy information about availability of computer code

Data collection	Confocal microscopy: Zeiss ZEN Blue 3.0. Flow cytometry: BD Aria instrument and FACSDiva software (version 8.0.1). RT-qPCR: Applied Biosystems 7900HT or QuantStudio 12K Flex instrument and software.
Data analysis	Code used to process and analyze single-cell RNA-seq data and bulk RNA-seq data are available on Github (https://github.com/gitlucyxu/SVZreprogramming). Software and package version numbers are as follows: Single-cell RNA-seq analysis, plotting: R (4.0.2), CellRanger (version 3.0.2 for whole-body reprogramming experiments; version 6.0.2 for SVZ-targeted reprogramming experiments), CITE-seq count (1.4.5), Seurat (3.1.2), sctransform (0.3), fgsea (1.14.0), biomaRt (2.44.1), MAST (1.14.0), org.Mm.eg.db (3.11.4), NCmisc (1.1.6), clusterProfiler (3.16.1), tidyverse (1.3.0), ggplot2 (3.3.2), ggpubr (0.4.0). Image analysis: QuPath (0.2.3), ImageJ (2.9.0), FIJI (1.53t). Flow cytometry: FlowJo (10). Plotting: GraphPad Prism (9.3.1) and R. Bulk RNA-seq analysis and plotting: R, TrimGalore (v0.6.6), STAR (2.7.10b), DESeq2 (1.40.1).

For manuscripts utilizing custom algorithms or software that are central to the research but not yet described in published literature, software must be made available to editors and reviewers. We strongly encourage code deposition in a community repository (e.g. GitHub). See the Nature Portfolio guidelines for submitting code & software for further information.

Data

Policy information about availability of data

All manuscripts must include a data availability statement. This statement should provide the following information, where applicable:

- Accession codes, unique identifiers, or web links for publicly available datasets
- A description of any restrictions on data availability
- For clinical datasets or third party data, please ensure that the statement adheres to our policy

Raw sequencing reads and processed files for single-cell RNA-seq are available at the Gene Expression Omnibus under accession number GSE224438. Raw sequencing reads and count files for bulk RNA-seq are available at the Gene Expression Omnibus under accession number GSE245385. Gene mapping was based on the mouse mm10 genome.

Research involving human participants, their data, or biological material

Policy information about studies with human participants or human data. See also policy information about sex, gender (identity/presentation), and sexual orientation and race, ethnicity and racism.

Reporting on sex and gender	This study did not include any human research participants.
Reporting on race, ethnicity, or other socially relevant groupings	This study did not include any human research participants.
Population characteristics	This study did not include any human research participants.
Recruitment	This study did not include any human research participants.
Ethics oversight	This study did not include any human research participants.

Note that full information on the approval of the study protocol must also be provided in the manuscript.

Field-specific reporting

Please select the one below that is the best fit for your research. If you are not sure, read the appropriate sections before making your selection.

☒ Life sciences ☐ Behavioural & social sciences ☐ Ecological, evolutionary & environmental sciences

For a reference copy of the document with all sections, see nature.com/documents/nr-reporting-summary-flat.pdf

Life sciences study design

All studies must disclose on these points even when the disclosure is negative.

Sample size	No statistical methods were used to predetermine sample size. Sample size was chosen based on availability of samples/animals and previous analysis of similar datasets (Dulken et al. 2019).
Data exclusions	Some samples that were run with the iOSKM cohort 1 and cohort 2 single-cell RNA-seq experiments are not included in this study because they were part of a separate study. These are indicated in the mouse metadata (Supplementary Table 1). Cells were excluded from scRNA-seq analysis based on pre-established standard quality criteria (Cells were filtered out if they contained greater than 10% mitochondrial reads or less than 500 genes. Cells showing strong expression of multiple sample barcodes were considered doublets and excluded from subsequent analysis, as were cells that could not be assigned to any sample barcode.)
Replication	Single-cell RNA-seq experiments (whole-body, and SVZ-targeted) were each performed twice, using two separate cohorts of mice that were processed on different days. Most other experiments were performed at least twice for replication, and data from all experiments are shown. The number of independent experiments is described in the figure legends and/or Methods. Information about independent experiments is provided in the Source Data Table.
Randomization	For in vivo experiments, animals were assigned to experimental vs. control groups based on starting weight and sex, to minimize the impact of these differences. Samples were processed in an alternating manner to minimize the impact of sample processing order. For in vitro experiments, randomization was not performed as each culture was split into both experimental and control groups.
Blinding	For image analysis, investigators were blinded to group allocation during analysis/quantification. For scRNA-seq, investigator performing dissections was blinded to group allocation.

Reporting for specific materials, systems and methods

We require information from authors about some types of materials, experimental systems and methods used in many studies. Here, indicate whether each material, system or method listed is relevant to your study. If you are not sure if a list item applies to your research, read the appropriate section before selecting a response.

Materials & experimental systems

n/a	Involved in the study
☐	☒ Antibodies
☒	☐ Eukaryotic cell lines
☒	☐ Palaeontology and archaeology
☐	☒ Animals and other organisms
☒	☐ Clinical data
☒	☐ Dual use research of concern
☒	☐ Plants

Methods

n/a	Involved in the study
☒	☐ ChIP-seq
☐	☒ Flow cytometry
☒	☐ MRI-based neuroimaging

Antibodies

Antibodies used

Western blot: OCT3/4 (1:2500, abcam ab181557, clone EPR17929), KPNB1 (1:2500, abcam ab2811, clone 3E9), SOX2 (1:1000, R&D AF2018, Lot KOY0317071), and TetR/rtTA (1:1000, Takara Bio 631132, clone 9G9); goat anti-rabbit-peroxidase (1:10,000, Calbiochem 401393), goat anti-mouse-peroxidase (1:10,000, Calbiochem 401215), rabbit anti-goat-peroxidase (1:10,000, Calbiochem 401515).
Immunostaining of brain sections: DCX (1:1000, Cell Signaling Technology 4604, Lot 7), Ki-67 (1:1000, Invitrogen/eBioscience, clone SolA15), mCherry (1:500, Invitrogen M11217, clone 16D7), Cre (1:500, Millipore Sigma MAB3120, clone 2D8), GFAP (1:1000, abcam ab53554, Lot GR3402854-1), SOX2 (1:500, R&D AF2018, Lot KOY0317071), NeuN (1:250, Millipore Sigma MAB377, clone A60), PSA-NCAM (1:2000, Invitrogen 14-9118-82, clone 12E3), EGFR (1:100, Millipore 06-847, Lot 3900816); donkey anti-rabbit, donkey anti-mouse, donkey anti-goat, and donkey anti-rat, conjugated to AF488, 568, 594, or 647 (1:500-1:1000, Invitrogen); or donkey anti-mouse IgM AF488 (1:500, Jackson ImmunoResearch 715-545-020)
Immunostaining of primary NSCs: DCX (1:1000, Cell Signaling Technology 4604), DCX (1:500, Millipore Sigma AB2253, Lot 3777998), GFAP (1:1000, abcam ab53554), Ki-67 (1:1000, Invitrogen/eBioscience, clone SolA15), mCherry (1:1000, Invitrogen, clone 16D7), GFP (1:500, abcam ab13970, Lot GR3361051-14), Cre (1:500, Millipore Sigma MAB3120, clone 2D8), TUJ1 (1:500, Biolegend 802001), O4 (1:500, R&D MAB1326, clone O4), EGFR (1:500, Millipore 06-847, Lot 3173794), Nestin (1:250, BD Pharmingen 556309, Lot 6084618), PSA-NCAM (1:2000, Invitrogen 14-9118-82, clone 12E3); donkey anti-rabbit, donkey anti-mouse, donkey anti-goat, donkey anti-rat, conjugated to Alexa Fluor (AF) 488, 568, 594, or 647 (1:1000, Invitrogen A-21206, A-31573, A10042, A-21202, A-31571, A-21447, A-21208, A-21209, A21247); donkey anti-mouse IgM-AF488 (1:1000, Jackson ImmunoResearch 715-545-020); goat anti-chicken IgY-AF488 (1:1000, Invitrogen A-11039); donkey anti-chicken IgY-AF488 (1:1000, Jackson ImmunoResearch 703-545-155); donkey anti-guinea pig-AF594 (1:250, Jackson ImmunoResearch 706-585-148).

Validation

All antibodies were validated by the manufacturers. Antibodies against cell type markers (DCX, GFAP, SOX2, PSA-NCAM, Ki-67, NeuN, EGFR, O4, Nestin) were selected based on extensive validation by the field. We additionally validated these based on known localization and morphology within cells and within the brain, as well as known expression or lack thereof in cell types of interest (e.g. NSCs vs. neurons). We additionally validated antibodies against exogenous/overexpression targets OCT4, rtTA, mCherry, Cre, GFP using the relevant negative and positive controls (e.g. Extended Data Fig. 1a-d, Extended Data Fig. 5h,n), and antibodies against mCherry, GFP using agreement with native fluorescence.

Animals and other research organisms

Policy information about studies involving animals; ARRIVE guidelines recommended for reporting animal research, and Sex and Gender in Research

Laboratory animals

Whole-body inducible OSKM mice [ROSA26(rtTA-M2); Col1a1(tetO-OSKM)] and conditional+inducible OSKM mice [ROSA26(lox-stop-lox-rtTA-IRES-EGFP); Col1a1(tetO-OSKM] were used. Young mice were 3-5 months old. Old mice were 18-28 months old. Both male and female mice were used for this study. Specific ages and sexes used in each experiment are indicated in the figure legends. Mice were housed with 12-hour light/dark cycles, ad libitum access to food and water in the cage, ~21°C temperature, and ~50% humidity.

Wild animals

This study did not involve wild animals.

Reporting on sex

Both male and female mice were used for this study. Mice were assigned to experimental groups to equalize the number of males and females in each group where possible. Specific numbers for each sex used in each experiment are indicated in the figure legends. Sex for each mouse in single-cell RNA-seq experiments is indicated in the mouse metadata (Supplementary Table 1). Sex-based analysis was not performed due to low statistical power.

Field-collected samples

This study did not involve samples collected from the field.

Ethics oversight

All animal procedures were performed according to protocols approved by the IACUC/AAPLAC of Stanford University (Protocol #8661).

Note that full information on the approval of the study protocol must also be provided in the manuscript.

Plants

Seed stocks	No plants were used in this study.
Novel plant genotypes	No plants were used in this study.
Authentication	No plants were used in this study.

Flow Cytometry

Plots

Confirm that:

☒ The axis labels state the marker and fluorochrome used (e.g. CD4-FITC).

☒ The axis scales are clearly visible. Include numbers along axes only for bottom left plot of group (a 'group' is an analysis of identical markers).

☒ All plots are contour plots with outliers or pseudocolor plots.

☒ A numerical value for number of cells or percentage (with statistics) is provided.

Methodology

Sample preparation	For live cell sorting for single-cell RNA-seq: SVZs from both hemispheres were carefully dissected under a dissecting microscope using forceps, scalpel with no.22 blade, and 22.5 degree stab knife. SVZs were minced, then digested in papain solution (14 U/ml, Worthington LS003119) for 10 min at 37oC. After centrifugation at 300g for 5 min at 4oC, liquid was removed and ovomucoid solution (0.7 mg/ml ovomucoid (Sigma-Aldrich T9253-1G), 0.5 mg/ml DNaseI (Sigma-Aldrich DN25-100MG), in DMEM/F12 (Gibco 11330057) was added. Tissue was triturated with a P1000 pipette to obtain single cell suspension. Cells were then layered onto 22% v/v Percoll (Sigma-Aldrich GE17-0891-01) in PBS and centrifuged at 700g for 10 min at 4oC without brakes to remove myelin debris. Supernatant, containing myelin and debris, was removed. Cell pellet was then resuspended in FACS buffer (1% BSA (Sigma A7979) + 0.1% glucose (Sigma G7021) in PBS) to wash and filtered through 40 um strainer. Cells were centrifuged at 300g for 5 min at 4oC, then resuspended in 70 ul of FACS buffer with DAPI (1 ug/ml, Thermo 62248). Live cells were isolated by FACS (Extended Data Fig. 8a) on a BD Aria sorter using a 100 um nozzle at 20 psi and collected in 750 ul FACS buffer in a protein low-bind microfuge tube (Eppendorf 0030108442). For analysis of primary NSCs: Primary NSCs were dissociated using accutase into single-cell suspension and washed in FACS buffer (PBS + 1% BSA + 0.1% glucose). Cells were resuspended in FACS buffer with DAPI (1 ug/ml) and filtered through a filter-cap 5 ml FACS tube before running on a BD LSRII flow cytometer.
Instrument	BD Aria II sorters and LSR II analyzers were used.
Software	BD FACSDiva software was used to acquire flow cytometry data, and FlowJo version 10 was used to analyze flow cytometry data.
Cell population abundance	Sorting was used to enrich for live cells for single-cell RNA-seq. Post-sort cell viability and lack of debris was visually verified under a light microsope during the establishment of this protocol.
Gating strategy	For live cell sorting for single-cell RNA-seq: scatter was used to exclude debris and doublets. DAPI was used to identify live cells (DAPI-). Full gating is in Extended Data Fig. 10. For analysis of primary NSCs: scatter was used to exclude debris and doublets. DAPI was used to identify live cells (DAPI-). Gates for mCherry or GFP were drawn based on a negative control sample. Full gating is in Extended Data Fig. 10.

☒ Tick this box to confirm that a figure exemplifying the gating strategy is provided in the Supplementary Information.